2016

TOWARDS ELUCIDATION OF THE MECHANISM OF BIOLOGICAL NANOMOTORS

Zhengyi Zhao
University of Kentucky, zzh246@g.uky.edu
Digital Object Identifier: https://doi.org/10.13023/ETD.2016.427

STUDENT AGREEMENT:

I represent that my thesis or dissertation and abstract are my original work. Proper attribution has been given to all outside sources. I understand that I am solely responsible for obtaining any needed copyright permissions. I have obtained needed written permission statement(s) from the owner(s) of each third-party copyrighted matter to be included in my work, allowing electronic distribution (if such use is not permitted by the fair use doctrine) which will be submitted to UKnowledge as Additional File.

I hereby grant to The University of Kentucky and its agents the irrevocable, non-exclusive, and royalty-free license to archive and make accessible my work in whole or in part in all forms of media, now or hereafter known. I agree that the document mentioned above may be made available immediately for worldwide access unless an embargo applies.

I retain all other ownership rights to the copyright of my work. I also retain the right to use in future works (such as articles or books) all or part of my work. I understand that I am free to register the copyright to my work.

REVIEW, APPROVAL AND ACCEPTANCE

The document mentioned above has been reviewed and accepted by the student's advisor, on behalf of the advisory committee, and by the Director of Graduate Studies (DGS), on behalf of the program; we verify that this is the final, approved version of the student's thesis including all changes required by the advisory committee. The undersigned agree to abide by the statements above.

Zhengyi Zhao, Student

Dr. Peixuan Guo, Major Professor

Dr. David Feola, Director of Graduate Studies

TOWARDS ELUCIDATION OF THE MECHANISM OF BIOLOGICAL NANOMOTORS

DISSERTATION

A dissertation submitted in partial fulfillment of the requirements for the degree of Doctor of Philosophy in the College of Pharmacy at the University of Kentucky

By

Zhengyi Zhao

Lexington, Kentucky

Co-Directors: Dr. Peixuan Guo, Professor of Pharmaceutical Sciences

and Dr. Steven Van Lanen, Professor of Pharmaceutical Sciences

Lexington, Kentucky

2016

ABSTRACT OF DISSERTATION

TOWARDS ELUCIDATION OF THE MECHANISM OF BIOLOGICAL NANOMOTORS

Biological functions such as cell mitosis, bacterial binary fission, DNA replication or repair, homologous recombination, Holliday junction resolution, viral genome packaging, and cell entry all involve biomotor-driven DNA translocation. In the past, the ubiquitous biological nanomotors were classified into two categories: linear and rotation motors. In 2013, we discovered a third type of biomotor, revolving motor without rotation. The revolving motion is further found to be widespread among many biological systems. In addition, the detailed sequential action mechanism of the ATPase ring in the phi29 dsDNA packaging motor has been elucidated: ATP binding induces a conformational entropy alternation of ATPase to a high affinity toward dsDNA; ATP hydrolysis triggers another conformational entropy change in ATPase to a low DNA affinity, by which the dsDNA substrate is pushed toward an adjacent ATPase subunit. The subunit communication is regulated by an arginine finger that extends from one ATPase subunit to the adjacent unit, resulting in an asymmetrical hexameric organization. Continuation of this process promotes the movement and revolving of the dsDNA within the hexameric ATPase ring. Coordination of all the motor components facilitate the motion direction control of the viral DNA packaging motors, and make it unusually powerful and effective.

KEYWORDS: Phi29 dsDNA Packaging Motor, Bio-nanomotor, RNA Nanotechnology, DNA Translocase, One-Way Revolving, ASCE Superfamily, AAA+ Superfamily

Zhengyi Zhao

Student's Signature

11/08/16

Date

TOWARDS ELUCIDATION OF THE MECHANISM OF BIOLOGICAL NANOMOTORS

By

Zhengyi Zhao

Dr. Peixuan Guo
Director of Dissertation

Dr. Steven Van Lanen
Co-Director of Dissertation

Dr. David Feola
Director of Graduate Studies

11/15/2016
Date

To my parents and family for their continued support

ACKNOWLEDGMENTS

I would like to express my deepest gratitude to my thesis advisor, Dr. Peixuan Guo, for his continued guidance and support which made this all possible. I am sincerely grateful that I was offered this opportunity to study at both the University of Kentucky and the Ohio State University to perform this intriguing research.

Many thanks also go to my committee members and examiner, Dr. Paul Bummer, Dr. Chang-Guo Zhan, Dr. David Rodgers, Dr. Steven Van Lanen, and Dr. Ren Xu for their sincere instruction and help. Without their diligence and attention to detail, completion of my qualifying exam and dissertation defense would not have been possible.

Furthermore, all members of Dr. Guo's laboratory have in the past and continue to be a valuable source of instruction not only on research matters and collaborations but on personal relationships and friendships alike. I would first like to acknowledge the members of the lab that have helped in training me to become a Ph.D. candidate. I would like to give my sincere gratitude especially to Dr. Dan Shu, Dr. Hui Zhang, Dr. Farzin Haque, Dr. Gian Marco De-Donatis, Dr. Chad Schwartz, and Dr. Huaming Fang for their kind help and instructions to my development as a research scientist. I am also thankful for the remainder of the lab, past and present members, who have contributed to my success: Dr. Yi Shu, Dr. Randall Reif, Dr. Zhanxi Hao, Dr. Jia Geng, Dr. Daniel Binzel, Dr. Mario Vieweger, Dr. Emil Khisamutdinov, Dr. Zhi Zhou, Dr. Xiaofang Jia, Dr. Ashwani Sharma, Dr. Taek Lee, Dr. Lei Lin, Dr. Aijun Hao, Dr. Cheng Li, Dr. Na Li, Dr. Nancy Wardle, Le Zhang, Shaoying Wang, Fengmei Pi, Hui Li, Nayeem Hossain, Daniel Jasinski, Zheng Cui, Eva House, Jeannie Haak, Yanqi Xie, Zhouxiang Ji, Sijin Guo, Erfu Yan, Hongran Yin,

Congcong Xu, Zhefeng Li, Megan Heitkemper, Ariel Wurm and Hongzhi Wang. I would like to also thank the work study students.

I have been lucky to have great outside collaborators during my tenure as a Ph. D. student and I would like to acknowledge them here:

Dr. Jingyuan Li (National Center for Nanoscience and Technology of China and Institute of High Energy Physics), Dr. Dong Wu (Shanghai iTech University), Dr. Zhi-jie Liu (Chinese Academy of Sciences), Dr. Bing Meng (Chinese Academy of Sciences), Dr. Hiroyuki Noji (The University of Tokyo), Dr. Christopher M. Yengo (Pennsylvania State University), Dr. Ian Grainge (University of Newcastle), Dr. Wah Chiu (Baylor College of Medicine), Dr. Oleg Tsodikov (University of Kentucky).

I would like to thank all other faculty and staff members throughout my graduate career, especially the graduate coordinators Catina Rossoll, director of graduate studies Dr. David Feola, and Dr. Jim Pauly in the Department of Pharmaceutical Sciences at the University of Kentucky. I thank them for their assistance in my transition from the University of Kentucky and carry out my CPT at the Ohio State University, and their kind help in organizing class schedules, reserving rooms, and facilitating living arrangements.

Finally, I would like to express my love and appreciation to my family: my mother Yamei Wang and my father Bo Zhao. Their encouragement and support mean the world to me and they continue to make me a better person.

My work was supported by the National Institute of Health grants R01-EB019036 and EB012135 to Dr. Peixuan Guo.

TABLE OF CONTENTS

LIST OF FIGURES

LIST OF ABBREVIATIONS

3WJ	Three Way Junction
AAA+	ATPase Associated with Various Cellular Activities
ASCE	Additional Strand Catalytic E
AFM	Atomic Force Microscopy
ATP	Adenosine Triphosphate
bp	Base pair
CE	Capillary Electrophoresis
DNA	Deoxy Nucleic Acid
dsDNA	Double Stranded Deoxy Ribonucleic Acid
E. Coli	Escherichia coli
eGFP	Enhanced Green Fluorescence Protein
EMSA	Electrophoresis Mobility Shift Assay
PAGE	Polyacrylamide Gel Electrophoresis
PFU	Plague Forming Unit
pRNA	Packaging Ribonucleic Acid
Rf	Arginine Finger
RNA	Ribonucleic Acid
smFRET	Single-Molecule Fluorescence Resonance Energy Transfer
ssDNA	Single Stranded Deoxy Ribonucleic Acid
TBE	89 mM Tris-borate, 2 mM EDTA
TBM	89 mM Tris, 200 mM Borate Acid, 5 mM $MgCl_2$
TEM	Transmission Electron Microscopy
TEV	Tobacco Etch Virus
TIRF	Total Internal Reflection Fluorescence
TMS	50 mM Tris pH 8.0, 100 mM NaCl, 10 mM $MgCl_2$

Chapter 1: Introduction and Literature Review

BRIEF SUMMARY:

Chapter 1 will give an overview about the phi29 dsDNA packaging motor and the current knowledge of various biomotors. The structure, function and application of the three main components in the phi29 motor in nanotechnology for diagnosis and therapeutics will be discussed in this chapter. The packaging models proposed in the past and the recent progress regarding the motor structures and motion principles will be included.

Chapter 2 focuses on the discovery of the third type of revolving motor without rotation, and the finding that these revolving motors are widespread among biological systems. The commonalities of these motors, together with the factors to distinguish revolving motors from rotation motors will be presented. Discussion of a variety of biomotors will be included in this paragraph for comparison through detailed biophysical, biochemical, and structural studies. Finding of the revolving motion is a breakthrough towards the understanding of motion mechanisms of various biomotors, and can be employed for the engineering of new synthetic structures for further applications.

Chapter 3 discusses about the factors that contribute to the one-way traffic property of viral DNA packaging motor. The one-way traffic of dsDNA translocation is facilitated by the involvement of several factors, including ATPase, channel chirality, channel inner loops, and four electropositive layers within the channel. The elucidation of one-way traffic mechanism of the biomotor shed lights on the approach for the construction of macromolecular species in a controlled fashion.

Chapter 4 will explain the sequential action of phi29 dsDNA packaging motor. The push-through one-way valve model has been further verified and moved forward with more details

regarding the biomotor subunit coordination. Arginine finger plays a role during the coordination of motor subunits, resulting in a dimer between two adjacent subunits bridged by arginine finger. This lead to formation of asymmetrical hexameric ATPase, which have been further supported by structural evidences in different ATPases.

Chapter 5 takes the findings from the previous chapters to construct an active biomotor with continuous single-direction motion. The understanding of the mechanism and function of biomotor components, including phi29 connector, pRNA, and ATPase, has been translated toward the manipulation of biomolecular building blocks to generate the active and controllable motor.

Chapter 6 will briefly talks about the current state and the future direction of the biomotors. Potential applications utilizing the motor packaging system will be discussed.

HYPOTHESIS:

Phi29 dsDNA packaging motor coordinates its components in a sequential action manner during its single-directional genome packaging process.

INTRODUCTION:

The unusual powerful phi29 dsDNA packaging motor.

The importance of bio-nanomotors (1) for nanotechnology is akin to that of mechanical motors to daily life. Mechanical motors power cars to drive us to destinations, and nanobiomotors translocate DNA and RNA to facilitate biological functions. These biomotors are extensively involved in dsDNA trafficking, which is critical to DNA repair, replication, recombination, chromosome segregation, DNA/RNA transportation, membrane sorting, cellular reorganization, cell division, bacterial binary fission and many other processes (2,3).

DsDNA viruses package their genome into a preformed procapsid against the internal pressure with a nanomotor powered by ATP. As one of the strongest molecular motor known so far, the phi29 motor can package DNA with a force up to 57pN-110pN at an initial rate of 100-150bp/sec (4). Phi29 packaging system was first constructed in vitro in 1986 (5) and showed to be composed of three main coaxial rings: a connector dodecamer, an ATPase hexamer, and a pRNA hexamer to gear the motor (6-9), which is unique in phi29 and makes the motor unusual powerful.

Biomotors are previously classified as linear and rotation motors, while the newly discovered revolving motion lead to a new category of biomotors isolated from the rotation motors --- revolving motors upon the elucidation of the packaging mechanism of phi29 motor. Different models have been proposed for the motor of dsDNA viruses in the past (10-15). One shared feature among these models is that the packaging process involves ATP-driven conformational entropy changes of the biomotor powering DNA motion. The most popular models in the past include: 1) Nut and bolt model as five-fold/six-fold mismatch connector rotating thread (16); 2) Compression-relax model (17-19); 3) Ratchet model (20); 4) Molecular lever model (21); and 5) Push through one-way valve model. Models 1) - 4) all assume that relative DNA rotation with the motor is necessarily involved during DNA movement. However, the discovery of the third type of biomotor with revolving motion without rotation has provided more clues towards the "push through one-way valve model", where the ATPase gp16 pushes dsDNA substrate into the procapsid through the static connector channel that functions as a valve. The ATPase gp16 and the motor connector channel work independently, though bridged by pRNA as an integrated motor.

Motor connector channel.

In many dsDNA viruses, their connector channels, also called portal proteins, dock onto the motor and serve as pathways for genome during its packaging process (22-25). After packaging,

the portal then functions as a docking site for tail components to complete virion assembly. Structural studies revealed that the portal proteins from all these virus and tailed bacteriophages, such as phi29, SPP1, T4, and T3, share a similar cone-shaped dodecameric structure (26). Taken phi29 dsDNA packaging motor as an example, its portal protein is composed of 12 protein subunits assembled into a cone structure with a diameter of 3.6 nm at the narrowest constriction (27). The portal is stable under even extreme pH conditions from pH 2 to pH 12 (28), and the packaged DNA was able to remain inside the procapsid under high centrifugal force (29). Phi29 connector has been successfully embedded into lipid bilayer and applied for single-molecule detection through conductance assays. With the voltage applied across the membrane, charged molecules passing through the channel will generate transient current blockade signals due to volumetric exclusion of ions from the pore. The results revealed the "one-way traffic" of phi29 motor from the external narrow end to the internal wide end (29-31).

It has been reported that all portal channels of dsDNA bacteriophages display a 30° tilted left-handed channel wall configuration to facilitate the one-way traffic of dsDNA into procapsid by a revolving manner without rotation (26,29,32,33). The one-way revolving mechanism is further supported by portal conformational changes observed during DNA packaging and ejection processes. For phi29 motor, conformational changes of the portal protein can be induced by DNA, pRNA, divalent metal ions through biochemical approaches, or by voltages as demonstrated in nanopore-based single-molecule detection (34-37). Such three-steps conformational changes are reported to be common in various bacteriophage including T3, T4, and SPP1 (37), and is agrees with the Cryo-EM imaging by comparing the conformation of free portals *in vitro* with those in the infectious virion (38). The left-handed portal channel assisting dsDNA advancement during

packaging will be prepared to transit towards a right-handed configuration in three steps for DNA ejection after DNA packaging is complete (26,30).

Mutations of the phi29 connector revealed that the internal loops and the inner lysine rings play an important role in DNA translocation through the channel. The channel loops serve as a ratchet to facilitate the advancement of the genome and prevent it from sliding out during the packaging process (27,31). Four positive lysine layers present at the internal channel wall interact with the negatively charged phosphate backbone of dsDNA (27,31,32). This electrostatic interactions will facilitate the DNA movement and slightly alter the speed of genome translocation. While lysine residues were not essential in viral DNA packaging as indicated by different mutations of the connector, with one exception when residue 234 on the internal loop was mutated and less virion production was observed, supporting the ratchet function of the connector internal loops for motor packaging (31).

Motor packaging RNA.

Packaging RNA is unique in phi29 dsDNA packaging motor, it has been extensively investigated (39-47) since its discovery in 1987 (7). pRNA is 117 nucleotides (nt) in length with independent folding of the ATPase gp16 interaction domain (8) and the motor binding domain (39-41,46-48). In 1988, the pRNA ring was determined to exist as a hexamer (49,50) (featured by Cell (51)) and further verified by Cryo-EM in 2000 (52). There were discrepancies concerning the structure, stoichiometry, and functioning of DNA translocation motors since then. Extensive studies through biochemical analysis (49-51), single molecule photobleaching study (53), gold labeling imaging by electron microscopy (EM) (54,55), and RNA crystal structure studies (56) have all revealed the hexameric assembly of pRNA, excluding the pentameric theory (13,57,58) and the five-fold/six-fold mismatch model (16). One key evidence came from the single molecule

photobleaching analysis of DNA-packaging intermediates, which showed the presence of all six copies of pRNA on the active motor during DNA translocation (53) (**Fig.** 3) with pRNA dimers as building blocks for the pRNA hexameric ring.

As one of the key components for resisting the large internal force during phi29 genome packaging, it is not surprised that an ultra-stable three way junction (3WJ) motif has recently been found within this pRNA molecule, which is unique for the unusual powerful motor (59,60). This 3WJ motif is resistant to 8 Molar urea, and does not dissociate even at extremely low concentrations both *in vitro* and *in vivo*. Detailed crystal structure analysis and single-molecule assays revealed that the 3WJ motif was coordinated by two divalent metal ions that contribute to the conformational changes and stabilization of the RNA tertiary structure (56).

This structural module of pRNA has been widely used as a building block for fabricating ultra-stable nanoparticles with controllable size and shape (61-63), and also as a carrier for targeting and delivery of therapeutic moieties including siRNA, miRNA, ribozyme, drug, and cancer targeting RNA aptamers (64-70). 3WJ derived RNA nanoparticles display little toxicity, favorable biodistribution and pharmacokinetic profiles (71), evidenced by the results that after systemically administered into mice, RNA nanoparticles showed strongly associated with intracranial xenograft tumor without accumulation in normal organs or tissues, and retain the activity of the harbored functionalities. The achievements of phi29 pRNA nanoparticles have led to the development of this RNA as a novel vehicle for applications in nanotechnology and nanomedicine (59,71-82).

Motor gp16 ATPase.

Phi29 motor functions with its ATPase gp16 as an engine utilizing the energy derived from ATP. In 1998, it was proposed by Guo that the mechanism of ATPase in viral DNA packaging

motors is similar to that of the hexameric ASCE including AAA+ superfamily, which is ubiquitous in DNA translocation process in biological systems (49). As a common feature of the ATPase in this superfamily, the critical Walker A (G/A-XXXXGK(T/S)) and Walker B motifs ((R/K)XXXXGXXXXLhhhhD) are assigned in phi29 gp16 ATPase, where G, A, K, T, S, R, L, D, X, and h represent glycine, alanine, lysine, threonine, serine, arginine, leucine, aspartic acid, standard amino acids, and a hydrophobic amino acid, respectively. In the case of phi29 ATPase, Walker A domain is shown to be responsible for ATP binding, and Walker B domain for ATP hydrolysis (6,33,83). With its ability to convert chemical energy from ATP into a conformational change inside the protein, a gain or loss of conformational entropy and the affinity for its substrate will be generated, resulting in a mechanical movement to either make or break contacts between macromolecules. These motion are widely involved in local or global protein unfolding, complex assembly/disassembly, or macromolecule transportation processes.

It has been reported that phi29 DNA packaging motor components work sequentially and cooperatively, including pRNA (84) and ATPase subunits (14,26,33), which allows the motor to continue to move without interruption. Hill constant and binomial distribution assay have revealed that one single inactive subunit was able to inactivate the whole oligomer (85,86). In the presence of dsDNA, a rearrangement occurs within the subunits of gp16 ATPase that enables them to communicate with each other and to "sense" the nucleotide state of the reciprocal subunit through an extremely high level of coordination in the function of the ATPase with the DNA substrate. Such inter-subunit communication was shown to be regulated by an arginine finger (87) by extending from one subunit to the adjacent one and bridge the dimer formation. Ultracentrifugation assays indicated the existence of both monomers and dimers in the ATPase. Further *in vitro* virion assembly assays of the isolated fractions showed that dimer alone did not show any assembly

activity, which can be restored upon the addition of monomers, agreeing with the previous finding that addition of fresh ATPase is required to re-initiate the activity of phi29 packaging intermediate (88). The transient formation of dimer inside the ATPase hexamer resulted in an asymmetrical structure of the ATPase, which is supported by many other biological motors (87,89,90). Binding of ATP to the ATPase subunit stimulates a conformational entropy alternation (26) that enables the ATPase subunit to bind dsDNA and prime ATP hydrolysis. A second entropic and conformational change triggered by ATP hydrolysis will then render the ATPase into a low affinity for dsDNA thus pushing the DNA to the next subunit. Continuation of this process promotes the movement and revolving of the dsDNA within the hexameric ATPase ring.

The final oligomeric state of gp16 ATPase in phi29 motor is a hexamer as proved by qualitative DNA binding assays, capillary electrophoresis assays (CE), and *in vitro* assembly inhibition assays combined with binomial distribution model (83), disagreeing with the pentameric model derived from the EM reconstruction (14,58), which is recently reported to be resulted from the asymmetrical structure of the ATPase intermediate during the sequential coordination as stated above.

Revolving motors: Distinct from Linear or Rotation Motors

Extensive studies based on phi29 dsDNA packaging motor has led to the discovery of a third type of revolving motor that is distinct from linear or rotation motors. The detailed introduction and comparison of these three types of biomotors was published in Guo P. et al. *Microbiology and Molecular Biology Reviews*, 2016. 80(1):161-86.

Chapter 2: The Third Type of Biomotor using Revolving Motion without Rotation

This chapter was reproduced (with some modifications) with permission from G. De-Donatis†, Z. Zhao† (co-first author), S. Wang, L. P. Huang, C. Schwartz, O. V. Tsodikov, H. Zhang, F. Haque and P. Guo. “Finding of widespread viral and bacterial revolving dsDNA translocation motors distinct from rotation motors by channel chirality and size”. Cell & Bioscience 4:30 (Jun. 2014).

Finding of Widespread Viral and Bacterial Revolving dsDNA Translocation Motors Distinct from Rotation by Channel Chirality and Size

Gian Marco De-Donatis[1,2,3†], Zhengyi Zhao[1,2,3†], Shaoying Wang[1,2,3], Lisa P. Huang[§], Chad Schwartz[1,2,3], Oleg V. Tsodikov[2], Hui Zhang[1,2,3], Farzin Haque[1,2,3], and Peixuan Guo[1,2,3]*

[1]Nanobiotechnology Center, [2]Department of Pharmaceutical Sciences, College of Pharmacy, [3]Markey Cancer Center, University of Kentucky, Lexington, KY, USA.

ABSTRACT

Background: Double-stranded DNA translocation is ubiquitous in living systems. Cell mitosis, bacterial binary fission, DNA replication or repair, homologous recombination, Holliday junction resolution, viral genome packaging and cell entry all involve biomotor-driven dsDNA translocation. Previously, biomotors have been primarily classified into linear and rotational motors. We recently discovered a third class of DNA translocation motors in Phi29 utilizing revolving mechanism without rotation. Analogically, the Earth *rotates* around its own axis every 24 hours, but *revolves* around the Sun every 365 days.

Results: Single-channel DNA translocation conductance assay combined with structure inspections of motor channels on bacteriophages P22, SPP1, HK97, T7, T4, Phi29, and other dsDNA translocation motors such as bacterial FtsK and eukaryotic mimiviruses or vaccinia viruses showed that the revolving motor is widespread. The force generation mechanism for revolving motors is elucidated. Revolving motor can be differentiated from rotation motors by their channel size and chirality. Crystal structure inspection revealed that revolving motors commonly exhibit channel diameters larger than 3 nm, while rotation motors that rotate around one of the two separated DNA strands within the channel feature a diameter smaller than 2 nm. Phi29 revolving motor translocated double- and tetra-stranded DNA that occupied 32% and 64% of the narrowest channel cross-section, respectively, evidencing that revolving motors exhibit channel diameters significantly wider than the dsDNA. Left-handed oriented channels found in revolving motors drive the right-handed dsDNA via anti-chiral interaction, while right-handed channels have been observed in rotation motors to drive the right-handed dsDNA via parallel threads. Tethering both the motor and the distal end of the dsDNA does not block DNA packaging, indicating that no rotation is required for motors of dsDNA pages, while a small-angle left-handed twist of dsDNA

that is aligned with the channel could occur due to the conformational change of the motor channel from a left-handed configuration for DNA entry to a right-handed configuration for DNA ejection for host cell infection.

Conclusions: The revolving motor is widespread among biological systems, and can be distinguished from rotation motors by channel size and chirality. The revolving mechanism renders dsDNA void of coiling and torque during translocation of the lengthy helical chromosome, thus resulting in more efficient motor energy conversion.

INTRODUCTION

Transportation of dsDNA from one cellular compartment to another is a prevalent process in all living systems. Many members of the ASCE (Additional Strand Catalytic E) superfamily are nanomotors with a hexameric arrangement of subunits that facilitate a wide range of functions, including dsDNA riding, tracking, packaging, and translocation, which are critical to many processes such as DNA repair, replication, recombination, chromosome segregation, transcription, and cellular reorganization (3,91). Despite their functional diversity, a common feature of the biomotors of this family is their ability to convert energy obtained from the binding or hydrolysis of ATP into mechanical energy which results in local/global protein unfolding, complex assembly/disassembly, or grabbing/pushing dsDNA for translocation (3,91-104). The hexagonal shape of the motor facilitates bottom-up assembly in nanomachine manufacturing (55,56,105-107).

Nanobiomotors have previously been classified into two main categories: linear and rotational motors, which have been clearly documented using single-molecule imaging and X-ray crystallography (108-113). During replication, dsDNA viruses translocate their genomic DNA into preformed protein shells (procapsids) (10-12,51,98,114-116). This entropically unfavorable process is accomplished by a nanomotor that uses ATP as an energy source (6,17,117-123). This dsDNA packaging motor consists of a connector channel and packaging molecules to carry out its activities. For 35 years, it has been popularly believed that DNA packaging in dsDNA viruses involves rotation motors (16), which is seemingly supported by the swivel structure in the crystal structures of all connector channels of bacteriophages (27,124,125). However, extensive investigations revealed that the dsDNA packaging motor channels do not rotate during motor actions (33,53,126-128). For example, the T4 DNA-packaging motor remains active when the

motor channel protein is crosslinked to the protein shell (126). Single-molecule imaging further verified that there is no rotation of the channel during packaging (127). These evidences have brought up a puzzle concerning how packaging can involve a rotation motor without the identification of any rotating components. In 2010, another question was raised regarding the inverse orientations of the Phi29 motor channel and dsDNA helices (29), which further questioned the involvement of rotational motion, since the rotation mechanism of dsDNA as a bolt threading onto a motor channel as a nut requires that the threads of the bolt and nut have the same directionality. Recently, we have discovered that bacteriophage Phi29 dsDNA packaging motor uses a revolving mechanism without rotation, coiling, or torque forces (**Fig. 2.1**) (32,33,83,102). The ATPase hexameric ring exercises a force to push the dsDNA through the dodecamer channel which acts as a one-way valve (29,102,103). Observation of this revolving mechanism establishes a third class of biomotors. This finding resolves many puzzles throughout the history of long-lasting studies on the motor (102,103).

As the translocation of dsDNA is a ubiquitous process in living systems and motors of all dsDNA bacteriophages share some common structural and functional features, we aimed at determining whether the revolving model discovered for Phi29 can generally be applied to other DNA packaging motors. Cellular counterparts that show a strong similarity to the Phi29 viral DNA packaging motor are the FtsK and SpoIIIE family, featuring a hexameric motor that transports DNA and separates the intertwined lengthy genomic dsDNA during cell division or binary fission (129-137). Unwinding of the supercoiled dsDNA resulting from rotation would lead to expensive energy consumption (138). The revolving mechanism adopted by biological systems during evolution, resembles an optimized mechanism for translocation of lengthy dsDNA genome without coiling. In this report, we analyze the motor mechanism regarding force generation of

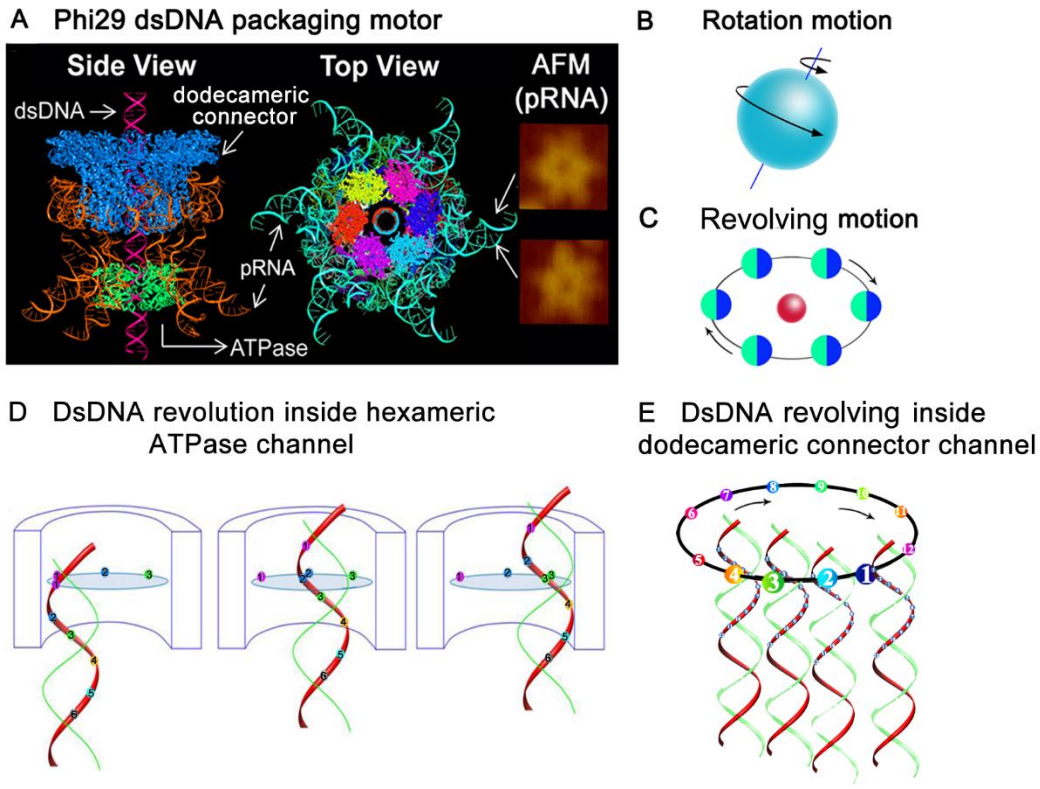

Figure 2.1. Illustration of rotation motions and revolving motions using Phi29 revolving motor as an example. (A) 3D structure of Phi29 dsDNA packaging motor in a side view and top view with a pRNA hexamer derived from the crystal structure (56), and the AFM (Atomic Force Microscopy) images of the pRNA hexamer with extended loops. **(B)** Illustration of rotation motors like the Earth *rotates* around its own axis. **(C)** Illustration of revolving motors like the Earth *revolves* around the Sun without rotation. **(D)** Illustration of the dsDNA revolving inside the hexameric ATPase channel. Only three of the six steps are shown. **(E)** Illustration of the dsDNA revolving inside the dodecameric connector channel, only four of the twelve steps are shown. Neither the channel nor the dsDNA needs to rotate during the revolving through channels.

Phi29 and compare its structure and mechanism to that of DNA packaging motors of SPP1, P22, T7, HK97, mimivirus, and vaccinia virus, as well as some cellular proteins such as FtsK and SpoIIIE. We also provide a simple way to distinguish between revolving and rotation motors by channel size and chirality.

MATERIALS AND METHODS

Incorporation of the connector channel into a planar bilayer lipid membrane

The method of inserting the connector with reconstituted liposomes into a lipid bilayer has been reported previously (139). Briefly, a Teflon film partition (aperture 200 μm in diameter) was used to separate a bilayer lipid membrane chamber (BLM) into *cis*- and *trans*- compartments. The aperture was painted two times with 0.5 uL of 3% (w/v) DPhPC n-decane solution, and the two compartments were filled with conducting buffer (1 M NaCl or 1 M KCl, 5 mM HEPES, pH 7.4). After formation of the lipid bilayer on the aperture, the lipid/connector complexes were added to the chamber and allowed to fuse with the planar lipid bilayer.

Construction of tetra-stranded DNA

Five strands were custom ordered from IDT, with the following sequences: Strand-1: 5'-CGC AGA CAT CCT GCC GTA GCC TGA GGC ACA CG-3'; Strand-2: 5'-CGT GTG CCT CAC CGA CCA ATG C-3'; Strand-3: 5'-GCA TTG GTC GGA CTG AAC AGG ACT ACG CTG GC-3'; Strand-4: 5'-GCC AGC GTA GTG GAT GTC TGC G-3'; Strand-5: 5'-TC AGT GGC TAC GGC ACC GT-3'. The five strands were annealed in stoichiometric ratio in TMS (Tris-magnesium saline) buffer (50 mM Tris-HCl, pH8.0, 100 mM NaCl and 10 mM $MgCl_2$) and purified in 12% (w/v) native PAGE, following reported procedures (140).

Single channel conduction assays for each membrane inserted connector channels

A pair of Ag/AgCl electrodes was connected directly into the *cis*- and *trans*- compartments to measure the current traces across the lipid bilayer membrane. The current trace was recorded using an Axopatch 200B patch clamp amplifier coupled with the Axon DigiData 1322A analog-digital converter (Axon Instruments) or the BLM workstation (Warner Instruments). All voltages reported were those of the *trans*- compartment. Data was low band-pass filtered at a frequency of 1 kHz, and acquired at a sampling frequency of 10-100 kHz. The Patch clamp 9.1 software (Axon Instruments) was used to collect the data, and the software Origin Pro 8.0 was used to analyze all the data.

Direct observation of DNA translocation

The stalled packaging intermediates containing biotinylated DNA were prepared by using non-hydrolyzable γ-S-ATP (88). The intermediates were then immobilized to perfusion chambers built from glass slides and coverslips. The 0.53 mm fluorescent streptavidin microspheres (Bangs Laboratories Inc.) were bound to the protruding, biotinylated DNA end of the intermediates. After restarting the packaging reaction by adding gp16 and ATP (88), an individual DNA-packaging event was observed. Epi-illumination was used. Sequential images with 8-bit digital resolution were recorded at 1 frame per second for 600 s. The pixel resolution of the images was 0.26 mm/pixel.

RESULTS AND DISCUSSION

Revolving and rotation motors can be distinguished by motor channel size

Previous observations that only one subunit of the hexamer binds to dsDNA at a time (33,100), as well as the cooperativity and sequential action among hexameric ATPase subunits (100), confirmed the revolving of dsDNA along the channel (33). In this revolving process, dsDNA

advances by sliding along the channel wall instead of proceeding through the center of the channel. Thus, the channel would be expected to be wider than the diameter of the dsDNA to ensure sufficient space for revolving. Inspection of the motor channel size in available crystal structures and cryo-EM data confirmed this expectation; while the width of dsDNA is 2 nm, the diameters of the narrowest region of the connector channels of Phi29 (6), SPP1 (21), HK97, the ATPase ring of T4 (141), as well as the dsDNA translocase FtsK (134) of bacteria, are all larger than 3 nm (**Fig. 2.2**).

On the other hand, the channels of rotation motors, such as replicative DNA helicases TrwB, E1, and DnaB (142-144), are smaller than 2 nm in diameter (**Fig. 2.2**). For rotation motors, the channel would thus be expected to have a similar width as the ssDNA to allow for the bolt and nut threading mechanism. Nonetheless, during some processes for certain rotation motors, only one strand enters the channel while the other remains outside (97,138,142-146). In these situations, local unwinding fluctuations of the dsDNA might cause separation of the two strands and facilitate the threading of the ssDNA strand into the center of the hexameric ring, as suggested by smFRET experiments (147-149). It has been reported that the ssDNA within the channel displays an A form helical structure (144), thus the channel diameter should be no larger than 2 nm to allow for contact between the DNA and the channel. The situation for branch migration is more complicated and beyond the scope of this manuscript. Overall, the above data indicates that the revolving motor can be distinguished from the rotation motor by the size of the motor channel.

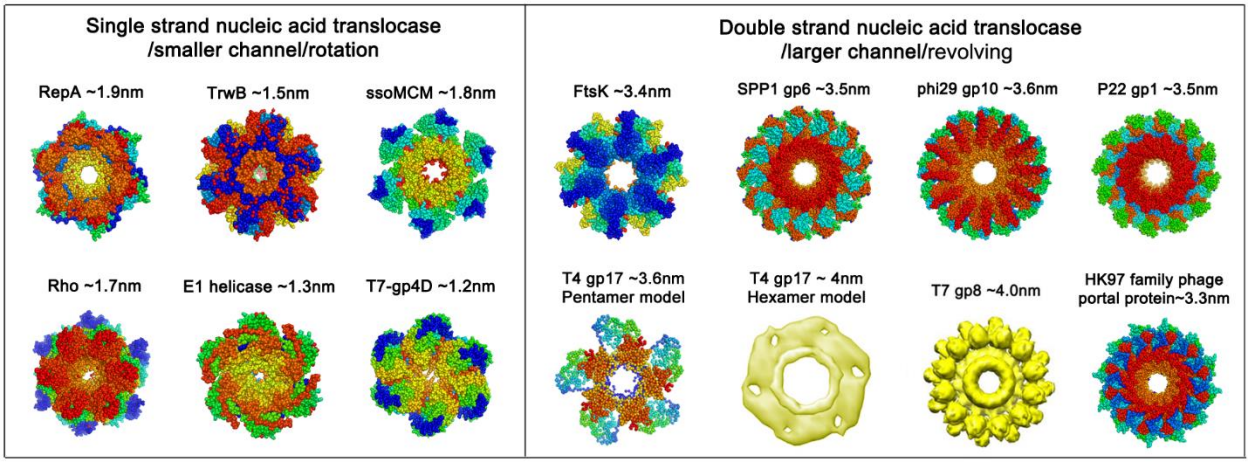

Figure 2.2. Comparison of the channel sizes between rotation (left panel) and revolving (right panel) biomotors. The motor channel of dsDNA phages shown in the right panel all have a channel size twice the width of dsDNA, make it impossible for a bolt and nut treading mechanism to work, thus supporting revolving rather than rotation mechanism. (PDB: RepA, 1G8Y; TrwB: 1E9R; ssoMCM, 2VL6; Rho, 3ICE; E1, 2GXA; T7-gp4D, 1E0J; FtsK, 2IUU; Phi29-gp10, 1H5W; HK97 family-portal protein, 3KDR; SPP1-gp6, 2JES; P22-gp1, 3LJ5; T4-gp17, 3EZK). The pentamer and hexamer models of T4 ATPase gp17 display a channel of 3.6 and 4.0 nm, respectively (141).

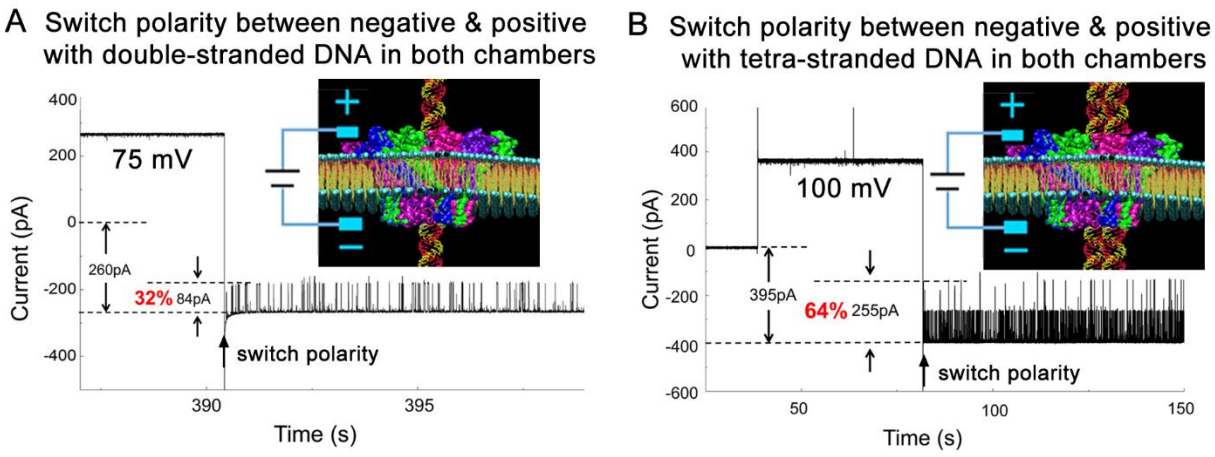

Figure 2.3. Nanopore conductance assay demonstrating large channel size. Current blockage of the channel by double-stranded was 32% **(A)** and by tetra-stranded DNA was 64% **(B)**, indicating that the size of the channel pore is large enough for the translocation of tetra-strand DNA. Switch of voltage polarity revealed that the channel allowed only unidirectional translocation of both dsDNA (A) and tetra-stranded DNA (B).

Conductance assay of single connector channels for translocation of tetra-stranded DNA reveals a three-fold width of Phi29 channels compared to dsDNA.

The channel size was further assessed by single-channel conductance assays using Phi29 connector channels as a model system. A current blockage of 32% was observed for translocation of dsDNA through the connector channel (**Fig. 2.3A**), consistent with the ratio of the cross-sectional areas of dsDNA ($(2/2)^2 \times 3.14 = 3.14$ nm^2) and channel ($(3.6/2)^2 \times 3.14 = 10.2$ nm^2, 10.2 nm^2 ÷ 3.14 nm^2 = 32%). For tetra-stranded DNA, which was constructed by DNA nanotechnology (150), when passing through the connector channel, a blockage of ~64% was observed (**Fig. 2.3B**). Thus, the cross-sectional area at the narrowest region of the Phi29 connector funnel is three-fold the area of the dsDNA. Such a big channel size makes it impossible for a bolt and nut tracing mechanism, and makes it likely that only one ATPase subunit at a time can bind to dsDNA (33,100).

Both dsDNA and tetra-stranded DNA show one-way translocation through the Phi29 motor channel, since the switch of the electrical polarity changed the dsDNA from passable to impassable or vice versa through the channel (**Fig. 2.3**). One-way traffic of tetra-stranded DNA reveals that the channel does not merely serve as a pathway, it plays an active role by forming contacts with translocating double- and tetra-stranded DNA.

The left-handed chirality of revolving motors is distinct from the right-handed chirality of rotation motors

From mechanistic and physical standpoints, revolving motors depend upon a left-handed channel while rotation motors require a right-handed channel, to match the right-handed orientation seen in both B-type DNA and A-type DNA helices. Recently, it has been reported that

the anti-chiral arrangement between the Phi29 channel and the dsDNA helices facilitates the revolving of the dsDNA for uni-directional translocation during packaging (32,33). Analysis of the crystal structures of the motor channel of SPP1 (21), T7 (151), HK97, P22 (125), and Phi29 (27) revealed that all of these motor channels display the anti-chiral arrangement between the channel and the DNA helices. The helical domains of the 12 protein subunits aligned to form the connector channels in all of these phages are tilted at 30º left-handed relative to the vertical axis of the channel, resulting in a configuration that runs anti-chiral to the right-handed dsDNA helices during packaging (**Fig. 4, 5A**). This structural arrangement greatly facilitates the controlled motion, supporting the conclusion that dsDNA revolves, instead of rotating, through the connector channel without producing coiling or torsional forces while touching each of the 12 connector subunits in 12 discrete steps of 30º transitions for each contact (33).

Sequence alignments do not show apparent homology among the portal proteins of SPP1, T7, and HK97 family phages. Protein sizes also vary among different bacteriophages, ranging from 36 kDa (Phi29 gp10), 57 kDa (SPP1 gp6), 59 kDa (T7 gp8), to 94 kDa (P22 gp1) (124,151). However, these portal proteins assemble into a propeller-like structure composed of 12 subunits with a central channel that acts as a valve for DNA translocation, and they all share very similar three-dimensional structures with several conserved regions that serve a common function in DNA packaging. Secondary structure prediction was carried out in search of structural similarities. The predicted secondary structures matched almost perfectly with the known 3D arrangements, confirming the validity of the results. Among almost all of the portal proteins, a very similar pattern of strands and helices with comparable spacing and length (**Fig. 4A**) was found, particularly a sequence of α-β-α-β-β-α stretch. Detailed analysis of quaternary structures has revealed that the 30º tilted helix exists in all portal proteins of P22, SPP1, Phi29, T7, and HK97 family phages (**Fig.**

4B). Further mapping studies have revealed that the position of the 30º tilt in the quaternary structure is located at the same conserved sequence at the last alpha helix of the α-β-α-β-β-α stretch (**Fig. 4A**), indicating that this 30º anti-chiral arrangement plays a critical role in dsDNA packaging as it has been conserved by evolution.

As aforementioned, the rotation motors should have a right-handed channel to ensure parallel threading to the right-handed DNA. Indeed, crystal structure studies of helicase-DNA complexes have verified the right-handed spiral configuration of the hexameric protein-DNA complex (**Fig. 5**) (144,152,153). In some cases, the motor channel adopts right-handed chirality only when the ring is distorted while in complex with DNA, such as RecA filament (152) and DnaB, which functions in a nonplanar hexameric conformation during their movement relative to DNA (144,153), otherwise, it remains as a closed symmetrical ring as observed in the absence of DNA (154). E1 helicase also adopts a right handed staircase pattern in the conformation of side chains when bound with DNA (155). All of these crystallographic studies suggest that these right-handed complexes use the rotation mechanism (or a mechanism similar to a rotation mechanism for RecA, where its monomers assemble on one end of the filament and disassemble on the other). It is also possible that the gp16 ATPase in the Phi29 dsDNA packaging motor also adopts a nonplanar filament assembled from continuously spiral hexamers (or assembled from dimers) rather than a planar closed ring during the DNA packaging.

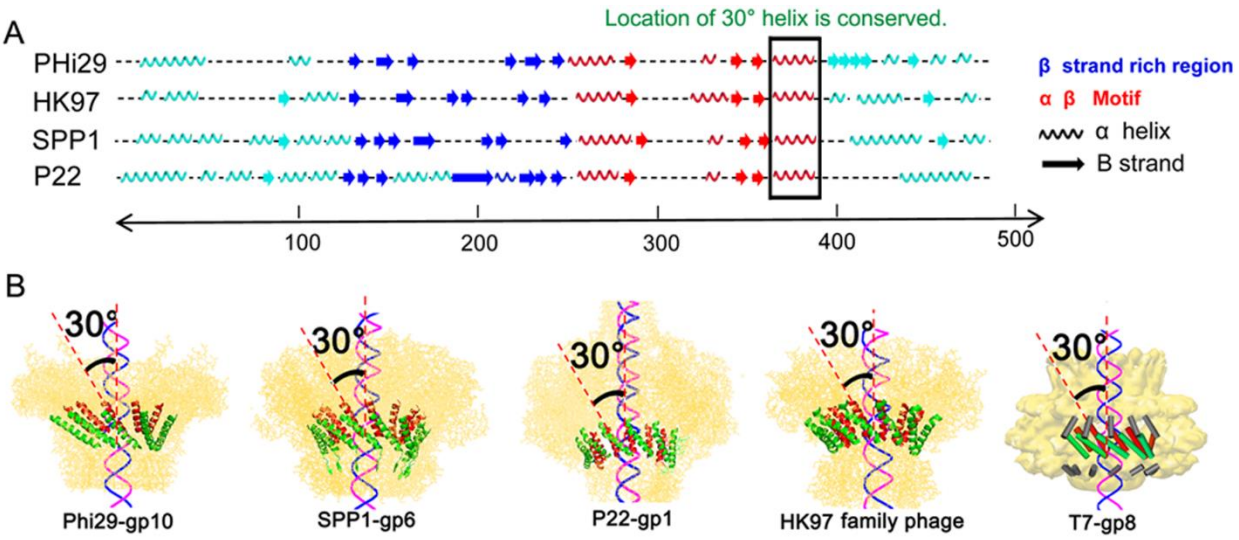

Figure 2.4. Different bacteriophages showed a left-handed channel wall with a 30º tilt. (A) The 3D structure of Phi29 (P04332), HK97 (Q6NFR1), SPP1 (P54309), P22 (P26744) were predicted using the program PredictProtein with default parameter (www.predictprotein.org), revealing the 30º left-handed regions correlated well with their respected crystal structures (PDB:Phi29-gp10, 1H5W; HK97 family-portal protein, 3KDR; SPP1-gp6, 2JES; P22-gp1, 3LJ5). The location of the 30º left-handed tilted helix in each bacteriophage connector protein subunit is framed, which all lay at the end of the α β motif. **(B)** The 30º tilt helix (red) is also shown in an external view in connector 3D structures of different bacteriophages, supporting the common mechanism that DNA revolves through the 30º tilted channel by an anti-chiral arrangement in dsDNA translocation.

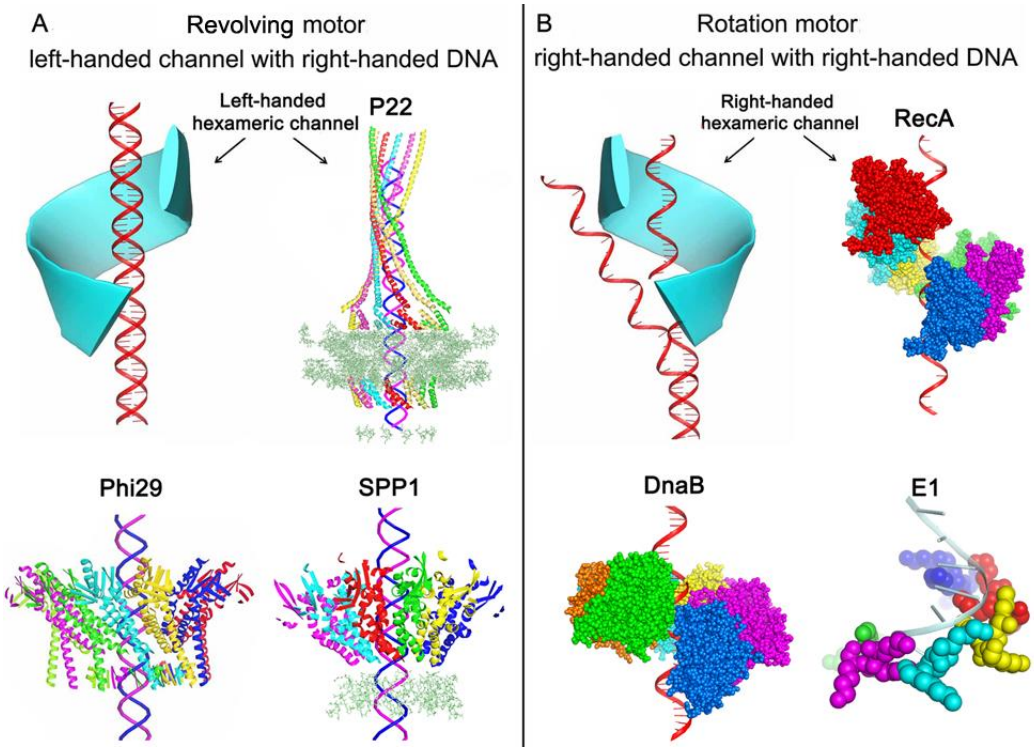

Figure 2.5. Chirality comparison of revolving and rotation motors. (A) In revolving motors, the right-handed DNA revolves within a left-handed channel, such as in the connector channels of bacteriophage Phi29 (27), P22 (125), and SPP1 (21). **(B)** In rotation motors, the right-handed DNA rotates through a right-handed channel *via* the parallel thread, with RecA (152), DnaB (144) and E1 helicase (155) shown as examples. For E1 helicase, only the inside right-handed hairpin staircases that traces along the ssDNA are shown.

Common force generation mechanism of dsDNA translocation motors in bacteria, eukaryotic and prokaryotic viruses

The recently discovered revolving motors use a hexameric ATPase to drive the advance of dsDNA in a sequential manner. Cellular dsDNA translocases also assemble into hexameric structures (96,97,156). The cellular components that show the strongest similarity to phage revolving motors are found in the bacteria FtsK and SpoIIIE family of the ASCE DNA motor group (129-131,137). Available evidences (131,134) lead to our hypothesis that these motors also use a revolving mechanism to translocate dsDNA without rotation. Indeed, translocation of dsDNA by FtsK at a rate of 1.6-1.75 base per ATP (131,134) quantitatively agrees with the Phi29 DNA packaging motor in which each ATPase subunit uses one ATP to package 1.75 nucleotide (6,32,33,83,102). Sequence studies of motor components of large eukaryotic dsDNA viruses, such as *Acanthamoeba poylphaga mimivirus* (APMV), and vaccinia viruses revealed that these viruses contain a dsDNA translocation motor that is similar to that of the FtsK-HerA superfamily (95,137,157,158), suggesting that these virus also use the revolving mechanism for dsDNA packaging. Computation studies provide strong evidence that Phi29 DNA packaging motor ATPase gp16, FtsK, and the mimivirus motor ATPase all fall into the FtsK-HerA superfamily with a configuration of a hexameric motor ring (95,137,157).

As shown in this report, quaternary structure analysis revealed that a left-handed, 30º tilted helix arrangement exists in the channel wall of dsDNA bacteriophages P22, SPP1, Phi29, T7, and HK97. During revolving of dsDNA through the channel, it advances by touching the side of the channel wall instead of proceeding through the center of the channel (33,159). As a result, the 30º left-handed direction for each transition between two connector subunits and the 30º alteration for dsDNA to advance 1/12 of helical pitch neutrally resulting in a zero gain, that is, no rotation occurs

for the dsDNA during the translocation. The proposed model of 60º per step of the FtsK hexamer (360º ÷ 6 = 60º) (131) agrees with the finding of 30º per step within the dodecamer connector channel (360º ÷ 12 = 30º) of all dsDNA bacteriophages and 60º per steps within the Phi29 hexameric ATPase gp16 (32,33,83,102).

Channel size and chirality are key factors in the identification of translocation motor types which can reveal the motor mechanism. The channel size is a physical confinement that can be used to distinguish revolving motors from rotation motors. As shown in this report, examination of the motor structures from X-ray crystallography reveals that revolving motor channels are larger than rotation motor channels. The finding that heteroduplex loop structures up to 19 bases can translocate through the phage lambda portal with the same efficiency as genome packaging (160) is another indication that the channel of lambda is wider than the dsDNA as well.

Revolving motors make contact with only one strand of the dsDNA in the 5' to 3' direction in order to revolve along the connector channel, which has been evidenced in various motors such as Phi29 (15,161) and T4 (19). The model that dsDNA interacts with the internal surface of the hexameric ring (131) is in agreement with the observation in FtsK that only one strand of the dsDNA touches the internal wall of the motor channel (32,33).

Besides, further analysis of the crystal structures of phage connectors among SPP1, P22, and Phi29 (27,162) revealed four potential-relaying electropositive lysine residues lying on the predominantly negatively charged connector channel surface. Although these four positively charged layers are nonessential for motor DNA packaging activity (11,31), they are reported to influence DNA translocation (31,163). Investigations into the detailed interaction of lysine residues with the bacteriophage genome during translocation revealed that the force generation mechanism of the relaying layers inside the channel wall altered the speed of DNA translocation

resulting in four pauses (32,102). The interaction between these positively charge lysine rings and the negatively charged phosphate backbone of the DNA suggests that the viral DNA packaging motor involves an electrostatic force in DNA translocation.

Furthermore, it has been reported that the dsDNA spooling in the filled capsid is a common phenomenon in all the T7, Phi29, ε15, P22, and λ phages (164-167). The revolving mechanism explains this spooling phenomenon. During packaging of DNA (32,33), dsDNA will spool within the procapsid naturally as a result of the revolving process. Since rotation is not involved, no coiling is generated and no free DNA terminus is required during spooling. Initially, extra room results in a random arrangement of the entering DNA, however, towards completion of packaging it spools tighter and tighter due to revolving, which results in a more ordered orientation of the dsDNA (164-167). In addition, the reported revolving mechanism of phage DNA packaging motors is also consistent with recent Cryo-EM imaging studies showing that the T7 dsDNA core tilts from its central axis (159).

DNA twists rather than rotates due to motor channel conformational changes during DNA translocation

Many connector channels of dsDNA bacteriophages (**Fig. 2.4**) adopt a left-handed channel wall to facilitate one-way traffic during dsDNA packaging into pre-assembled protein shells (29,32). The conformational changes of the channel have been reported associated with this packaging process (30,38). Such conformational changes allow conversion of the left-handed connector after completion of DNA packaging towards the opposite configuration, thus facilitating DNA one-way ejection into host cells for infection. Indeed, three steps of conformational changes of the Phi29 connector (**Fig. 2.6A**) (30), as well as discovered in the DNA packaging motor of SPP1 (Wang and Guo, unpublished data). Noticeable conformational differences between isolated

Phi29 connectors and connectors in virions confirm such a structural transition after DNA packaging (38). In the Phi29 crystal structure, the connector subunit displays a left-handed 30º tilt (**Fig. 2.4**). However, when treated as a rigid body, the crystal structure clearly does not fit into the Cryo-EM density maps, indicated by a correlation coefficient as low as 0.55. After manual adjustments, the correlation coefficient was improved to 0.70, resulting in a 10° twist of the connector towards the connector axis (38). On the other hand, the N-terminal external region is difficult to adjust to fit as a rigid body into other parts of the connector density. It was found that the N-terminal external region underwent significant conformational shift in the DNA-filled capsid (38). It was concluded that angular twisting and restructuring of the connector core subunit are promoted by the interactions among Phi29 DNA and its structural proteins (38). Due to the dsDNA alignment with the channel wall (32,33,83,102,103) and the relatively static C-terminal internal region, a significant conformational shift in the N-terminal external region then results in a clockwise twist of the dsDNA when viewed from the C-terminus (**Fig. 2.6**).

Recently, it has been reported that a small angular twist of 1.5 degree per nucleotide was observed during dsDNA packaging in Phi29 (168). Observation of such a small angular deviation per nucleotide can be explained by these conformational changes of the connector (**Fig. 2.6**). As evidenced above (38), if the N-terminal external region is shifted more significantly than the internal C-terminal region, a leftward twist of the DNA will occur during revolving along the connector channel (**Fig. 2.6B**). This is in agreement with the observed clockwise twist of 1.5 degree per nucleotide relative to the C-terminus of the connector (168).

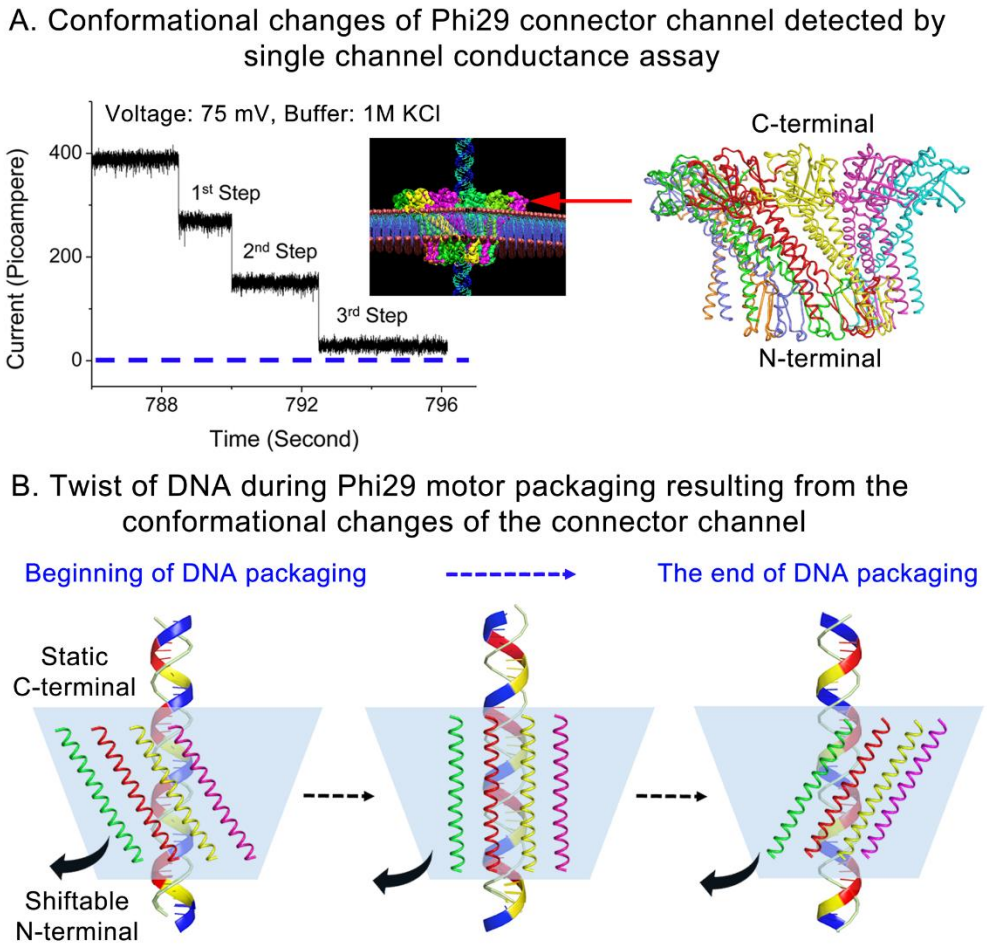

Figure 2.6. Illustration of dsDNA twisting during translocation due to channel conformational changes. (A) Discrete three step-wise conformational changes of Phi29 connector channel were detected by single channel conductance assay with the connector embedded in lipid bilayer. The external view of the crystal structure of the connector channel is shown on the right. **(B)** The C-terminal of the connector inside the procapsid is more static than the external N-terminal. As a result, the N-terminal of the connector may shift leftwards during the DNA packaging, leading to the clockwise twist of the DNA that aligns within the connector channel wall.

The reported twist of 1.5 degree per nucleotide or 15.75º per helical pitch of 10.5 bp during dsDNA packaging cannot be taken as the rotation mechanism in which 360º per pitch or ~34º per base pair are required. Furthermore, the reported increase in the frequency of DNA twisting per nucleotide with increase in capsid filling, is in agreement with the observation that the conformational change of the channel accelerates towards the end of the packaging process (30). This is logical since the dsDNA is aligned with the wall of the connector channel, and when DNA packaging is close to completion, a final conformation will be adopted and a more obvious twisting will be observed to prepare the channel for DNA ejection toward host infection.

Single-molecule real-time imaging and force spectroscopy revealed that no rotation occurs during DNA translocation

In order to validate the model of revolving without the need for rotation, several single-molecule imaging experiments were carried out (**Fig. 2.7, 2.8**). A micrometer-sized fluorescence bead was attached to the distal end of the Phi29 genomic dsDNA. DNA translocation was directly observed in real-time by single-molecule imaging microscopy to detect fluorescence images revealing the displacement of the bead (53,128). No rotation was found in these traces (**Fig. 2.7**). To exclude the possibility that the lack of rotation is a result of bond freedom between the beads and DNA or due to the difficulty in optical discrimination due to the spherical nature of the beads, a cluster of magnetic beads was attached to the end of the Phi29 DNA to generate a label with an asymmetric shape (**Fig. 2.7B**) (128). Experiments using different setups for DNA packaging in a vertical (**Fig. 2.7A**) and horizontal orientation (**Fig.** 2.7B) (128) have been repeated many times and no rotation of DNA was observed. Polarization studies have been used to study biomotors such as T4 helicase (147). The polarization analysis of Phi29 DNA packaging motor did not find a rotation phenomenon either (**Fig.** 2.8).

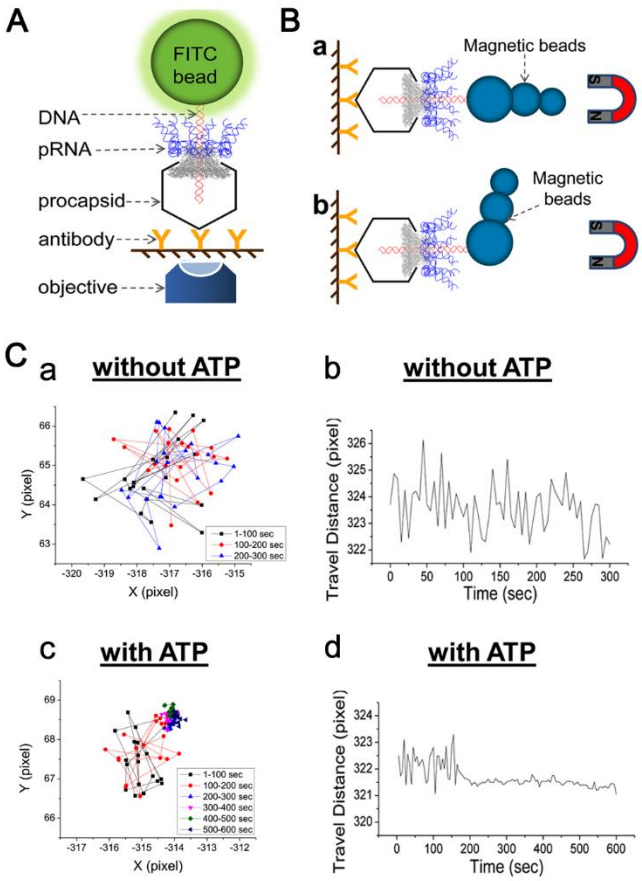

Figure 2.7. Demonstration of no DNA rotation by real-time direct observation of single motor DNA packaging. Procapsid was immobilized in glass and the distal end of dsDNA was tethered to a bead. DNA is packaged vertically **(A)** or horizontally **(B)** towards the slide surface (graphic is not drawn to scale). **(C)** The motion of the bead is tracked during DNA packaging without (a and b) and with (c and d) the addition of ATP to the sample. The motion of the bead ceased at later times only when ATP was added (c) and (d) due to the physical restriction of DNA being completely packaged. (a) and (c) show the trajectories of the bead. Different colors represent different time ranges during the translocation. (b) and (d) show the changes in beads travel distance versus time.

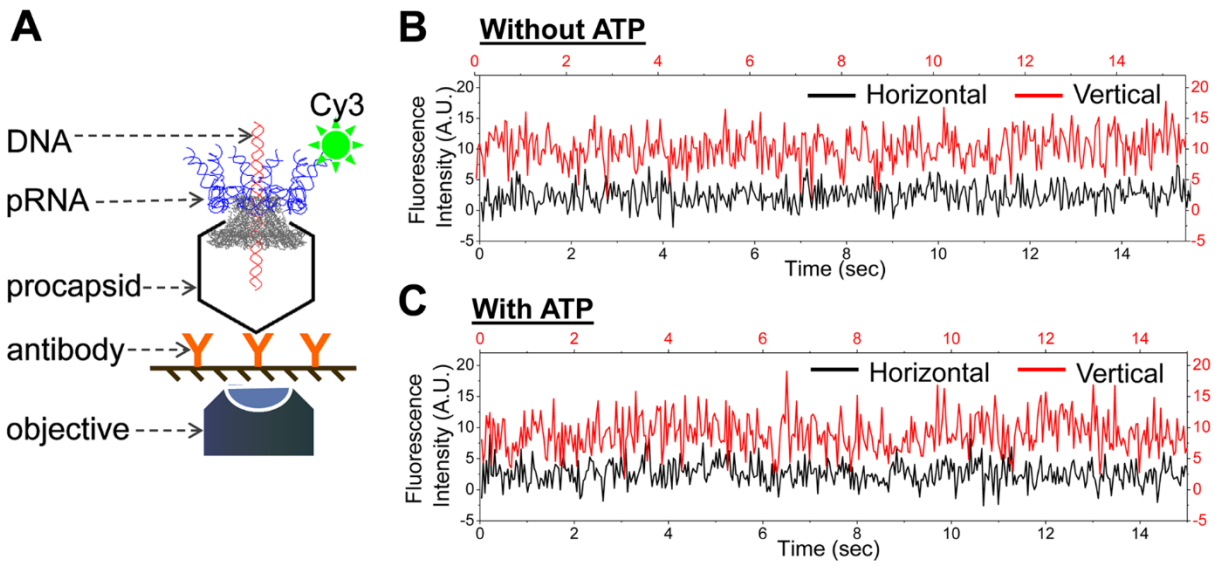

Figure 2.8. Single molecule polarization detection to investigate motor rotation. (A) Experiment design of single molecule polarization detection on motor pRNA rotation during DNA packaging. The motor was stalled by γ-S-ATP and the rotation of pRNA ring can be excluded since no anti-correlated signals of a single Cy3 fluorophore in horizontal (H) or vertical (V) channels were observed. **(B and C)** Typical time trajectories of Cy3 fluorescence intensity in horizontal (black) and vertical (red) channels (B) without and (C) with the addition of ATP to restart the packaging.

The mechanism where no DNA rotation is required during packaging is further supported by the observation that in bacteriophage T4, both DNA ends are tethered to the portal throughout DNA packaging once the packaged DNA persistence length of about 500 bp is reached, suggesting that no rotation is needed and DNA does not get tangled up (19,169). All these observations support a revolving mechanism for phage DNA packaging without the need for rotation.

CONCLUSIONS

The revolving mechanism is a common feature shared by many DNA translocation motors. Inspections of structural data from eukaryotic and prokaryotic dsDNA translocases suggest that revolving and rotation motors can be distinguished by measuring the size and chirality of the DNA translocation channel. The channel of revolving motors are larger than 3 nm, while the channels of rotation motors are smaller than 2 nm in diameter. Revolving motors use a left-handed channel to drive the right-handed dsDNA in an anti-chiral arrangement, while some rotation motors use parallel threads with a right-handed channel. Revolving motors hold both strands of the dsDNA within the channel, while some rotation motor hold only one strand of the DNA inside the channel (97,138,142,144-146). Such revolving motors are void of dsDNA coiling (33,102,138). A small-angle left-handed twist of dsDNA, which is aligned with the channel, takes place due to the conformational shifts of the motor channel from a left-handed configuration for DNA entry to a right-handed configuration for DNA ejection for host cell infection, however, no dsDNA rotation is required for DNA packaging.

ACKNOWLEDGEMENTS

We would like to thank Dr. Guo-Min Li for his valuable comments. The work was supported by NIH grants R01 EB012135. The content is solely the responsibility of the authors and does not necessarily represent the official views of NIH. Funding to Peixuan Guo's Endowed Chair in

Nanobiotechnology position is from the William Fairish Endowment Fund. PG is a cofounder of Kylin Therapeutics, Inc., and Biomotor and RNA Nanotech Development Co. Ltd.

Chapter 3: One-Way Traffic of Viral DNA Packaging Motor

This chapter was reproduced (with some modifications) with permission from Z. Zhao, E. F. Khisamutdinov, C. Schwartz and P. Guo. “Mechanism of one-way traffic of hexameric phi29 DNA packaging motor with four electropositive relaying layers facilitating antiparallel revolving”. ACS Nano. 7:4082-4092 (May 2013).

Mechanism of One-Way Traffic of Hexameric Phi29 DNA Packaging Motor with Four Electropositive Relaying Layers Facilitating Anti-Parallel Revolving

Zhengyi Zhao[†], *Emil Khisamutdinov*[†], *Chad Schwartz*[†] *and Peixuan Guo**

Nanobiotechnology Center, Markey Cancer Center, and Department of Pharmaceutical Sciences, College of Pharmacy, University of Kentucky, Lexington, KY, 40536, USA

[†] Contribute Equally

ABSTRACT

The importance of nanomotors in nanotechnology is akin to that of mechanical engines to daily life. The AAA+ superfamily is a class of nanomotors performing various functions. Their hexagonal arrangement facilitates bottom-up assembly for stable structures. Bacteriophage phi29 DNA-translocation motor contains three co-axial rings: a dodecamer channel, a hexameric ATPase ring, and a hexameric pRNA ring. Viral DNA-packaging motor has been believed to be a rotational machine. However, we discovered a revolving mechanism without rotation. By analogy, the earth revolves around the sun while rotating on its own axis. One-way traffic of dsDNA translocation is facilitated by five factors: 1) ATPase changes its conformation to revolve dsDNA within hexameric channel in one direction; 2) the 30° tilt of the channel subunits causes an anti-parallel arrangement between two helices of dsDNA and channel wall to advance one-way translocation; 3) unidirectional flow property of the internal channel loops serves as a ratchet valve to prevent reversal; 4) 5'-3' single-direction movement of one DNA strand along the channel wall ensures single direction; and 5) four electropositive layers interact with one strand of the electronegative dsDNA phosphate backbone, resulting in four relaying transitional pauses during translocation. The discovery of a riding system along one strand provides a motion nano-system for cargo transportation and a tool for studying force generation without coiling, friction, and torque. The revolving of dsDNA among 12 subunits offers a series of recognition sites on DNA backbone to provide additional spatial variables for nucleotides discrimination for sensing applications.

INTRODUCTION

Biological nanomotors are ubiquitous. The AAA+ (ATPases Associated with diverse cellular Activities) superfamily of proteins is a class of biological nanomotors with a wide range of functions, including DNA translocation, tracking, and riding.(95,170-176) These motors show great potential for use in nanotechnological applications and have proven to be as important to nanotechnology as mechanical motors are to daily life. Most members of this family fold into hexameric arrangements;(170,171,173,174,176-179) since all angles are factors of 360^{o}, this hexagonal structure with an interior angle of 120^{o} and external angle of 60^{o} could facilitate bottom-up assembly or simple fabrication to produce a stable structure or arrays. Despite their functional diversity, the common characteristic of these motors is their ability to convert chemical energy obtained from the hydrolysis of the γ-phosphate bond of ATP into a mechanical force and physical motion; a process usually involving a shift in entropy and a change in conformation of the motor building block. This change of conformation generates a gain or loss of affinity for its substrate, leading to mechanical movement by breaking contacts between macromolecules; assembly or disassembly of the complex; induction of substrate unfolding; and promotion of translocation of DNA, RNA, proteins, or other macromolecules. In a cellular environment, these activities underlie processes critical to DNA repair, replication, recombination, chromosome segregation, DNA/RNA transportation, and many others.(2,3)

In both prokaryotic and eukaryotic cells, DNA needs to be transported from one cellular compartment to another. During replication, dsDNA viruses translocate their genomic DNA into preformed protein shells, termed procapsids (for review, see (10-12,180)). This entropically unfavourable process is accomplished by a nanomotor that uses ATP as an energy source.(6,17,120,181) The dsDNA translocation motor consists of a protein channel and two

molecules that carry out its activities:(7,49,53) an ATPase (6,8,9,22,182-185) and, in the phi29 bacteriophage, a hexameric RNA ring. Our discovery 25 years ago proved that the larger molecule serves as part of the ATPase complex used in energy production, and the smaller one is responsible for binding to the dsDNA substrate.(6,49) This notion has now become well-established.(10-12,180) The connector contains a central channel encircled by 12 copies of the protein gp10 that serve as a pathway for dsDNA translocation.(27,186) This dodecameric connector protein has shown great potential in nanotechnology and nanomedicine applications because of its ability to form peptide-mediated,(187,188) as well as nucleotide-mediated,(107) self-assembled nanoparticles. Also advantageous is the realization that it can be constructed into multilayers (189,190) and single layer patterned arrays,(106) and it has a high sensitivity for real time sensing of nucleotides and single chemicals.(139,191)

In 1978, an attractive model with five-fold/six-fold rotation mechanism for bacteriophage dsDNA packaging was proposed.(16) Since then, it has been popularly believed that viral DNA translocation motors are rotating machines.(16,27,112) Many other intriguing translocation models have subsequently been proposed for the motor of dsDNA viruses.(12-15,192) The most well-studied system is the bacteriophage phi29 DNA translocation motor, constructed in 1986.(5) In 1987, an RNA component was discovered on the translocation motor,(7) and subsequently, in 1998, this RNA particle was determined to exist as a hexameric ring (49,50) (featured by *Cell* (51)). Based on this structure, it was proposed that the mechanism of phi29 viral DNA translocation is similar to that used by other hexameric DNA tracking motors of the AAA+ family.(49) This notion has induced fervent debates concerning whether the motor is a hexamer or a pentamer.

In a rotational model, at least one of the three coaxial rings in the translocation motor, or the dsDNA itself, should rotate during dsDNA translocation. Several published data has confirmed that none of the motor components, including the connector, the dsDNA, and the ATPase gp16, rotate during DNA translocation.(53,126-128) For example, studies combining the methods of single-molecule force spectroscopy with polarization-sensitive single-molecule fluorescence optical trapping(127) proved that the connector does not rotate. This was further supported by an experiment in which the connector was covalently linked to the capsid protein of a procapsid, making rotation of the connector within the procapsid impossible.(126,127,193) When the connector and the procapsid were fused to each other, rotation of the connector within the procapsid was not possible. However, the motors were still active in translocating dsDNA and producing active viruses, implying that connector rotation is not necessary for DNA translocation. Our single molecule studies using beads tethered to the end of dsDNA has revealed that dsDNA was still packaged into the procapsid even with such tethering.(53,128) The results raised a question regarding the operation of the phi29 DNA translocation motor, since it does not follow the rotational mechanism. Thus, this seemingly simple rotary machine was still a mystery. Although the application of this motor in nanotechnology has been attempted,(106,107,139,187-191) demonstration of its potential has been diminished by opposing literature regarding the motor mechanism. Elucidation of its operating mechanism is essential for the field of nanobiotechnology.

Recently, we discovered a novel mechanism for the viral DNA translocation motor: the motor uses a revolving mechanism without involving the rotation of any of the motor components or coiling of dsDNA.(194) The motor contains six copies of ATPase gp16.(195) During DNA translocation, dsDNA revolves unidirectionally along the dodecameric channel wall. ATP binding to one ATPase subunit stimulates the ATPase to adapt a conformation with a high affinity to bind

dsDNA. ATP hydrolysis induces a new conformation with a lower affinity for dsDNA, thus pushing dsDNA away and transferring it to an adjacent subunit by a power stroke. One ATP is hydrolyzed in each one of the six transitional steps, and six ATPs are consumed in one helical turn of 360°. As demonstrated with Hill constant determination, binomial assay, cooperativity and sequential analysis, transition of the same dsDNA chain along the channel wall, but at a location 60° different from the last contact, urges dsDNA to move forward 1.75 base pairs with each step (10.5 bp/turn ÷ 6ATP = 1.75 bp/ATP). Through evolution, nature has conceived a clever revolving machine to translocate the DNA double helix while avoiding the difficulties associated with DNA supercoiling, friction, and torque force during rotation. The revolving without rotation model could resolve a big conundrum troubling the past 35 years of painstaking investigation of the mechanism of these DNA packaging motors. With the revolving mechanism, dsDNA continues to advance without the need for rotation! The one-way traffic property of the motor has previously been reported,(29) but the mechanism has remained enigmatic. In this paper, we elucidate how the motor components coordinate to revolve the dsDNA, ensure a one-way traffic mechanism, and continuously advance dsDNA without reversing.

MATERIALS AND METHODS:

In Vitro Virion Assembly Assay

Purified *in vitro* components were mixed and subjected to the virion assembly assay, as previously described.(196) Briefly, newly assembled infectious virions were inoculated with *Bacillus* bacteria and plated. Activity was expressed as the number of plaques formed per volume of sample (pfu/ml).

Electrophoretic Mobility Shift Assay (EMSA).

The fluorescently tagged protein was shown to possess similar assembly and packaging activity as compared to wild-type.(100,197) Cy3-dsDNA (40 bp) was prepared by annealing two complementary DNA oligos containing Cy3 labels (IDT) at their 5' ends and purifying them with a 10% polyacrylamide gel. Samples were prepared in 20 μl buffer A (20 mM Tris-HCl, 50 mM NaCl, 1.5% glycerol, 0.1 mM Mg^{2+}). Samples were incubated at ambient temperature for 20 min and then loaded onto a 1% agarose gel (44.5 mM Tris, 44.5 mM boric acid) and electrophoresed at 4°C for 1 hr at 8 V/cm. The eGFP-gp16 and Cy3-DNA samples were analyzed by a fluorescent LightTools Whole Body Imager using 488 nm and 540 nm excitation wavelengths for GFP and Cy3, respectively.

Single-pore Conductance Assay for DNA Translocation.

The preparation of connector-containing liposomes, the insertion of the connector into the planar bilayer lipid membrane (BLM), and the electrophysiological measurements of DNA thought the channel have been described previously.(28,29,139) Briefly, the phi29 connector was inserted into a BLM by vesicle fusion after obtaining connector reconstituted liposomes. A BLM chamber (BCH-1A from Eastern Sci LLC), was used to form horizontal membrane, and a thin Teflon film with an aperture of 70-120 μm (TP-01 from Easter Sci LLC) or 180-250 μm (TP-02) in diameter was used as a partition to separate the chamber into cis- and trans- compartments. For connector insertions, 1-2 μL of liposome stock solution was diluted by 10-20 fold and was directly added to the cis compartment. A pair of Ag/AgCl electrodes connected directly to the head-stage of a current amplifier were used to measure the current across the BLM. The current was recorded by an Axopatch 200B patch clamp amplifier coupled with the Axon DigiData 1322A or Axon DigiData 1440 analog-digital converter (Axon Instruments). All the electrical signals were obtained from the trans-compartment. Data was low band-pass filtered at a frequency of 1 kHz

and acquired at 500 μs intervals per signal. The PClamp 9.1 software (Axon Instruments) was used to collect the data, and the software Clampfit was used for data analysis. Conductance measurements were determined using the slope of the current trace induced by a ramp voltage after a definite insertion of a gp10 connector was observed. Solution conductivity was measured using a Pinnacle 542 conductivity/pH meter (Corning Inc.).

RESULTS AND DISCUSSION:

The Unique Structure of The Three Coaxial Hexameric Rings of Phi29 Motor Ensure One-Way Traffic.

The phi29 DNA-translocation motor is composed of three coaxial rings (**Fig. 3.1**): a hexameric ATPase ring that serves as the force generating machine; a dodecameric channel that serves as a path for dsDNA;(27,29,186) and a hexameric RNA ring that connects and gears the connector and the ATPase.(56,66,197) The one-way traffic phenomenon has been verified by voltage ramping, electrode polarity switching,(29) and sedimentation force assessment.(29) However, the mechanism for controlling the one-way translocation had not been elucidated.

Most recently, we discovered that the motor uses a revolving instead of a rotation mechanism,(194) which greatly promotes our understanding of this one-way property. We found that the motor uses five different modules to control the direction of translocation: (1) the motor ATPase plays a major role in producing energy to push the dsDNA to advance toward the connector *via* dsDNA revolving within the channel;(194,195) (2) the 30° tilt and the anti-parallel arrangement between the two helixes of dsDNA and the connector channel subunit enhance the translocation of dsDNA in a single direction; (3) the unidirectional flow property of the internal channel loops serves as a ratchet valve to prevent reversal of dsDNA; (4) the 5'-3' single-direction

movement of one strand of dsDNA along the phi29 motor connector channel wall ensures a unidirectional motion; and (5) four relaying lysine layers interact with a single strand of the dsDNA phosphate backbone, resulting in four steps of transition and pausing during dsDNA translocation.

ATPase Pushes the DsDNA to Revolve in One Direction along Its Hexameric Channel.

The ATPase gp16 controls the one-way traffic by two mechanisms. The first mechanism is the "Push through a One Way Valve" mechanism,(11,29,31,100) and the second one is the revolving of dsDNA along the dodecameric channel wall.(195) The following is the force generation mechanism from the ATPase gp16. ATPase exists in a hexameric form (**Fig. 3.1B**).(195) The binding of ATP to one gp16 subunit stimulates it to adapt to a conformation with a higher affinity for dsDNA, while ATP hydrolysis forces gp16 to assume a new conformation with a lower affinity for dsDNA, thus pushing dsDNA away from one subunit and transferring it to an adjacent subunit (**Fig. 3.2**).(100,194) Such physical transition pushes the DNA through the one-way valve channel, urging the dsDNA to advance inwards to enter the procapsid, but not in reverse. This conclusion was supported by gel shift assays. In the absence of γ-S-ATP, a non-hydrolysable derivative of ATP, the binding of gp16 to DNA is weak (**Fig. 3.3**, **lane 3**). However, after the addition of γ-S-ATP the binding efficiency of gp16 to DNA increased significantly (**Fig. 3.3**, **lane 4**) since the complex is frozen by the non-hydrolysable ATP. This evidence supports the above conclusion that ATP induces a conformational change in gp16 that causes it to assume a high affinity conformation for dsDNA binding. More significantly, when ATP was added to the gp16-γ-S-ATP-dsDNA complex, rapid ATP hydrolysis was observed (100) and gp16 dissociated from the dsDNA. This indicates that after hydrolysis, gp16 undergoes a further conformational change that produces an external force against the dsDNA and pushes the substrate away from the motor complex by a power stroke. This also agrees with the result shown in **Fig. 3.3**, **lane 5**; providing

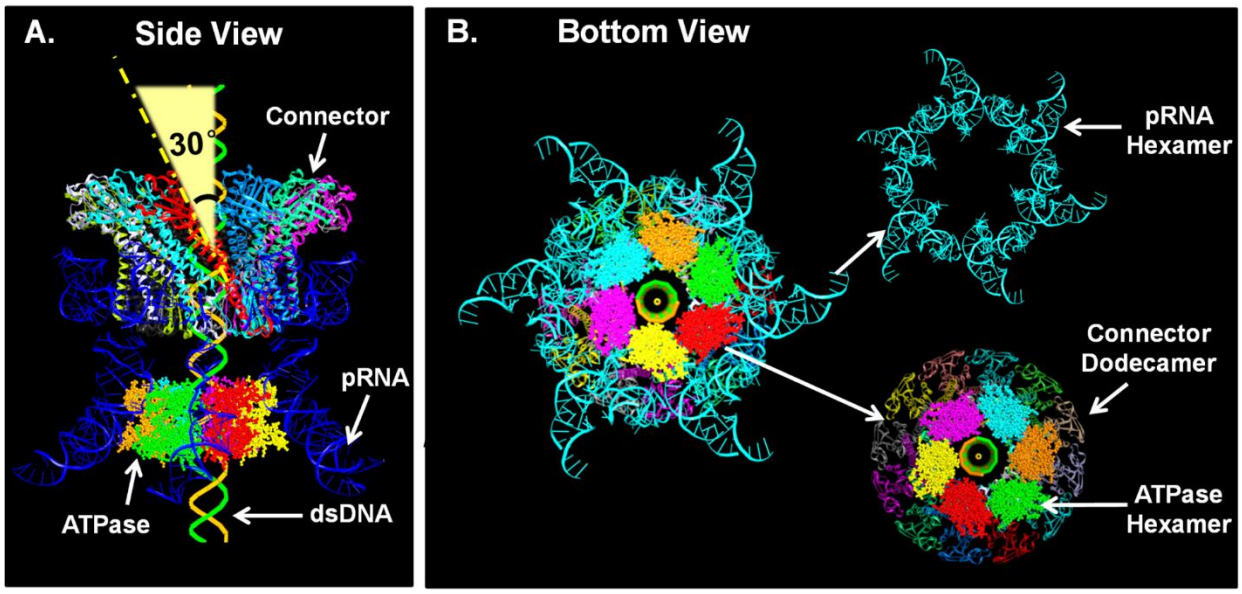

Figure 3.1. Illustration of phi29 DNA-packaging motor structure. Side view (A) and bottom view (B). The 30° tilt of the helix of the connector subunit and its anti-parallel with dsDNA helix is depicted (A). The three coaxial rings: pRNA hexamer, ATPase hexamer and connector dodecamer in the phi29 DNA packaging motor are depicted (B).

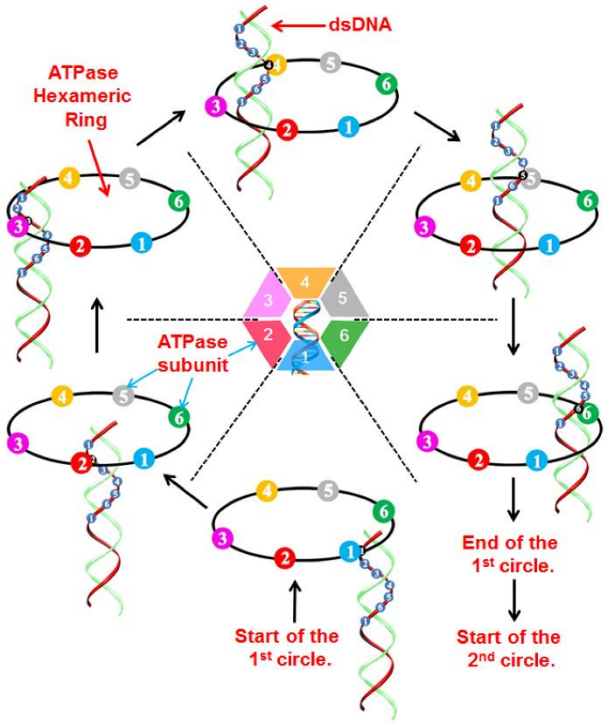

Figure 3.2. Schematic of the revolving mechanism in translocating genomic DNA. The binding of ATP to one subunit stimulates gp16 to adapt to a conformation with a higher affinity for dsDNA. ATP hydrolysis forces gp16 to assume a new conformation with a lower affinity for dsDNA, thus pushing dsDNA away from the subunit and transferring it to an adjacent subunit. Rotation of the hexameric ring or the dsDNA is not required since the dsDNA chain is transferred from one point on the phosphate backbone to another.

evidence for the existence of two ATPase conformations under different conditions with various ATP concentrations.

The second mechanism of one-way traffic control is directed *via* dsDNA revolving through the gp16 hexameric ring in one direction (**Fig. 3.2**). During DNA translocation, only one strand of the dsDNA interacts with the dodecameric channel wall, and neither the dsDNA nor the hexameric ATPase rotates (**Fig. 3.2**). One ATP is hydrolyzed in each transitional step, and six ATPs are consumed for one helical turn of 360°, or 10.5bp (base pairs). As demonstrated with Hill constant determination, binomial assay, cooperativity and sequential analysis, transition of the same dsDNA chain along the channel wall, but at a location 60° different from the last contact, urges dsDNA to revolve forward with a single orientation at 1.75 bp (10.5 bp per turn ÷ 6 ATP = 1.75 bp/ATP).(122,126)

The 30° Tilting of Channel Subunits Causes An Anti-Parallel Arrangement between Two Helices Resulting in Revolving in A Single Direction.

A cone-shaped central channel is encircled by 12 copies of the protein connector subunit gp10 and serves as a pathway for dsDNA translocation.(27,186) The wider C-terminal end, 13.6 nm in diameter, is buried inside the procapsid. The narrower N-terminal end is 3.6 nm in diameter and allows dsDNA to enter. The connector is a one-way valve that only allows dsDNA to move into the procapsid unidirectionally,(139) as verified by voltage ramping, electrode polarity switching, and sedimentation force assessment.(29) All 12 gp10 subunits are tilted at a 30° angle and encircle the channel in a configuration that runs anti-parallel to the dsDNA helix residing in the channel. The anti-parallel arrangement between the two helices of the connector subunit, and the helix of the dsDNA, can be visualized in an external view (**Fig. 3.4A**), with dsDNA potentially making contact at each connector subunit (**Fig. 3.4**).

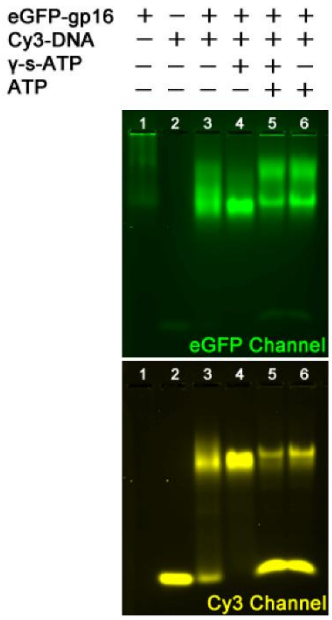

Figure 3.3. EMSA of eGFP-gp16 configurations with short Cy3-dsDNA and ATP or γ-S-ATP. The GFP channel shows migration of the ATPase and the Cy3 channel shows the migration of the dsDNA. The eGFP channel lane 5 clearly shows 2 distinct bands of gp16 after addition of ATP indicating the presence of two conformations of gp16.

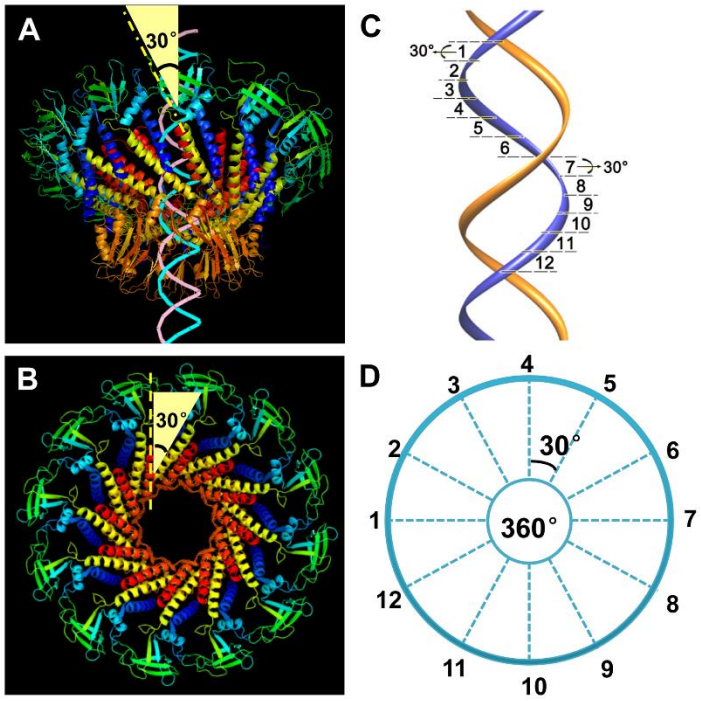

Figure 3.4. Illustration showing the anti-parallel configuration between connector subunit and DNA helix. External view (A) and internal view (B) of the anti-parallel configuration of connector and DNA as dsDNA revolves through the connector. One twelfth of a dsDNA helix is 30°(C), which is the angle dsDNA revolves to advance between two adjacent connector subunits (D). The contact at every 30° for twelve 30° transitions resulted in translocation of one helical turn of the dsDNA through the connector (B).

The anti-parallelism exhibited by the helices argues against a bolt and screw rotation model, since a screw thread and the corresponding whorl should match. The 30° tilt of the subunits matches perfectly with the 30° transitions that the dsDNA helix exhibits during revolving (360° ÷ 12 = 30°). In each step of revolving that moves the dsDNA to the next subunit, the dsDNA physically moves to a second point on the channel-wall, keeping a 30° angle in between the two segments of the DNA strand (**Fig. 3.4**). This structural arrangement enables the dsDNA to touch each of the 12 connector subunits in 12 discrete steps of 30° transitions for each helical pitch (**Fig. 3.4**). Nature has created and evolved a clever machine that advances dsDNA in a single direction while avoiding the difficulties associated with rotation, such as DNA supercoiling, as seen in many other processes. For reference, the Earth *rotates* around its own axis every day, but *revolves* around the sun every 365 days.

Unidirectional Flow of the Internal Channel Loops Provides A Vector Force as A Ratchet Preventing DNA Reversal.

The phi29 connector allows dsDNA to translocate from its N-terminal (narrower end) to its C-terminal (wider end).(139) In our most recent findings, like other ion channels that play a critical role in regulating ions in and out of membranes, the phi29 motor channel gates in three discrete steps in response to high voltage or ligand binding.(29,30) We have constructed a mutant connector in which the internal loops, which have been believed to play a role in DNA packaging, with residues 229-246 (27,31) were deleted. The viral assembling activities of procapsids bearing this mutant connector were assessed by *in vitro* virion assembly. It was found that procapsids with the loop-deleted connector failed to produce any virions, as compared to wild-type procapsids in which the assembly activity was about 1×10^8 pfu/ml (plaque forming units per millilitre) (**Fig. 3.5B**). Other findings from our lab and other groups have revealed that the channel loops play a

critical role in the one-way traffic mechanism of dsDNA; and that the packaged dsDNA reverses and slides out after being packaged into the mutant procapsid.(12,30,31,163,198) The channel loops may act as a clamp during DNA translocation and prevent the DNA from sliding out, supporting the "push through one-way valve" model in which the direction of DNA migration is regulated by the loops inside the channel (31) (**Fig. 3.5A**). The application of single-pore conductance assay revealed a one way-traffic of normal connector channel and two-way traffic of internal channel loop-deleted connector (**Fig. 3.6**). DNA traffic was probed by applying a ramping potential (**Fig. 3.6 left panel**) and by switching the voltage polarity (**Fig. 3.6 right panel**) that crossed the membrane. Due to the negative charge of the phosphate backbone, DNA migrates from the negative toward the positive electrode. In the presence of DNA in both *cis*- and *trans*-chambers under a ramping potential, DNA translocated *via* the single-channel BLM only at the negative potential when channel entrance (the narrow-end which locates outside the procapsid) faced the negative electrode (**Fig. 3.6A**). On the contrary, DNA translocation was observed only at the positive potential when the channel turned upside down (**Fig. 3.6B**). Furthermore, in the presence of DNA in both *cis*- and *trans*-chambers under a constant voltage, DNA translocation *via* the single-channel could be turned on and off depending on the polarity of the voltage(29) (**Fig. 3.6E**). This correspondence to polarity switching was dependent upon the orientation of the connector in the BLM, which was determined by nanogold blocking assay.(29) When no DNA translocation was observed under negative potential, switching the voltage to positive potential resulted in DNA translocation (**Fig. 3.6E**), and vice versa. The results strongly support that dsDNA can only pass through the wild type connector channel in one direction. When the internal loops of the connector were deleted, the two-way traffic of DNA was observed using both scanning potential (**Fig. 3.6C**) and polarity switching (**Fig. 3.6F**). So far, the two-way traffic of DNA has not been detectable for

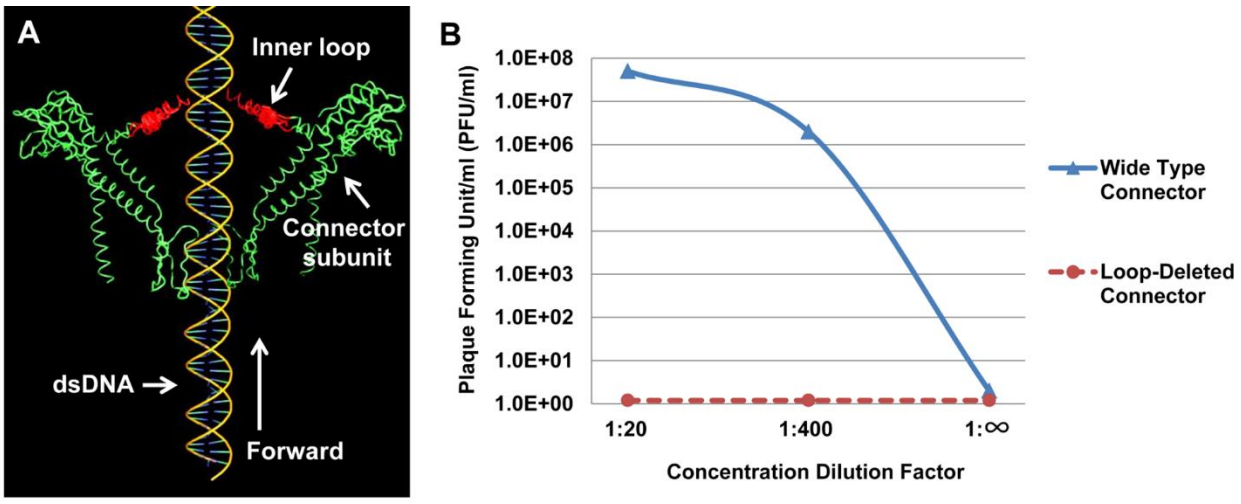

Figure 3.5. Influence of the flexible inner channel loops on DNA movement and virion assembly assay. (A) The flexible loop within the connector channel functions to interact with the DNA, facilitating the DNA to move forward, but blocking the reversal of DNA during DNA packaging. (B) Two dilution factors of wild-type procapsid show high virion assembly activity (~10^7 pfu/ml), while procapsids harboring the connectors with internal loops deleted are of a very low virion assembly activity. The loops are assumed to facilitate the forward movement of DNA and enhance the DNA one-way traffic mechanism, but not the reverse.

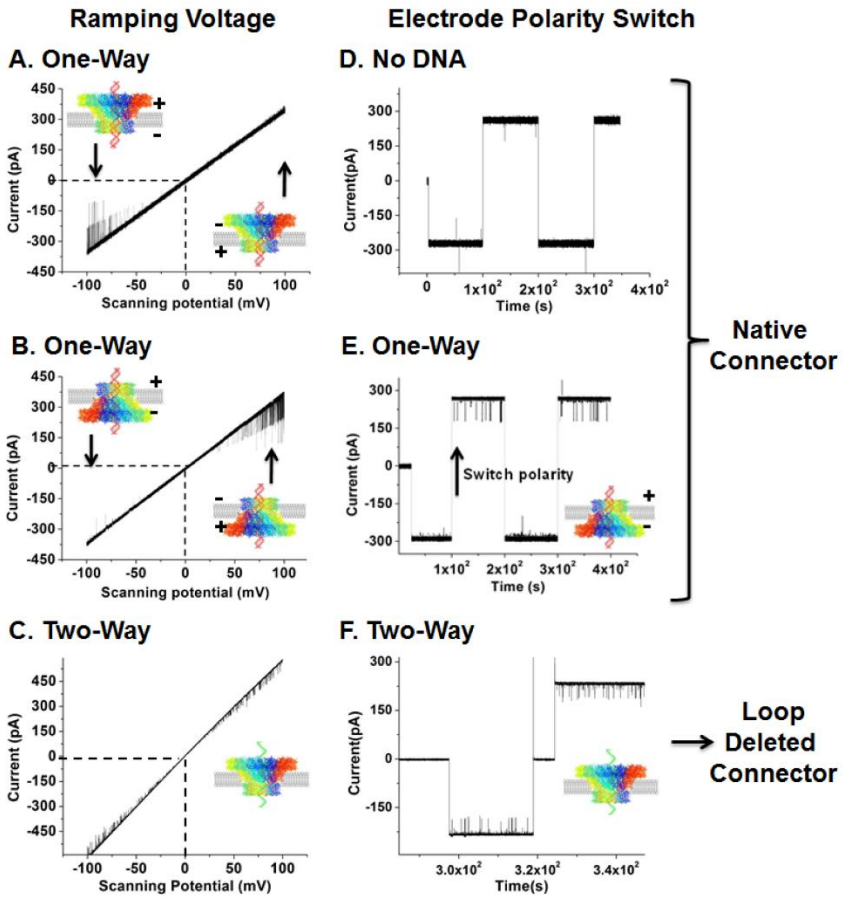

Figure 3.6. Single-pore conductance assay for DNA translocation through phi29 connector. Unidirectional translocation of dsDNA through wide type phi29 connector was shown under a ramping potential from -100mV to +100mV (A,B) and by switching polarity (E). ssDNA exhibits a two-way traffic property through internal loop-deleted connector, as shown by ramping potential (C) and by switching polarity (F). (D) The negative control without DNA.

wild type connector under the current experimental conditions.(34) In summary, the conductance assay with specific mutant connectors demonstrated that the internal flexible loops are essential for the one-way traffic of the motor. Together with the finding that procapsids harbouring modified connectors with internal channel loop mutation or deletion lose the capability to retain DNA after packaging,(163) as well as our finding that the procapsids harbouring modified connectors with internal channel loop deletion decrease the virion assembly efficiency (**Fig. 3.5B**), we concluded that the internal flexible loops play a key role in the one-way traffic property of viral DNA packaging motors during DNA translocation.

The 5'-3' Single-Direction Movement of One DNA Strand Along Channel Wall Ensures Unidirectional Motion.

Our extensive investigations into data modeling and literature have led to the following conclusions: the motor only contacts one strand, not both, of the dsDNA in the 5' to 3' direction in order to revolve along the connector channel.(15) While single-stranded DNA cannot be packaged, dsDNA with the 3'-end extended can revolve along the channel one helical turn of 10.5 bp. This notion has been based upon the revolving (but not the rotation) model and agrees with our studies on phi29 DNA packaging of phi29 genomic DNA containing single-stranded gaps.(161) The gap-containing dsDNA were produced *in vitro*, and the DNA packaging function was assayed in agarose gel electrophoresis using the defined *in vitro* phi29 assembly system.(196,199) We found that phi29 DNA with single-strand gaps was not packaged at full genome length. Because of such, we created two gaps: one at the left end (5883 bp) and one at the right end (14421 bp) of the phi29 DNA genome. Only the 5.9 kb DNA fragment between the left end of the genome and the first gap were packaged.(161) The right end fragment was not packaged. The result suggests that a single-strand gap in the DNA is a structural alteration that can cause the packaging motor to stop;

and that the packaging direction is from 5' to 3', since the phi29 packaged the left end of the genome first. Our model is supported by the finding by Black and co-workers who reported that a 3' single-strand overhang was packaged under conditions extending from the 100 bp duplex.(19) A 3'-extension up to 12 bases did not inhibit translocation, whereas 20 or more bases significantly blocked the T4 motor in DNA packaging. The 20-base gap was consistently found to be vulnerable, whether it was at the 3' end or in the middle of the DNA strand.(19) These results support the notion that the motor can revolve one complete turn of 360° with a single-stranded structure and that dsDNA revolves along the motor using a single strand in the 5' to 3' direction. The data is also supported by experimental data involving optical tweezers showing that dsDNA is processed by having contact with an unknown component on one strand of DNA in the 5' to 3' direction; the modification of phi29 DNA in the 5' to 3' direction stopped dsDNA packaging;(15) as well, that modification with 10 bases is tolerable, but 11 bases is not.(15)

Four Electropositive Relaying Layers Interact with the Electronegative DNA Backbone, Resulting in Four Steps of Transitional Pauses.

Connector crystal analysis (27) has revealed that the dominantly negatively charged phi29 connector interior channel surface is decorated with 48 positively charged lysine residues, existing as four relaying 12-lysine rings derived from the 12 protein subunits that enclose the channel (**Fig. 3.7**). The four lysine rings (K200, K209, K234, and K235) are scattered inside the channel and have been proposed to play a role in DNA translocation.(27) However, we have found that mutation of one layer of the four lysine rings does not significantly affect motor action.(31)

Here we further investigate the detailed interaction of lysine residues with the bacteriophage genome during translocation. When DNA revolves through the connector, it goes through 12 subunits of the connector per cycle, and we hypothesized that only one strand touches

the channel wall. Thus, during the entire 360° revolving, the negatively charged phosphate backbone will be in contact with the same positively charged layer of the lysine ring. One 360° revolving corresponds to 10.5 bp for each helical turn of the B-type dsDNA. This results in an imperfect match ($10.5 \div 12 = 0.875$) of sequential contact between the base, which has the negatively charged DNA phosphate group, and the channel subunits, which contains the positive-charged lysine ring (**Fig. 3.7**).

On average, each of the four lysine layers will be responsible for contact with three subunits (12 subunits ÷ 4 layers = 3 subunits). This value indicates that for every three subunits, 2.6 bp ($0.875 \times 3 = 2.6$ bp) will be translocated through the connector. At each step, a 12.5% mis-match occurs $\left(1 - (10.5 \div 12)\right)$ x $100\% = 12.5\%$. After three transactions with three subunits, a 37.5% variation will occur (12.5% x 3 = 37.5%), and the charge/charge interaction will be weakened due to distance. The phosphate interacts with the optimally charged lysine in the next subunit, and the distance variation due to this mismatch will be compensated for by introducing next lysine layer (**Fig. 3.7**). The contact point between the phosphate and the lysine then shifts to the next lysine ring. The transition results in a slight pause during DNA advancement. When dsDNA translocates through three subunits, the heading phosphate of the DNA will have to transition into the next lysine layer in order to compensate for the imperfect match between the phosphate and each lysine residue during DNA advancement through the connector. Thus, the four layers of the lysine ring will result in four pauses of DNA translocation. We found that the mutation of only one layer of the four lysine rings does not significantly affect motor function,(31) indicating that the interaction of the lysine with the phosphate is only the auxiliary force and not the main force necessary for motor action. This also indicates that the uneven speed of the four-step pauses caused by the four lysine layers is not the essential function of the motor. This would explain why

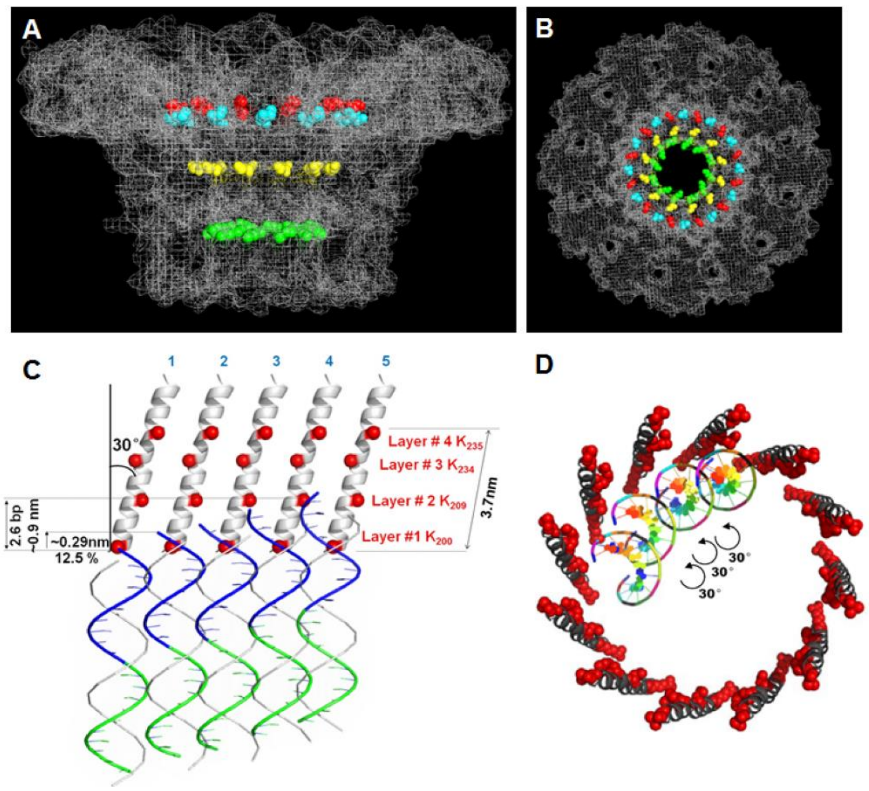

Figure 3.7. Structure of the phi29 channel showing the four lysine rings scattered inside the inner wall of the connector. Side view (A) and top view (B) of the connector, showing K200 (magenta) and K209 (yellow). The 229 (cyan) with 246 (red) show the boundary of the connector inner flexible loops that harbor the other two lysines. Due to the flexibility of the loop, the crystal structure of this loop is not available, and the known boundary of the loop was used to show the location. Side (C) and Top view (D) of the detailed scheme of DNA revolving through connector are shown. In this figure, the related position of the dsDNA and the connector subunit are displayed as three dimensional and viewed at different angles; the position of the dsDNA is different between two channel subunits, even though the DNA itself does not rotate.

the lysine layer and the 10.5 base per patch are not a perfect match, and why the distance of the layers are not constant.

Based on the crystal structure, the length of the connector channel is ~7 nm. Vertically, these four lysine layers fall within a 3.7 nm (27) range and are spaced approximately ~0.9 nm apart. The lysine residues K234 and K235 lie in the inner loop of the connector between residues 229 to 246, which were missing in the crystal structure; so the two residues close to the boundary of the inner loops were represented and were used to estimate the location (**Fig. 3.7**). Since B-type dsDNAs have a pitch of 0.34 nm/bp, ~2.6 bp per rise along its axis between two lysine layers can be used in translocation ($0.9\ \mathrm{nm}/0.34\ \mathrm{nm.\,bp^{-1}} = \sim 2.6\ \mathrm{bp}$). This value agrees with the recently data demonstrating the presence of four-step of pauses during dsDNA translocation process, as measured by optical tweezers using single molecule analysis.(13,14) It was demonstrated that each step translocated 2.5 base pairs and each circle translocated 10 base pairs of dsDNA.(13,14) The step size is in a good agreement with our finding described above. However, the authors interpreted the four pauses caused by four lysine rings into the rotation model driven by four motor ATPase. Thus, they found that their model is in disagreement with both the hexamer (11,49,50,52,53,55,56) and pentamer (58,200,201) models. Subsequently, the authors proposed a model in which phi29 DNA packaging motor is a pentamer, but one subunit of the pentamer was inactive, resulting in four motor subunits that generate four power strokes or bursts in rotation. Their rotation model is contradictory to our revolving mechanism described above showing that the four pauses are due to the presence of four lysine layers in the connector (**Fig. 3.7**).(194,195)

ACKNOWLEDGEMENTS:

The work was supported by NIH grants R01 EB012135 to PG, who is a co-founder of Kylin Therapeutics, Inc, and Biomotor and Nucleic Acids Nanotech Development, Ltd.

Chapter 4: Sequential Action Motion in phi29 dsDNA Packaging Motor

This chapter was reproduced (with some modifications) with permission from Z. Zhao, G. De-Donatis, C. Schwartz, H. Fang, J. Li and P. Guo. “Arginine fingers regulates sequential action of asymmetrical hexameric ATPase in dsDNA translocation motor”. Molecular and Cellular Biology. In press (Jul. 2016).

Arginine Finger Regulates Sequential Action of Asymmetrical Hexameric ATPase In dsDNA Translocation Motor

Zhengyi Zhao[1,2], Gian Marco De-Donatis[2], Chad Schwartz[2], Huaming Fang[2], Jingyuan Li[3], and Peixuan Guo[1,2] *

[1]Division of Pharmaceutics and Pharmaceutical Chemistry, College of Pharmacy; and Department of Physiology & Cell Biology, College of Medicine, The Ohio State University, Columbus, OH, USA

[2] College of Pharmacy, University of Kentucky, Lexington, KY, USA

[3]Institute of High Energy Physics, Chinese Academy of Sciences, Beijing, China

Running Title: Arginine finger primes sequential action of ATPase

ABSTRACT

Biological motors are ubiquitous in living systems. Currently, how the motor components coordinate the unidirectional motion is elusive in most cases. Here we report that the sequential action of the ATPase ring in the DNA packaging motor of bacteriophage phi29 is regulated by an arginine finger that extends from one ATPase subunit to the adjacent unit to promote noncovalent dimer formation. Mutation of the arginine finger resulted in the interruption of ATPase oligomerization, ATP binding/hydrolysis, and DNA translocation. Dimer formation re-appeared when arginine mutants were mixed with other ATPase subunits that can offer the arginine to promote their interaction. Ultracentrifugation and virion assembly assays indicated that ATPase was presenting as monomers and dimer mixtures. The isolated dimer alone was inactive in DNA translocation, but the addition of monomer could resume the activity, suggesting that the hexameric ATPase ring contained both dimer and monomers. Moreover, ATP binding or hydrolysis resulted in conformation and entropy changes of the ATPase with high or low DNA affinity. Taken together, it is concluded that arginine finger regulates sequential action of the motor ATPase subunit by promoting the formation of the dimer inside the hexamer. The finding of asymmetrical hexameric organization is supported by structural evidences of many other ATPase systems, showing the presence of one noncovalent dimer and four monomer subunits. All these provide clues for why the asymmetrical hexameric ATPase gp16 of phi29 was previously reported as pentameric configuration by cryo-EM. Since contact by the arginine finger renders two adjacent ATPase subunits closer than other subunits, the asymmetrical hexamer would appear as a pentamer by cryo-EM, a technology that acquires the average of many images.

INTRODUCTION

The ASCE (Additional Strand Catalytic E) superfamily including AAA+ (ATPases associated with various cellular activities) superfamily is a broad class of proteins among which several nano-biological molecular motors or nanomotors are listed. Nanomotors facilitate a wide range of functions (3,84,91,101,202,203), many of which are involved in DNA replication, repair, recombination, chromosome segregation, protein degradation, membrane fusion, microtubule severing, peroxisome biogenesis, gene regulation, DNA/RNA transportation, bacterial division, and many other processes (2,3,131,204-206).

Despite their functional diversity, ring-shaped P-loop NTPases share two conserved modules with Walker A and a Walker B motifs (6) exerting their activity through the ATP-dependent remodeling for translocation of macromolecules. The Walker A motif is responsible for ATP binding, while the Walker B is for ATP hydrolysis (207,208). This energy transition can result in either a gain or loss of substrate affinity, therefore generating a mechanical force exerted on the substrate to produce a mechanical motion. This motion will lead to a contact with or a separation from the substrate molecule, resulting in molecule folding/unfolding, complex assembly/disassembly, or translocation of DNA, RNA, protein or other substrates (209).

Both the revolving mechanism and the sequential reaction mechanism adapted by biological systems through evolution are efficient methods of unidirectional translocation of lengthy dsDNA genome, with minimum consumption of energy and without tangling or coiling (26,32,33,83,103,203). However, both the revolving mechanism and/or the sequential reaction mechanism for DNA translocation requires a signal communication from one component to another in the motor complex. It has been reported that ASCE ATPases contain one arginine finger motif along with the Walker A and Walker B motifs (137,142,210,211). In the active ATPase ring,

the arginine residue is located in proximity to the γ-phosphate of the bound ATP in the adjacent ATPase subunit (95,211-213). Arginine finger has been confirmed to associate with the formation of the ATP binding pocket (95,137,214-216). To understand how the motor component coordinates its motion necessary for unidirectional DNA translocation activity and sequential action of the ATPase ring, we analyzed the role of Arginine finger motif in the ATPase core of the dsDNA translocation motor. It was found that this motif controls the formation of the coordinating dimer inside the hexamer of the motor ATPase. The dimer however is not static but shifts and alters with time, following a sequential manner, and this sequential reaction mechanism is regulated by arginine finger.

MATERIALS AND METHODS

Cloning, mutagenesis and protein purification.

The engineering of eGFP-gp16 and the purification of the gp16 fusion protein have been reported previously (197). eGFP-gp16 mutants including arginine finger mutant R146A, Walker A mutant G27D, and Walker B mutant E119A as well as mCherry-gp16 mutant R146A were constructed by introducing mutations in the gp16 gene by Keyclone Technologies.

Glycerol gradient ultracentrifugation.

50 μl of eGFP-gp16 (500 μg/ml) were dropped on the top of 5 ml linear 15-35% glycerol gradients in a TMS buffer. After centrifuging at 35000 rpm in a SW55 rotor at 4 °C for 22 hr, the gradients were collected into 31 fractions from bottom to top and measured using a plate reader under 488 excitation before being applied to *in vitro* assembly assay.

Electrophoretic mobility shift assay (EMSA).

Fluorescently-tagged protein that facilitates detection and purification was shown to possess similar assembly and packaging activity as compared to wild-type (100,197). The EMSA method has been described previously (33,83). The gp16 mutants or wild-type were mixed with 33 bp Cy5-dsDNA in the presence or absence of ATP and γ-S-ATP. Samples were incubated at ambient temperature for 20 min and then loaded onto a 1% agarose gel (44.5 mM Tris, 44.5 mM boric acid) and electrophoresed at 4 °C for around 1 hr at 8 V/cm. The eGFP-gp16, mCherry-gp16, and Cy5-DNA samples were analyzed by a fluorescent LightTools Whole Body Imager using 488 nm, 540 nm, or 635 nm excitation wavelengths for GFP, mCherry, and Cy5, respectively.

Protein structure prediction and analysis.

I-TASSER (217) was used to predict the structure of the subunit of gp16 through a threading algorithm. The structure prediction processed without restraint, allowing the server to select the template. The N-domain (1-180 aa) of the predicted structure adopts a RecA-like fold, which is the conserved structure for many oligomeric ATPases, including T7 gp4 and FtsK. The RMSD between the predicted structure (N-domain of gp16) and FtsK (beta-domain) after the structure alignment is around 3 Å. The predicted structure (monomer) was then used to construct a hexameric structure of gp16 with *P. aeruginosa* FtsK (pdb ID: 2IUU) as the template (134). VMD was used to render the image of the structure (218).

Proteinase probing assay.

3 μl of his-gp16 (2 mg/ml) was mixed with trypsin (0.5 μg) and different amounts of ATP (0 nmol, 16 nmol, 32 nmol, 64 nmol, 128 nmol, 256 nmol, 512 nmol, 1 μmol) in the enzyme reaction buffer: 50 mM NaCl, 25 mM Tris pH8, 0.01% Tween 20, 0.1 mM $MgCl_2$, 2% glycerol, 1.5% PEG 8000, 0.5% Acetone, and 5 mM DTT. Fresh DTT was added into the buffer right before

the reaction. The final volume for this reaction system was 30 μl. The samples were incubated in room temperature for 30 min and applied on 12% SDS-PAGE.

Tryptophan intrinsic fluorescent assay.

8 μl SUMO-gp16 (1 μg/μl) was incubated with different amount of ATP in the reaction buffer (0.005% Tween 20, 1.5% PEG 8000, 0.5% Acetone, and 2 mM Tris pH 8.0). The fluorescent intensity of the samples was immediately measured through a spectra-fluorimeter under wavelength excitation at 280 nm.

ATPase activity assay.

Enzymatic activity *via* fluorescent labeling was described previously (184). Briefly, a phosphate binding protein conjugated to a fluorescent probe that senses the binding of phosphate was used to assay ATP hydrolysis.

***In vitro* assembly inhibition assay.**

Purified *in vitro* components were mixed and were subjected to virion assembly assay as previously described (196). Briefly, newly assembled infectious virions were inoculated to *Bacillus* bacteria and plated. Activity was expressed as the number of plaques formed per volume of sample (pfu/mL).

RESULTS

Hypothesis of motor motion mechanism to be tested.

Most biological motor ATPases assemble into hexameric rings with a motion process stimulated by ATP (6). For the phi29 dsDNA translocation motor, our hypothesis is that: (1) An arginine finger is present in the phi29 motor ATPase gp16. (2) The arginine finger outstretches to the

upstream adjacent ATPase subunit to serve as a bridge for the formation of a dimeric sub-complex and regulates the sequential action of the subunits in the hexameric ATPase ring. (3) One ATPase dimer and four monomers are present in the hexameric ring. (4) ATP binding results in the reshaping of the conformation and change of the entropic landscape of gp16. (5) Due to the DNA-dependent ATPase activity (6), binding of DNA to ATP/gp16 complex resulted in ATP hydrolysis, leading to a second conformational and further entropy change of the ATPase to a low DNA-affinity configuration that allows the release of dsDNA for its concomitant transfer to the adjacent subunit.

The model speculates that ATPase undergoes a series of conformational changes during DNA binding and ATP hydrolysis that are organized in a sequential manner, and that this sequential mechanism is coordinated by arginine finger (**Fig. 4.1**), with the supporting data described below.

Identification of arginine finger motifs in phi29 gp16 ATPase.

Gp16 shares the common ATP binding domain typical of all ASCE, including AAA+ proteins (91,99). This domain contains very well conserved motifs responsible for ATP binding and ATP hydrolysis (207) which have been previously identified as Walker A (6) and Walker B motifs (83), respectively. However, the detailed information about its arginine finger motif remained elusive. Sequence alignment was subsequently performed with similar ASCE proteins to identify this motif (**Fig. 4.2A**). From the alignment, we identified the position of the arginine fingers (residue 146) localized after beta-4 as seen in other ATPases, which correlates well with the known structural information and consensus sequences for this motif found in other proteins (95,134,219-221) (**Fig. 4.2A**). Single mutant R146A gp16 was produced and examined for its ATPase activity. As expected, the arginine finger mutant was severely impaired in the activity for

both ATP hydrolysis activity (**Fig. 4.2B**) and DNA binding in the presence of γ-s-ATP (**Fig. 4.2C**), possibly due to the impaired affinity for γ-s-ATP similar to the Walker A mutant (83). On the contrary, the Walker B mutants retained their binding affinity for DNA in the presence of γ-s-ATP and were also sufficient in binding DNA in the presence of ATP, although they could not hydrolyze ATP (33,83).

The arginine finger outstretches to the upstream adjacent ATPase subunit to serve as a bridge for the formation of a dimeric sub-complex.

Arginine finger has been reported to have various functions, including the major role in subunit communications by pivoting upon ATP hydrolysis to trigger the conformational changes of the subunits of the ATPase (91,142,222-226). The formation of the dimeric complex of gp16 in the absence of ATP was demonstrated by different approaches: glycerol gradient ultracentrifugation (**Fig. 4.3**), electrophoresis mobility shift assay (EMSA) (**Fig. 4.4A-C**), size exclusion chromatography, and native gel electrophoresis (83). These assays were based on the previous finding that fusion of the GFP protein to the N terminal of the gp16 did not interfere with activity of the ATPase gp16 in DNA packaging (182,183,197). It was found that mutation of the Arginine finger abolished dimer formation within the ATPase (**Fig. 4.3**). Although the Arginine mutants alone could not form dimers, interactions were observed when they were mixed with either the wild-type or other mutants that contained an intact arginine finger, which can provide an arginine residue for dimer formation (**Fig. 4.3**). The disruptive effect of Arginine finger mutation on assembly ability was also reflected in the protein activity, since it was

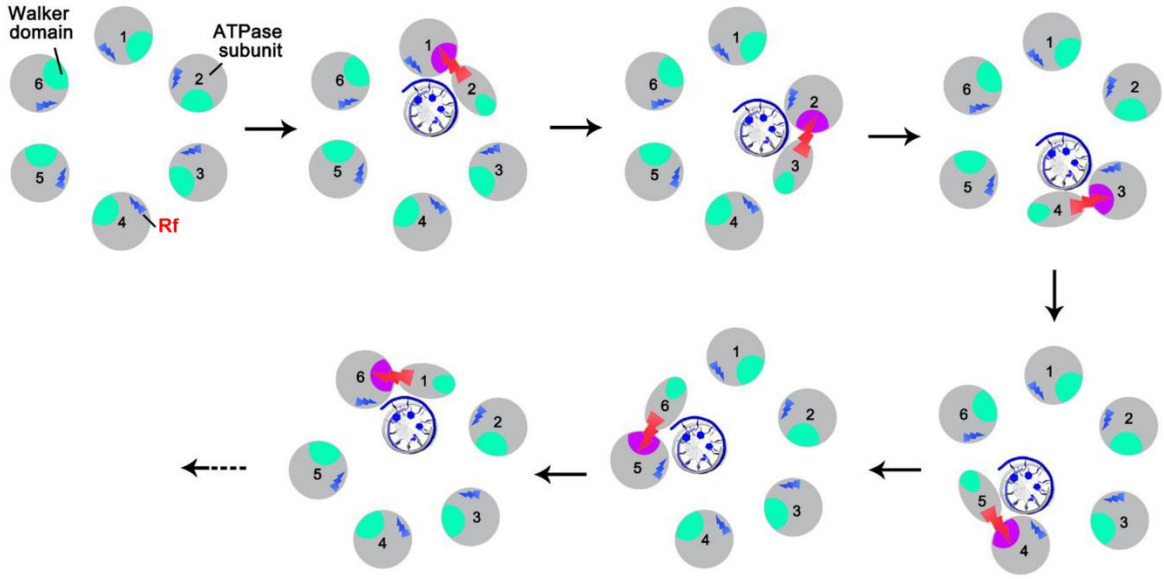

Figure 4.1. Proposed mechanism of ATPase coordination regulated by arginine finger.

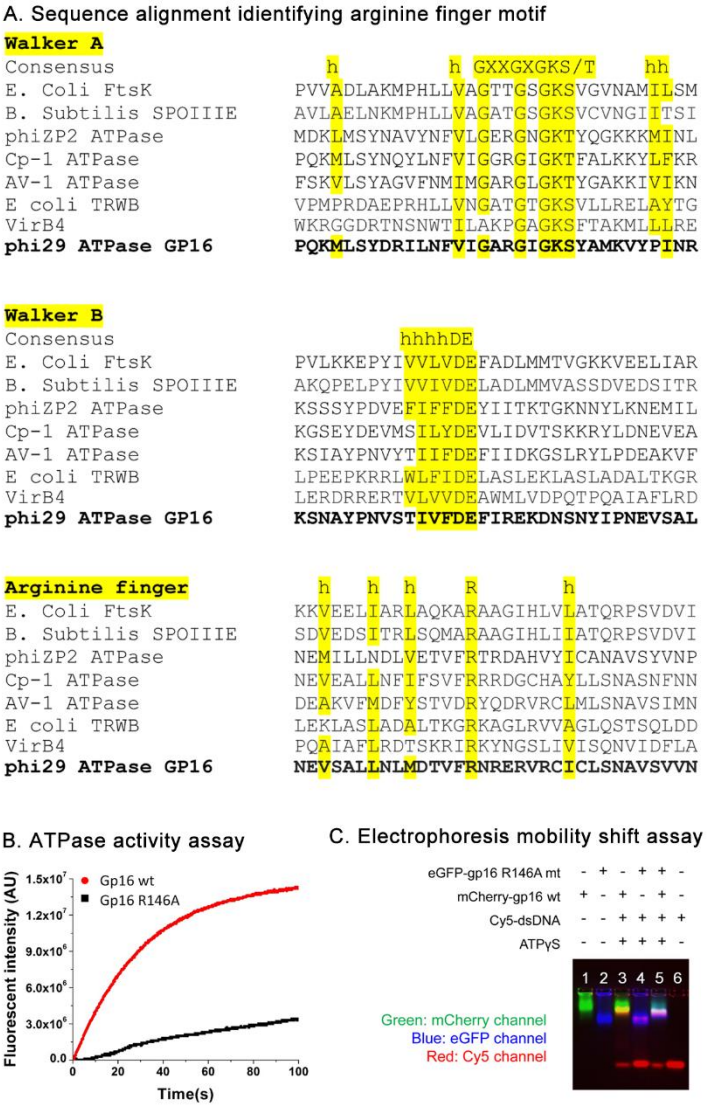

Figure 4.2. Identification and characterization of arginine finger in phi29 gp16 ATPase. (A) Sequence alignment among gp16 ATPase with other ATPase in the same family, indicating the location of the Walker A, Walker B, and arginine finger (R) motifs of gp16 ATPase which are well aligned with previously established domains (6,95,134,219-221). "h" represents hydrophobic residue. (B-C) ATP binding and hydrolysis activity assay of gp16 Arginine mutant. After the R146 residue is mutated, gp16 ATPase loses its ATP hydrolysis activity in B and DNA binding activity shown by EMSA in C.

observed that one single inactive subunit of an arginine finger mutant was able to inactivate the whole ATPase ring in an assembly inhibition assay (**Fig. 4.4D-E**).This supports the idea that in the ATPase ring, one adjacent wild-type ATPase provided an arginine finger to interact with the arginine mutant, and the lack of one arginine in the entire ring completely abolished the activity of the whole ring.

To get a better understanding of the structural role of Arginine finger, we modeled a gp16 hexameric ring using I-TASSER (217) and Phyre2 softwares (227). The gp16 sequence aligned well with the crystal structure of the hexameric FtsK DNA translocase of *E. coli* (**Fig. 4.5**). Using this model, we observed that the position of the Arginine finger of one subunit of gp16 outstretches to the active site of a neighboring subunit. The predicted structure showed that the Arginine finger was part of the ATP binding pocket (**Fig. 4.5**). The structural model provides an explanation for the observed cooperativity behavior in the hexameric ring of gp16. Not surprisingly given the importance in the formation of the active site, mutations in Arginine fingers greatly impaired the ability of gp16 to bind to ATP, to hydrolyze ATP (**Fig. 4.2B**), to bind to DNA (**Fig. 4.2C**), and consequently to package DNA (**Fig. 4.4E**).

Both dimer and monomer forms were present in gp16 hexamer.

As demonstrated in the above sections, arginine finger serves as a bridge between two independent subunits, thus forming a transient dimeric subunit. In wild-type g16 it was observed that both dimer and monomer forms were present in solution, as revealed by glycerol gradient centrifugation experiments. The molecular weight relative to such fractions was confirmed by protein markers calibrating through the same assay (BSA (66 kDa) localized around fraction 23, Alcohol dehydrogenase (140 kDa) around fraction 18, and beta-Amylase (200 kDa) around fraction 15.

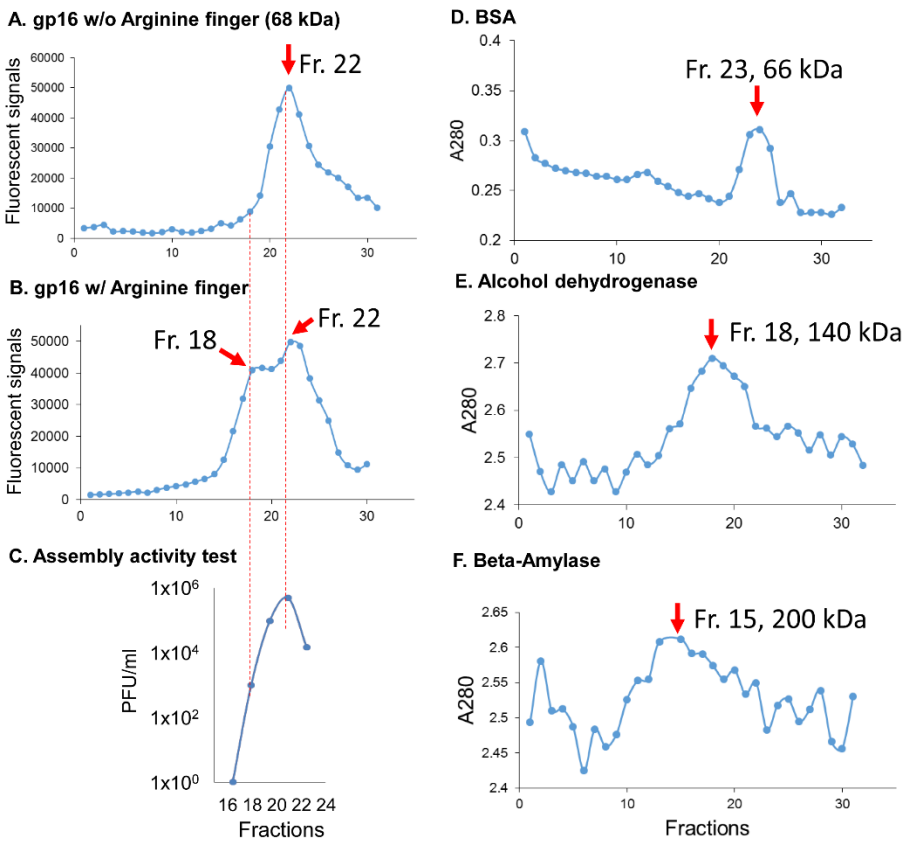

Figure 4.3. Ultracentrifugation assay showing the presence of both dimers and monomers in gp16 ATPase rings. One peak of eGFP-gp16 R146A (A) and two peaks of eGFP-gp16 wild-type (B) were shown after parallel ultracentrifugation in 15-35% glycerol gradient, indicating that both monomers and dimers were formed in gp16 wild-type, while dimer formation is interrupted by the mutation of arginine finger. (C) The isolated gp16 dimers did not show any viral assembly activity, supporting the previous finding that the addition of fresh gp16 monomers is required for re-initiating DNA packaging intermediates. (D-F) Ultracentrifugation fractions of protein markers including BSA (66 kDa), Alcohol dehydrogenase (140 kDa), and beta-amylase (200 kDa) are shown, with their peak locations around fractions 23, 18 and 15, respectively, to mark the separation of the monomer and dimer of gp16 ATPase.

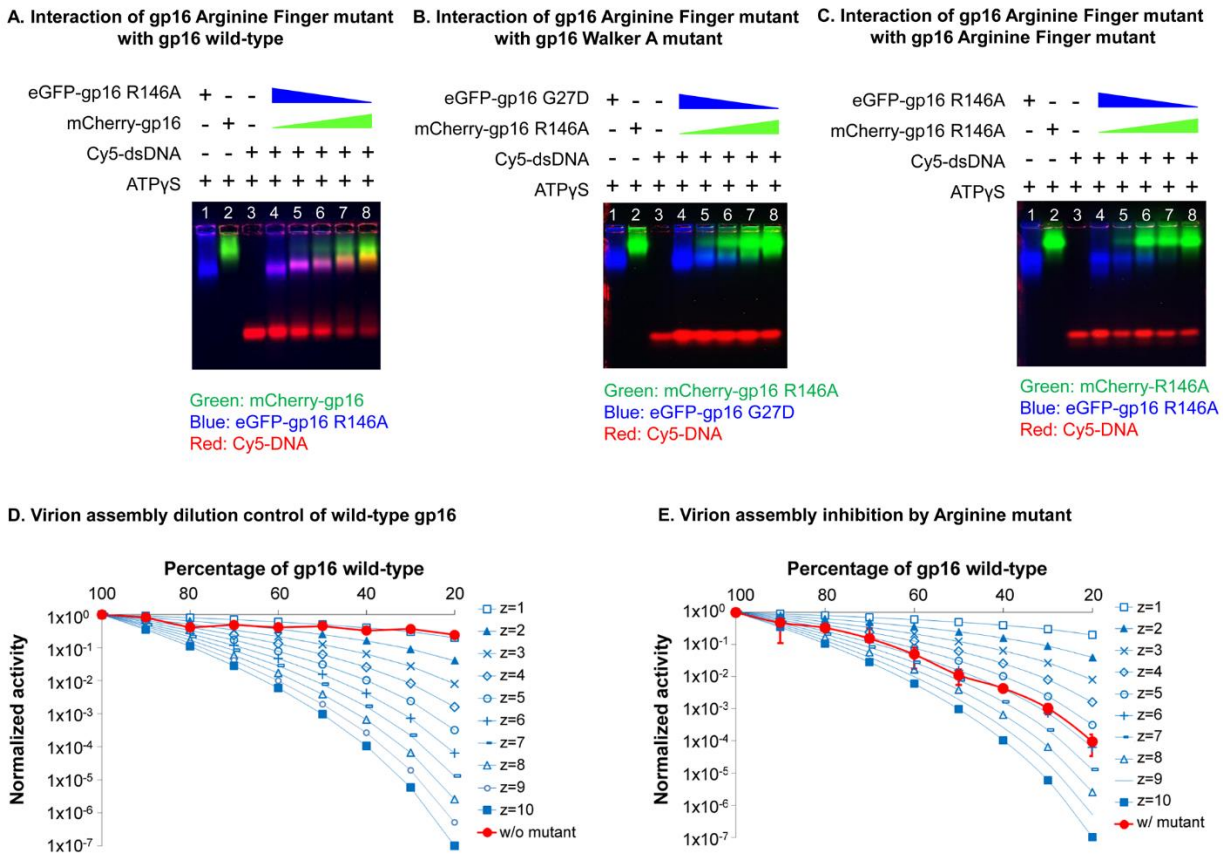

Figure 4.4. Inter-subunit interaction of gp16 arginine mutant with other gp16s. (A-C) EMSA showing the interaction of gp16 arginine finger mutant with (A) gp16 wild-type, (B) gp16 Walker A mutants, and (C) arginine finger mutants. Interactions between gp16 arginine finger mutants with gp16 wild-type or gp16 Walker A mutants are demonstrated by the band shift of both ATPase and DNA in the gel, while no obvious band shifts were observed when arginine finger mutant ATPases were mixed together. (D-E) Binomial distribution assay to show the blockage ot ATPase arginine finger mutant on motor packaging activity. Different ratios of buffer (D) or eGFP-gp16 arginine finger mutants (E) were mixed with wild-type gp16 ATPase for the in vitro virion assembly activity assay.

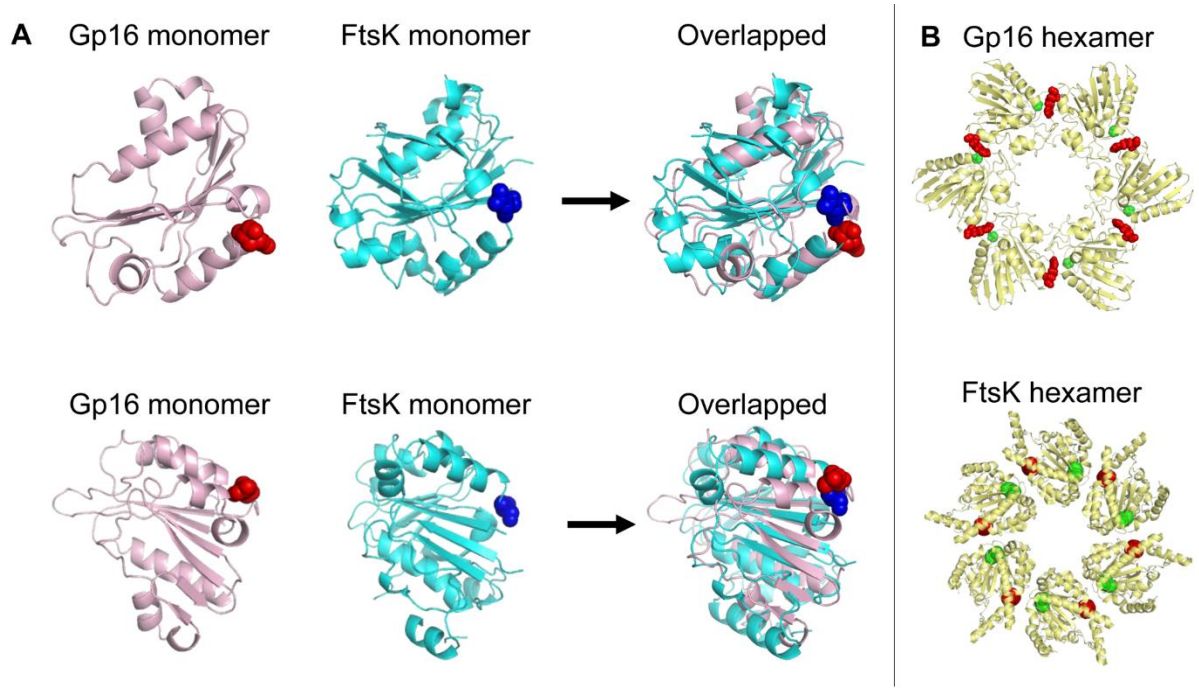

Figure 4.5. Prediction and comparison of gp16 structure. (A) Structural comparison between the crystal structure of FtsK monomer (pdb ID: 2IUU, cyan), and gp16 ATPase model (pink). The arginine finger is highlighted as a sphere. (B) Comparison of the predicted gp16 hexamer and FtsK hexamer. The ATPase gp16 hexamer structure was constructed using the predicted monomer structure in (A) and the *P. aeruginosa* FtsK (pdb ID: 2IUU) as templates (134). VMD was used to render the image of the structure (218). The ATP domains are highlighted as spheres: residue 27 (green, the conserved Walker ATP domain) and residue 146 (red, the arginine finger). The interaction of arginine finger with the upstream adjacent subunit is evidenced by the proximity of the Red and Green spheres in both the constructed structure of gp16 hexamer and FtsK hexamer crystal structure.

We thus proceeded to test the packaging activity of the different fractions of gp16 ATPase recovered from the gradient. Interestingly it has been observed that DNA packaging activity was retained with the fractions containing monomers, while fractions containing only dimers displayed no DNA packaging activity (**Fig. 4.3C**). These results agree with the finding that the addition of fresh gp16 monomer to the DNA-packaging intermediates is required for re-initiating motor DNA packaging activity and the conversion of the intermediates into infectious viruses (88).

ATP binding resulted in the change of conformation and entropic landscape of gp16.

ASCE proteins undergo a cycle of conformational changes during ATP binding and hydrolysis with basically 2 major states: high or low affinity for the DNA substrate. In recent publications (11,33,83,100) we proposed a similar model for gp16, in which binding to ATP exerted an effect on the conformational state of the protein that predisposes binding to DNA (high affinity). Conversely, ADP would promote another conformational state, in which DNA binding is not favorable. This notion together with the observation that arginine finger has a role in regulating both the conformational state of gp16 and its interaction with the adjacent subunit prompted us to question whether the effect of ATP binding on gp16 was able to modify not only the conformation of the DNA binding portion of the protein, but also the structural characteristics of gp16 altogether. We thus tested if ATP binding was able to alter the shape of gp16 by partial proteolysis treatment and tryptophan intrinsic fluorescence assay (**Fig. 4.6A-B**). Interestingly, both assays indicated a conformational change in the gp16-ATP complex. Moreover, as visible from the partial proteolysis test, the protection from proteolysis is indicative of a larger population of gp16 with constrained conformation before ATP binding.

An electrophoretic mobility shift assay was also employed to study the interaction between ATPase and dsDNA in the presence of γ-S-ATP, a non-hydrolyzable ATP analog. Stronger

binding of gp16 to dsDNA was observed when gp16 was incubated with γ-S-ATP (**Fig. 4.6C**), suggesting that the gp16/dsDNA complex is stabilized through addition of the non-hydrolyzable ATP substrate.

Hydrolysis of ATP transformed the ATPase into a second conformation with low affinity for dsDNA, thus pushing the dsDNA toward an adjacent ATPase subunit.

Consequent to the first structural change, it was also observed that the binding of ATP/gp16 complex to DNA resulted in ATP hydrolysis and also the passage to a second conformational change with a low DNA-affinity configuration (6,9,184). This explains the finding in 1987 that the phi29 DNA packaging protein gp16 is a DNA dependent ATPase (6). Such a state resulted in the release of dsDNA for its concomitant transfer to the adjacent subunit. The conclusion was also supported by the finding that the addition of normal ATP promoted the release of dsDNA from the gp16-γ-s-ATP-dsDNA complex (**Fig. 4.6D**).

DISCUSSION

Phi29 genomic DNA packaging involves multi-components including a 12-subunit connector, a hexameric pRNA ring(7,49), and an ASCE ATPase gp16 hexamer. Great interest has arisen about this packaging system for its intriguing mechanism of action and for its useful applications in nanotechnology (6,59,70,191,228-231). It has been demonstrated that pRNA works as a point of connection between the ATPase and the connector (8), and that the hexameric ATPase (33,83) provides the pushing force for the packaging of genomic DNA, acting in coordination with the connector that acts as a one-way valve (11,29,232). Nanobiomotors have been previously classified into two main categories: linear and rotational motors. These two categories have been clearly documented in single molecule imaging and X-ray crystallography (108-113).

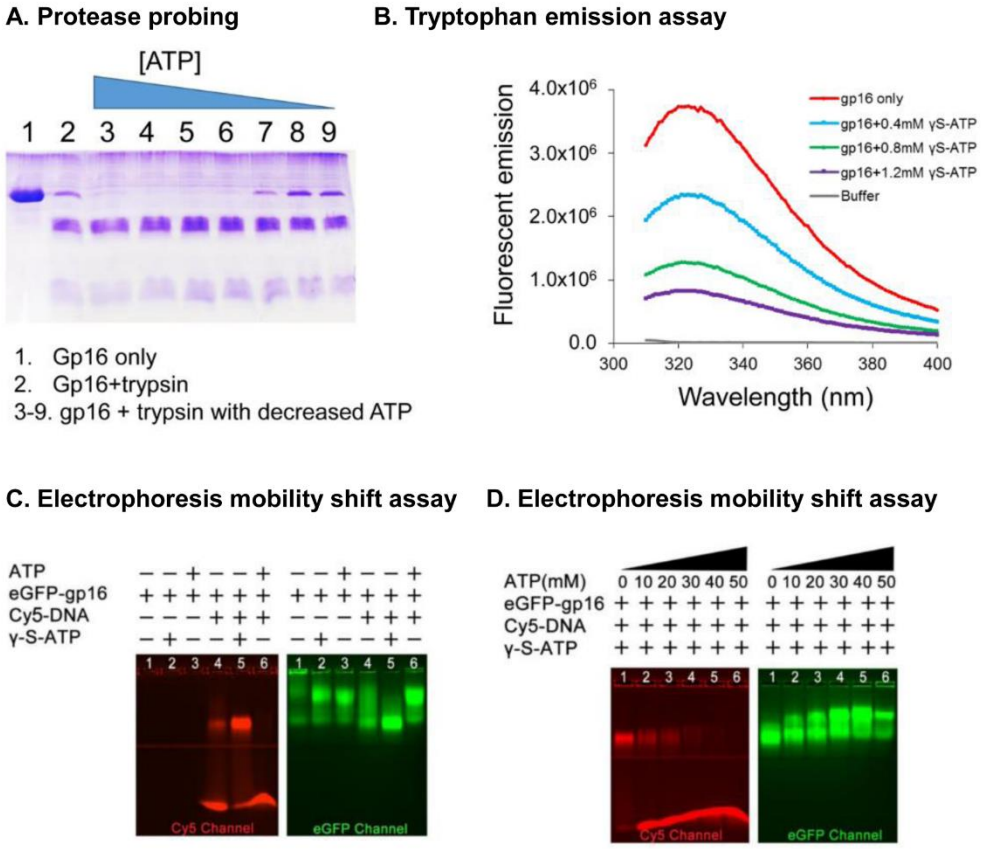

Figure 4.6. Demonstration of gp16 conformational changes and entropic landscape alteration upon ATP binding and hydrolysis. (A) Trypsin probing showed that the ATPase digested band is decreased with a reduced amount of ATP added into gp16 ATPase samples. (B) Intrinsic tryptophan fluorescent assay showing the signal changes of ATPase upon adding different concentrations of ATP. (C) EMSA showing that gp16 ATPase binds to ATP and undergoes a conformational change that has a high affinity for DNA, and ATP hydrolysis triggers a second conformational change of gp16 ATPase with a low affinity for DNA. (D) Increasing DNA is released from gp16 ATPase/DNA/ATP complex upon the addition of increased amount of ATP that can be hydrolyzed by the gp16 ATPase.

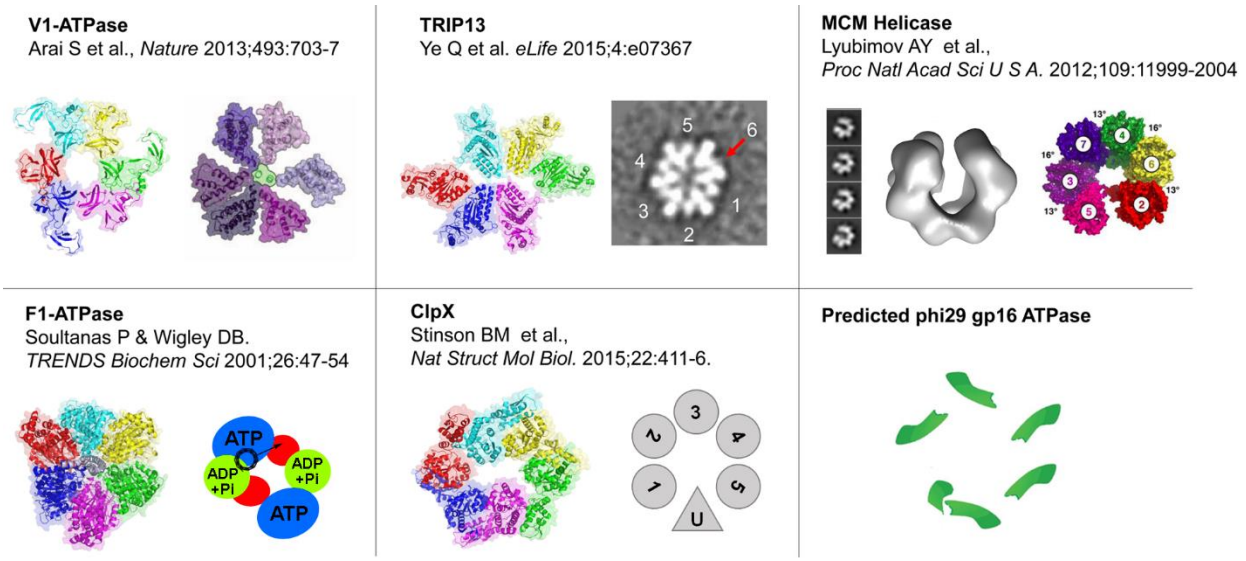

Figure 4.7. Asymmetrical structure of various ATPase hexamers. Structure illustrations of V1-ATPase (adapted from (89) with permission from Nature Publishing Group), TRIP13 (adapted and modified from (233) with permission from eLife Sciences Publications, licensed under CC BY-NC-SA), ClpX (adapted and modified from (234) with permission from Nature Publishing Group), MCM helicase (adapted from (90) with permission from National Academy of Sciences), and F1-ATPase (235) are shown as representatives of asymmetrical hexamers. PDB ID: V1-ATPase, 3VR5; TRIP13, 4XGU; F1-ATPase; ClpX, 4I81. EM ID: ssoMCM, EMD-5429.

Recently, it has been discovered that the phi29 dsDNA packaging motor uses a revolving mechanism that does not require rotation or coiling of the dsDNA (32,33,83,102). The finding of the revolving mechanism establishes a third class of biomotors, resolving many puzzles and debates throughout the history of painstaking studies on the motor (102,103).

The ATPase hexameric ring exerts a force, pushing the dsDNA in a sequential manner to advance through the dodecamer channel which acts as a one-way valve (29,57,84,102,103). The interest in the sequential revolving mechanism lies in the fact that it elegantly integrates all the known functional and structural information about the packaging core (the ATPase, pRNA and connector). Moreover, it offers solutions for many questions that arise when investigating the DNA packaging phenomenon (i.e. coordination between energy consumption and DNA packaging, ability to translocate a long strain of dsDNA without coiling or tangling). However, in order to have a sequential mechanism (which has been proposed for many proteins belonging to the family of AAA+/ASCE) (216,236,237), several conditions need to be fulfilled. The most important are: A) Only 1 or 2 subunits of the oligomer are able to bind the substrate with the same affinity exhibited in the entire hexamer. B) Both ATPase activity and translocation activity need to demonstrate negative cooperativity when one subunit is able to bind ATP; it is not able to hydrolyze the nucleotide (as in the case of the Walker B mutation). C) Only the ATP bound state of the protein is the unique state that efficiently binds to DNA.

We demonstrated that this is indeed the case for the phi29 motor ATPase (33,100). One important question that then arises with the demonstration of the sequential mechanism is, how can the different subunits of the ATPase sense the ATP binding/DNA binding state of others? In the present work, we addressed this question by identifying the arginine finger motifs of the ATPase gp16 by sequence alignment and proved that arginine finger is an essential motif that

participates in the formation of the ATP binding pocket by examining the behavior of gp16 mutants with the Arginine finger removed. The gp16 mutated in Arginine finger was unable to package DNA, to hydrolyze ATP, or to bind to DNA. The profile of gp16 in ultracentrifugation indicated the presence of a mixture of monomeric and dimeric forms. Mutation of the Arginine finger eliminated the capacity of gp16 to assemble into dimeric forms. Arginine finger motifs were thus shown to link two subunits to each other since the arginine motif of one subunit participates in the formation of the ATP binding site of the next subunit (**Fig. 4.7**). The importance of the dimer is moreover evidenced as shown by DNA packaging assay, in which the reconstituted hexamer of gp16 can efficiently pack DNA inside the procapsid only when ultracentrifuge fractions containing both dimeric and monomeric gp16 are mixed together (data not shown) (88).

In the sequential action of gp16, we proposed that one subunit of the hexamer binds to the DNA, subsequently hydrolyzing ATP to perform a translocation of a certain number of base pairs of DNA (6,122). The DNA is then passed to the subsequent subunit, and the process is repeated. It is intriguing to notice that the position and function of ATPase offers the possibility of carrying the information of ATP/DNA binding from one ATPase subunit to another, with a cooperative behavior of gp16 seen in the case of other mutants (Walker B mutations) (33).

The sequential action mechanism of phi29 ATPase is essential for optimal translocation efficiency. This mechanism integrates well with our overall model of the revolving motor and the "push through one way valve" model (11,33). Without the coordination during the energy production of gp16, the cycles of binding and release of DNA would create futile cycles of ATP hydrolysis, inhibiting the unidirectional translocation process (32,33,100). Arginine fingers thus act as an integrator of information for the entire process of DNA packaging. Years of evolution

have created an efficient biomotor, one that can be used in the future for applications in nanotechnology (203,228).

Furthermore, the conclusion of asymmetrical hexameric coordination was supported by structural computation, X-ray diffraction and Cryo-EM imaging of other hexameric ATPase systems (**Fig. 4.7**) (89,233-235). These results could provide some clues for why the asymmetrical hexameric ATPase of gp16 of phi29 and gp17 of T4 was previously interpreted as having a pentameric configuration by cryo-EM. Since the two adjacent subunits of the ATPase could interact with each other and form a closer dimer configuration, this dimer will appear as a monomeric subunit different from the others, and the hexameric ring is asymmetrical (**Fig. 4.7**).

ACKNOWLEDGEMENTS

The work was supported by NIH grant R01-EB012135 and R01-EB019036 to PG. The content is solely the responsibility of the author and does not necessarily represent the official views of NIH. Funding to Guo's Endowed Chair position in Nanobiotechnology position is by the William Fairish Endowment Fund, to Guo's Sylvan G. Frank Endowed Chair position in Pharmaceutics and Drug Delivery is funded by the CM Chen Foundation. P.G. is a consultant of Oxford Nanopore and RNA Nanobio, Ltd.

Chapter 5: Construction and Motion Direction Control of Bio-Nanomotor

This chapter was reproduced (with some modifications) with permission from Z. Zhao, H. Zhang, D. Shu, C. Montemagno, J. Li and P. Guo. “Construction of Asymmetrical Hexameric Biomimetic Motors with Continuous Single-Directional Motion by Sequential Coordination”. Small. In press (2016).

Construction of Asymmetrical Hexameric Biomimetic Motors with Continuous Single-Directional Motion by Sequential Coordination

*Zhengyi Zhao[1], Hui Zhang[1], Dan Shu[1], Carlo Montemagno[2], Jingyuan Li[3] and Peixuan Guo[1]**

[1]College of Pharmacy; College of Medicine/Department of Physiology & Cell Biology/Dorothy M. Davis Heart and Lung Research Institute, The Ohio State University, Columbus, OH, USA

[2]Chemical and Materials Engineering and Ingenuity Lab, University of Alberta, Edmonton, Alberta, Canada

[3]CAS Key Laboratory for Biomedical Effects of Nanomaterials and Nanosafety, National Center for Nanoscience and Technology of China and Institute of High Energy Physics, Beijing, China

ABSTRACT

The significance of bionanomotors in nanotechnology is analogous to mechanical motors in daily life. Here we report the principle and approach for designing and constructing biomimetic nanomotors with continuous single-directional motion. These bionanomotors are composed of a dodecameric protein channel, a six-pRNA ring, and an ATPase hexamer. Based on recent elucidations of the one-way revolving mechanisms of phi29 DNA packaging motor, various RNA and protein sequences were designed and tested by single-molecule imaging and biochemical assays, resulting in the production of active motors. Single-directional motion was attributed to three operation elements: 1) An ATPase hexamer containing ATP-interacting domains for alternative DNA binding and pushing regulated by the sequential acting arginine finger that bridges two adjacent ATPase subunits into a non-covalent dimer, resulting in an asymmetrical hexameric complex with one dimer and four monomers; 2) a dsDNA translocation channel as a one-way valve; 3) a hexameric pRNA ring geared with left-/right-handed junctions. Motion assessments revealed that only one inactive subunit of pRNA or ATPase was sufficient to completely block the motion thus defined as K=1, confirming sequential action for single direction motion based on the principle of binomial distribution and Yang Hui's Triangle.

INTRODUCTION

The ubiquitous intriguing nanomachines in living organisms have inspired numerous biomimetic strategies and human achievements. Biological macromolecules of DNA, RNA and proteins are essential and powerful chemical building blocks of all organisms based on their intrinsically defined features at the nanometer scale. (66,238) Construction of self-propelling nanomotors have been a popular subject in the field of nanotechnology. (239-260) The emerging field of nanotechnology has led to the advancement of biomaterials engineering and synthetic biology. (261-263) Although the construction of biological nanomotors has been extensively studied, (5,128,196,199) the key step to make these bionanomotors applicable in nanodevices and nanomachines is to functionalize these motors and control their continuous single-directional motion. Here we report one such principle and approach by designing and constructing an artificial biomimetic phi29 dsDNA packaging motor that can move continuously in one direction. This nanomachine is composed of a 3.6 nm dodecameric protein channel and six protein ATPase that are geared by six pRNA (packaging RNA) and driven by ATP (**Fig. 5.1**). (5)

The motion direction of the dsDNA was controlled by ATPase, connector and pRNA systems. In the ASCE (Additional Strand Catalytic E) ATPases superfamily, one well-conserved ATP domain contains one arginine finger motif along with the Walker A and Walker B motifs.(137,210,211,264) Located in proximity to the γ-phosphate of the bound ATP in the adjacent ATPase subunit,(95,211-213) arginine finger has been reported to be involved in the formation of the ATP activity pocket.(87,95,137,214-216) Elucidation of the principle of how arginine finger mediates the sequential action of ATPase has shed light on the realization of controlling motor motion direction.

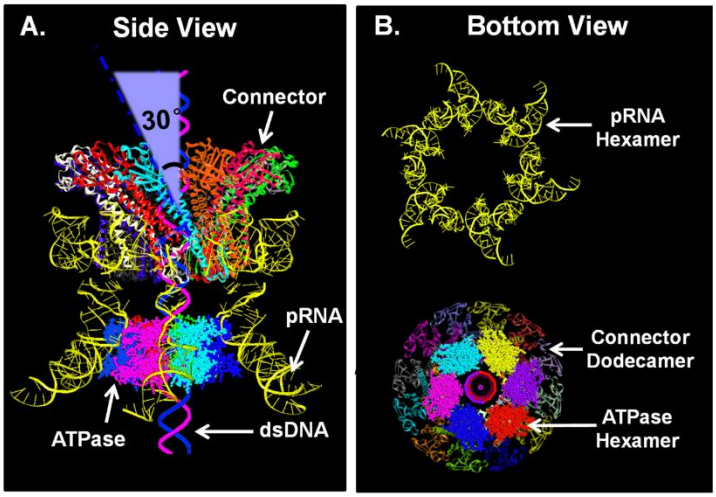

Figure 5.1. Illustration of the components of phi29 motor. (A) Side view and (B) Top view of the phi29 dsDNA packaging motor composed of the three co-axial rings of the dodecameric connector, hexameric pRNA ring, and hexameric ATPase ring.

Furthermore, the connector channel as a one-way valve for DNA advancement is another key factor for the control of the uni-directional movement of the biomotor. With the contribution of all three coaxial rings in the motor, the constructed motor, though tiny, is considered as one of the most powerful biological motor ever constructed to date.

MATERIALS AND METHODS

Cloning, mutagenesis and protein purification

The engineering of eGFP-gp16 and the purification of the gp16 fusion protein have been reported previously. (197) The eGFP-gp16 mutant R146A and mCherry-gp16 mutant R146A were constructed by introducing mutations in the gp16 gene (Keyclone Technologies).

Glycerol gradient ultracentrifugation

50 μl of eGFP-gp16 (500 μg/ml) were dropped onto 5 ml linear 15-35% glycerol gradients in TMS buffer. After centrifuging at 35000 rpm in a SW55 rotor at 4 °C for 22 hr, the gradients were collected into 31 fractions from bottom to top and measured using plate reader under 488 excitation before being applied to *in vitro* assembly assay.

Electrophoretic Mobility Shift Assay (EMSA)

Fluorescently tagged protein that facilitates detection and purification was shown to possess similar assembly and packaging activity as compared to wildtype.(100,197) The EMSA method has been described previously.(33,83) The gp16 mutants or wild-type were mixed with 33bp Cy5-dsDNA in the presence or absence of ATP and γ-S-ATP. Samples were incubated at ambient temperature for 20 min and then loaded onto a 1% agarose gel (44.5 mM Tris, 44.5 mM boric acid) and electrophoresed at 4°C for around 1 hr at 8 V/cm. The eGFP-gp16, mCherry-gp16,

and Cy5-DNA samples were analyzed by a fluorescent LightTools Whole Body Imager using 488 nm, 540 nm, and 635 nm excitation wavelengths for GFP, mCherry, and Cy5, respectively.

CE experiments to determine ratio of gp16 to bound dsDNA

CE (capillary electrophoresis) experiments were performed on a Beckman MDQ system equipped with double fluorescence detectors (at 488 nm and 635 nm excitation wavelengths). A bare borosilicate capillary with a total length of 60 cm and a 50 μm inner diameter were used. Assay conditions contained separation buffer of 50 mM Tris–HCl, 100 mM sodium borate at pH 8.00, 5 mM $MgCl_2$, 10% PEG 8000 (w/v), 0.5% acetone (v/v), 3 μM eGFP-gp16 monomer, and variable amounts of ATP and DNA.

In vitro assembly assay

Purified *in vitro* components, including prohead-connector, pRNA, genome DNA, ATPase, and tail proteins were mixed and subjected to virion assembly assay as previously described.(196) Briefly, newly assembled infectious virions were inoculated to *Bacillus* bacteria and plated. Activity was expressed as the number of plaques formed per volume of sample (pfu/mL). Different fractions of samples were isolated from the glycerol gradient and added into the system for their activity test.

Observation of gp16 motion

Double-stranded lambda DNA (48 kbp) was tethered between two polylysine coated 4 μm silica beads. (265) The dsDNA was bound between beads by back-and-forth infusion of DNA over the beads for 10 min; binding occurred as a result of charge-charge interactions. The back and forth motion of DNA over the polylysine beads stretched the DNA taut and lifted the chain above the surface by the 4 μm silica beads as visualized under the microscope. The incident angle of the

excitation beam in objective-type TIRF (total internal reflection fluorescence) was adjusted to a sub-critical angle in order to image the samples a few microns above the surface, yielding a low fluorescence background. (265) To-Pro-3 was used to confirm the formation of the DNA tightropes. After the DNA tightrope was formed, a 30 μL mixture with a final concentration of 1 nM Cy3-gp16 with 100 nM unlabeled gp16 in buffer B (25 mM Tris, pH 6.1, 25 mM NaCl, 0.25 mM $MgCl_2$) was infused into the sample chamber for binding to the stretched DNA. After 30 min incubation, 30 μL of a solution containing anti-photobleaching reagents (53) was infused into the chamber in order to prevent photobleaching of less photostable fluorophores and to detect binding. Movies were taken after the chamber was washed with buffer C (25 mM Tris, pH 8, 25 mM NaCl, 0.25 mM $MgCl_2$). A comparison was made of washings with buffer C, with and without 20 mM ATP. Since the DNA has been fixed by charge interactions and the protein fixed by binding affinity to the tethered DNA, washing does not remove pertinent material. Sequential images were acquired with a 0.2 s exposure time at an interval of 0.22 s, with a laser of 532 nm for excitation. The movies were taken for about 8 min, or until the Cy3 fluorophores lost their fluorescence due to photobleaching. Image J software was utilized to generate kymographs to show the displacement of the Cy3-gp16 spots along the DNA chains.

Direct observation of DNA translocation

The stalled packaging intermediates containing biotinylated DNA were prepared by using non-hydrolyzable γ-S-ATP. (88) The intermediates were then immobilized through IgG prohead antibody to perfusion chambers built from glass slides and coverslips. The fluorescent streptavidin microspheres (0.56 μm) were bound to the protruding, biotinylated DNA end of the intermediates. After restarting the packaging reaction by adding gp16 and ATP, (88) an individual DNA-packaging event was observed. Epi-illumination was used, and sequential images were recorded.

RESULTS AND DISCUSSION

Screening of pRNA sequences to control motor motion

pRNA is an essential component of the motor.(7) Six pRNA monomers form a hexameric ring through interactions between four bases in every two adjacent pRNA loops.(49) A minimum length of 117-nucleotide in each pRNA is required. Each pRNA contains five single-base bulges, one three-base bulge, one bifurcation bulge, one bulge loop and two stem loops (**Fig. 5.2**). To select the RNA sequences with activity to gear the motor, 18 different hexamer pRNAs were constructed following the method reported previously.(45,49) All these mutant pRNAs were competent in binding to the procapsid with an efficiency equal to that of the wild type pRNA. However, incorporation of only one mutant, either pRNAdCCA (with CCA bulge deletion, **Fig. 5.2,** red box) or pRNAtrun (truncated at the 5'- and 3- ends, **Fig. 5.2**, blue box), into the hexameric loop completely obliterated the motor function in DNA packaging activity. The fact that one inactive pRNA is sufficient to block the function of the entire motor has been defined as K = 1. (230,231,266) In binomial distribution, K =1 for the hexametric RNA ring implies that six RNA molecules worked sequentially. (84,100,266)

Screening of connector sequences to control motor motion

The channel of the phi29 motor functions as a dodecameric ring and serves as a pathway for the dsDNA to enter the procapsid during the packaging process. The protein subunit of the connector was modified to screen for active mutants for motor construction. This was achieved by adjusting the inner loop of the connector protein, or by applying terminus extensions or truncations to the connector protein. The inner loops of the connector are also involved in the one-way traffic of DNA translocation during motor packaging (**Fig. 5.3A**, **left**). (31,32) A similar internal loop is

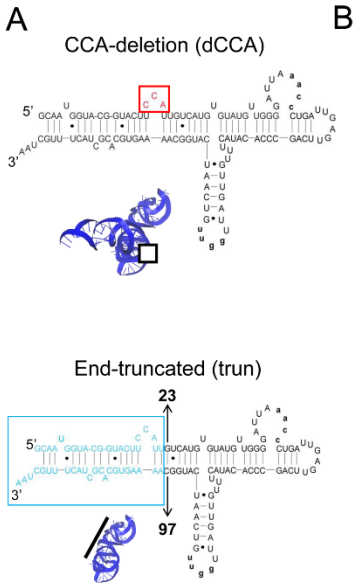

B

End-truncated (trun)			CCA-deletion (dCCA)		
Name	Structure	Activity (pfu/ml)	Name	Structure	Activity (pfu/ml)
3(DD)		10^8	3(DD)		10^8
3(Dd)		~ 0	3(Dd)		~ 0
3(dd)		~ 0	3(dd)		~ 0
2(DD) +1(Dd)		~ 0	2(DD) +1(Dd)		~ 0
1(DD) +2(Dd)		~ 0	1(DD) +2(Dd)		~ 0
2(TTT)		10^8	2(TTT)		10^8
2(TTt)		~ 0	2(TTt)		~ 0
2(ttt)		~ 0	2(ttt)		~ 0
(TTT) +(TTt)		~ 0	(TTT) +(TTt)		~ 0

Figure 5.2. Impact of different pRNA mutations on motor activity. (A) Sequence of pRNA monomer with CCA bulge (upper panel) or 5'/3' end (lower panel) highlighted in the box. The illustrations of the corresponding 3D structures are shown. The bars symbolize the end-truncation, and the empty squares symbolize the CCA-deletion. (B) Viral assembly activity of pRNA hexamers with different designs. Each color symbolizes one purified dimer or trimer. The uppercase **D** and **T** symbolize the normal dimer and trimer, respectively. The lower case **d** and **t** symbolize the mutant dimer and trimer, respectively.

also found in the portal protein of SPP1 (**Fig. 5.3A, right**). Single-pore conductance assay has been utilized to test the performance of the phi29 connector channels. With the channel embedded and voltage applied across the membrane, the translocation of the negatively charged DNA through the channel can be detected. With the wild-type connector, DNA translocation events occurred only at negative potential when the channel entrance faced the negative electrode, and vice versa. (29,32) In contrast, DNA translocated through the channel from both directions when using the loop-deleted connector. (32,34) The results strongly support that the internal loops of the connector are one of the key factor for the one-way traffic of dsDNA, (32,34) and that the direction of DNA translocation through the motor can be controlled by tuning the internal loop of the channel protein. Fusion of a small peptide to the N-terminus or C-terminus of gp10 generated different gp10 extensions named gp10-Nhis, gp10-Nstrephis, and gp10-Cstrep, with the tobacco etch virus (TEV) cleavage site incorporated. (267) The mutant procapsid with N-terminal extensions (gp10-Nex) demonstrated a 100 fold reduction in virion assembly compared to the wild-type procapsid (**Fig. 5.3B, C**). Removal of the extended sequence by TEV cleavage restored the phi29 virion assembly activity. On the other hand, the procapsids with C-terminal extensions (gp10-Cex) was slightly impaired in assembly activity (10-fold drop) (**Fig. 5.3B, C**). gp10-Ntrun with N-terminal residues 1-14 truncation and C-terminal strep tag extension was generated. To further define the sequence requirement for building the dodecameric architecture, residues 1-37 or 1-48 of gp10 were removed and tested. Residues 11-37 constitute one entire α-helix running from the narrow end to the wide end of the connector, followed by residues 38-48 which form a β-sheet at the relaxed wider end of the connector. It was obvious that this α-helix was intimately related to connector assembly. Its removal disrupted the balance and self-interaction of gp10 subunits in a connector, or worse, impaired gp10 protein folding which led to insoluble aggregates.

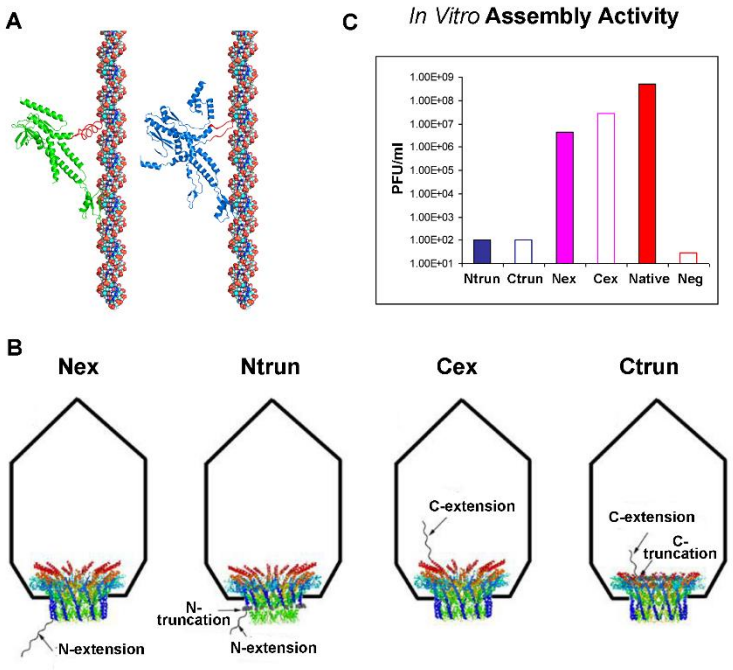

Figure 5.3. Impact of different connector mutations on motor activity. (A) Illustration of the internal loop in the phi29 portal protein (left) and SPP1 portal protein (right), showing their function as a ratchet for the one-way translocation of the DNA during genome packaging. (B) Illustration of procapsids with side view of the mutant connectors based on PDB: 1h5w. (C) Comparison of procapsid activity with equal amount of procapsid protein.

In addition, truncation of the flexible region of C-terminal 25 residues generated procapsid-Ctrun with normal morphology but with its virion assembly completely blocked. We speculate that the C-terminal region plays an important role inside the procapsid to facilitate DNA packaging.

Screening of the motor ATPase with different sequences of ATPase pockets to control motor motion

Previously, it has been reported that the phi29 DNA packaging motor adapts sequential action for its coordination among subunits. (33,84) More recently, this coordination has been shown to be mediated by the arginine finger motif in the gp16 ATPase of phi29. (87) Phi29 motor ATPase gp16 shares the common ATP activity domain typical of all members of the ASCE superfamily, (91,99) including the very well conserved motifs responsible for ATP binding and ATP hydrolysis,(207) which have been previously identified as Walker A (6) and Walker B motifs,(83) respectively. Sequence alignment studies have further revealed a common arginine residue.(95,134,219-221) The alteration in arginine 146 severely impaired ATP hydrolysis activity and motor DNA binding activity, as confirmed by EMSA (Electrophoresis Mobility Shift Assay) and capillary electrophoresis assay, showing the approximately 4-fold reduction of the binding affinity of gp16 arginine finger mutant with dsDNA compared to that of wild-type gp16 (**Fig. 5.4**).

The presence of a non-covalent dimer of the ATPase gp16 has been shown by different approaches including electrophoresis mobility shift assay (EMSA), glycerol gradient ultracentrifugation, and native gel electrophoresis (**Fig. 5.4**).(83) Dimer formation requires that at least one of the adjacent subunits can provide an intact arginine for the inter-subunit interaction, since dimers were produced when the arginine-free ATPase was mixed with the wild type with an intact arginine, but not with the arginine-free ATPase (**Fig. 5.4**). Furthermore, it was shown that one single inactive subunit of arginine 146-free ATPase was able to completely, other than

partially, block the function of the entire motor, (87) that is, K = 1 in binomial distribution as described above, which implies that six ATPase molecules worked sequentially. (230,231,266)

The hexameric structure of gp16 ATPase has been constructed with *P. aeruginosa* FtsK (PDB ID: 2IUU) as a template(134) based on its predicted monomer structure using I-TASSER (268) software. The core structure of both N-domain of gp16 and beta-domain of FtsK with the length of 127 residues were aligned. And the RMSD of backbone carbon atoms in these core structure were calculated. Considering of the size of these two proteins and the protein structure after alignment, an RMSD of 3Å can effectively reflect that gp16's N-domain adopts same fold as FtsK's beta-domain. (269,270) The model showed that the position of arginine 146 in one ATPase subunit outstretches to the ATPase domain in a neighboring subunit (**Fig. 5.5**), which agrees with our data showing the cooperative behavior in the hexameric ATPase ring. As demonstrated above, it is concluded that arginine finger serves as a bridge between single subunits to form non-covalent dimers.

ATP binding and hydrolysis triggers conformational entropy changes of ATPase with high or low DNA binding affinity

ASCE proteins undergo a cycle of conformational changes upon ATP binding and hydrolysis with two major states: high or low affinity for the substrate.(271) In recent publications,(11,33,83,100) a similar model of sequential action for gp16 has been reported. Partial proteolysis treatment and tryptophan intrinsic fluorescence assays indicated a conformational change in the gp16-ATP complex, more specifically, a more constrained and less conformational entropy for gp16 before ATP binding. EMSA, capillary electrophoresis assays, and FRET assays showed stronger binding of gp16 to dsDNA when incubated with γ-S-ATP (**Fig. 5.4**), suggesting

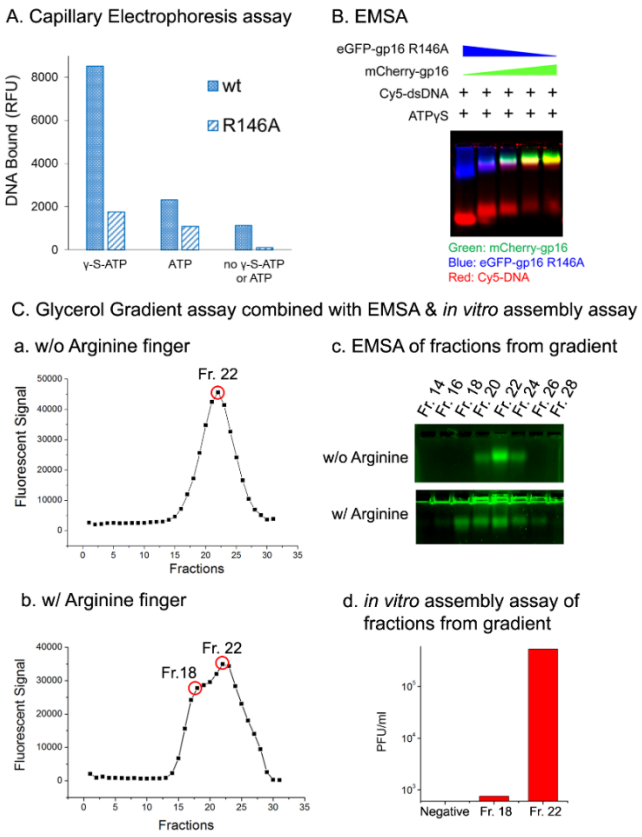

Figure 5.4. ATP binding and hydrolysis activity assay of gp16 arginine finger mutant and inter-subunit interactions of ATPase. (A) Capillary Electrophoresis assay for the binding affinity test of different gp16 with dsDNA. (B) Interactions between gp16 arginine finger mutants with gp16 wild-type are shown by the band shift of both ATPase and DNA in the gel. (C) Both dimers and monomers exist in gp16 ATPase rings. In 15%-35% glycerol gradient, one peak for eGFP-gp16 R146A (a) and two peaks for eGFP-gp16 wild-type (b) were observed after parallel ultracentrifugation, indicating that dimer formation is interrupted by the mutation of arginine finger. The fractions derived from the gradient have been applied to EMSA (c) and *in vitro* assembly activity assay, confirming the formation of dimers mediated by the arginine finger. The isolated gp16 dimer fraction (Fr. 18) showed significantly reduced activity compared to the monomers (Fr. 22) (d).

that the gp16/dsDNA complex is stabilized upon addition of the non-hydrolysable ATP substrate. The isolated gp16 dimer fraction (Fr. 18) showed significantly reduced activity compared to the monomers (Fr. 22) (d), supporting the previous finding that the addition of fresh gp16 monomer is required for re-initiating DNA packaging intermediates. (88)

As a dsDNA-dependent ATPase, (6,9,184) binding of the gp16/ATP complex to dsDNA resulted in ATP hydrolysis, leading to its second round of conformational entropy change to a low DNA-affinity configuration, and subsequently to the release of dsDNA for its concomitant transfer to the adjacent downstream subunit. An increased ATP hydrolysis rate has been observed when the ATPase is bound to DNA, indicating a global structural alternation in the protein upon DNA binding/release.(100) Taken together, a mechanism of ATPase for dsDNA translocation is proposed (**Fig. 5.6**) for constructions of active motors, showing that the energy consumption status corresponds to the inter-subunit communication primed by the arginine finger. The resulting asymmetrical hexameric intermediate was supported by many other hexameric ATPase systems based on structural computation, X-ray diffraction and Cryo-EM imaging (**Fig. 5.6**).(89,233-235) The results provide clues as to why the hexameric ATPase gp16 of phi29 and gp17 of T4 were previously interpreted as having a pentameric configuration by cryo-EM.(58,141)

Single-molecule real-time imaging of the biological active motor with continuous motion

The motion of the constructed artificial ATPase motor without the dodecameric channel and the RNA ring was confirmed by single-molecule fluorescence imaging (**Fig. 5.7**). Purified ATPase was labeled with Cy3 fluorescent dye and incubated with DNA, which is tethered between two polylysine beads. The motion of fluorescent spots representing the ATPase complexes was observed along the DNA chains through real-time recording, which confirmed the translocating activity of ATPase along dsDNA. Next, the successful construction of the artificial motor

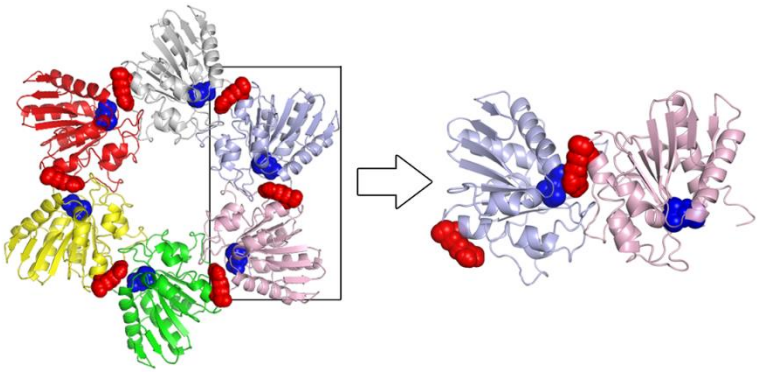

Figure 5.5. Illustration of inter-subunit interaction inside gp16 ATPase. Gp16 ATPase hexameric ring was constructed (left panel), and the interaction between two adjacent subunits (right panel) has been shown with the arginine finger highlighted in the red sphere and Walker domain (represented by E119 residue in Walker B domain) highlighted in the blue sphere. The interaction of arginine finger with the upstream adjacent subunit is supported by the relative location of the related domains.

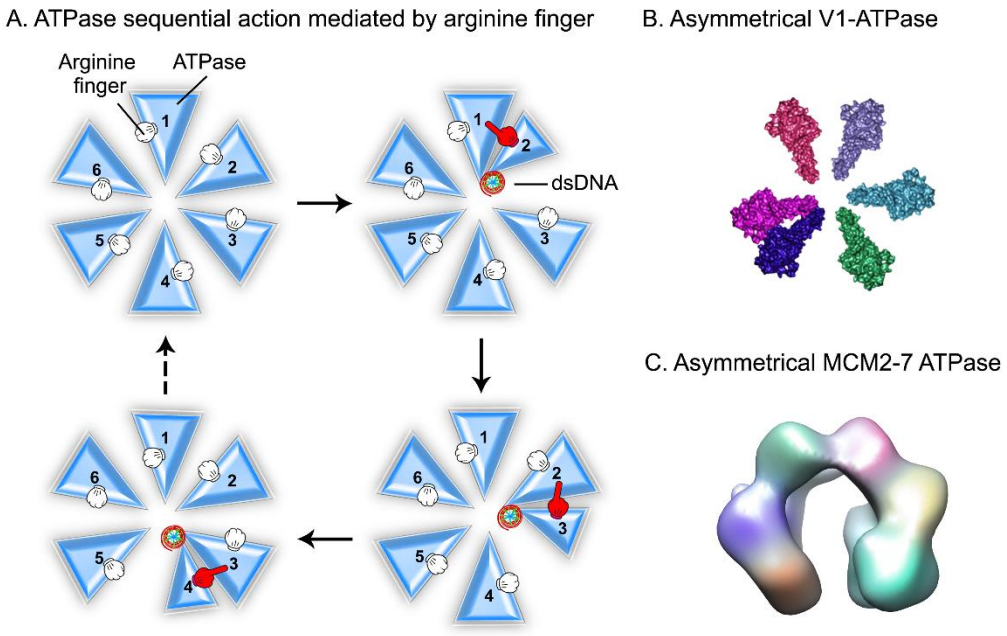

Figure 5.6. Asymmetrical ATPase structure caused by sequential action. (A) ATPase coordination with a series of conformational changes during DNA binding and ATP hydrolysis as regulated by the arginine finger, resulting in the asymmetrical configuration of ATPase. (B) The asymmetrical structures have also been found in many other biomotors, including V1-ATPase (89) (B) and MCM2-7 protein (EM accession:EMD-5429) (90) (C).

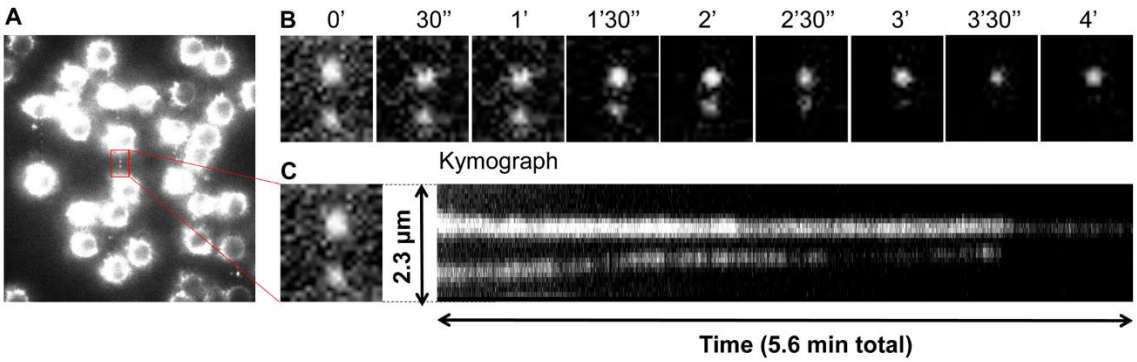

Figure 5.7. Single-molecule detection of the continuous ATPase translocation on dsDNA. (A) The gp16 complex labeled with Cy3 (33) moved along the dsDNA chain tethered between two polylysine coated beads. (B) The motion of the Cy3-gp16 complex was analyzed by *Image J* and (C) a kymograph was generated to demonstrate the motion of the ATPase.

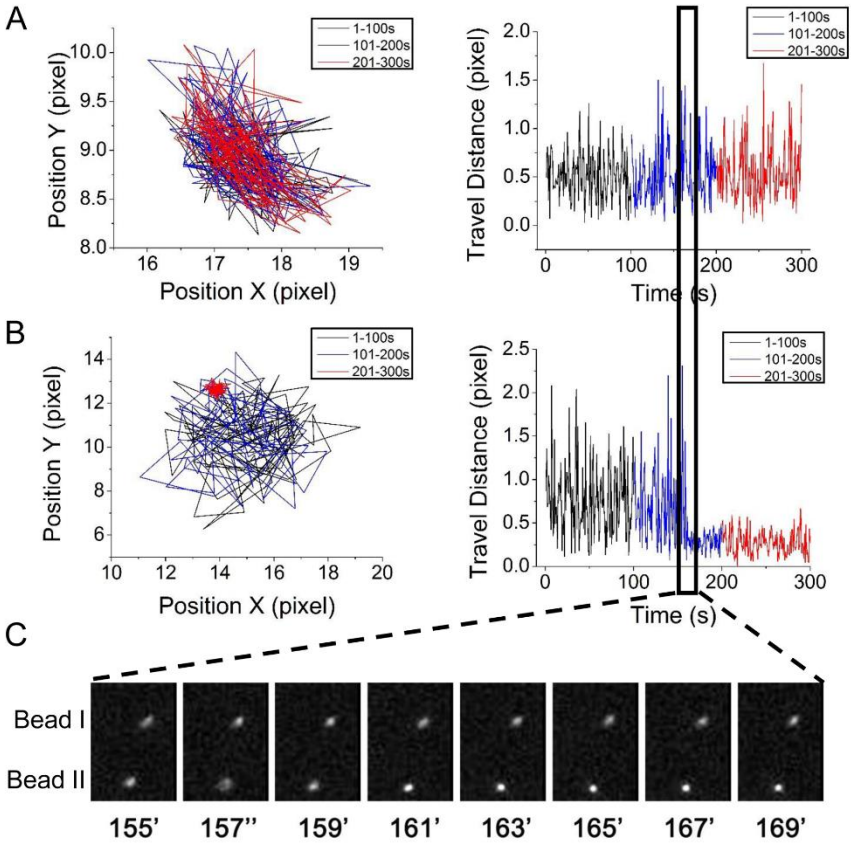

Figure 5.8. Single-molecule detection of continuous DNA translocation in the phi29 biomotor. Comparison of the trajectories and travel distance of microspheres attached to the end of DNA in two different packaging intermediates Beads I (A) and Beads II (B). Beads I showed random Brownian motion. Bead II also showed Brownian motion at the beginning, however, such motion ceased after around 150 seconds, indicating the end of the translocation event. The stalling of the dsDNA serves as evidence of uni-directional translocation. (C) Sequential images of a fluorescent microsphere attached to DNA, corresponding to when Beads II tends to stop as indicated in the figure.

containing both dodecameric ring and RNA hexamer to drive dsDNA was tested by fluorescence imaging in real time. DNA translocation was recorded through the biomotor constructed with all active motor components. The functional motor was stalled using non-hydrolysable γ-S-ATP, isolated (53,88) and then attached to a slide. The distal end of the dsDNA was labeled with a biotin moiety and attached to a fluorescent streptavidin-coated microsphere. After addition of ATP, the continuous motion of the motor was resumed and observed by real-time fluorescence microscopy through epi-illumination (**Fig. 5.8**).

Analysis of the motion in x, y, and z dimensions showed that the swing distance of the microsphere was reduced as the motion process was close to the end of packaging. As a control, the microsphere exhibited a mainly linear and static Brownian motion when the stalled motor was not restarted, indicating that the constructed motor was functional in continuous DNA translocation with a one-way direction (**Fig. 5.8**). Single directional motion of the motor was also detected in real time using a horizontal setup with biomotors assembled in the procapsids, (128) which confirmed the successful construction of the artificial motor with the control of motion direction.

CONCLUSIONS

Based on the one-way revolving mechanism of the phi29 dsDNA packaging motor, we have successfully constructed phi29 biomimetic nanomotors with altered and modified pRNA, ATPase and protein channel with single-directional motion. Arginine finger bridges two adjacent ATPase subunits to form a non-covalent dimer, resulting in an asymmetrical hexameric complex. Single direction motion of the dsDNA was controlled by three sets of operation elements: 1) the asymmetrical hexameric ATPase containing one dimeric and four monomeric subunits that hold

an ATP-interacting domain to regulate alternative DNA binding and also push an arginine finger to control the sequential action; 2) the dsDNA translocation channel that serves as a one-way valve to ensure single direction advancement and to prevent the reversal of the dsDNA; 3) the hexameric pRNA ring geared with their left and right-hand loops. Assessment of the resulting constructs revealed that one inactive subunit of pRNA or ATPase is sufficient to completely, other than partially, block the function of the entire motor. The finding of K = 1 implies sequential action with single directional motion, based on the criterion of binomial distribution and Yang Hui's Triangle.

ACKNOWLEDGEMENTS

The authors would like to thank Mario Vieweger for the analysis of single-molecule recording. The work was supported by NIH grant R01-EB012135, and R01-EB019036 to PG. Funding to P.G.'s Sylvan G. Frank Endowed Chair position in Pharmaceutics and Drug Delivery is by CM Chen Foundation. P.G. is a consultant of Oxford Nanopore and NanoBio RNA Technology Co. Ltd. The content is solely the responsibility of the authors and does not necessarily represent the official views of NIH.

Chapter 6: Future Direction of DNA Packaging Motors

The phi29 DNA-packaging nanomotor (7) is a biomolecular motor, which can package its genome into the procapsid through revolving with the energy from the binding and hydrolysis of ATP. It is one of the strongest biological motors known by far, capable of generating force up to 57-110 pN (4). In addition, it is the most efficient *in vitro* DNA packaging system, with up to 90% of the genomic DNA being packaged into its procapsid. All motor components have been constructed to be viable, visible outside native environment for stability and detection. Viral components are a new generation of nano-scale building blocks that are robust, have the ability to self-assemble and operate outside their natural environment. The host of Phi29 bacteriophage, *Bacillus Subtilis,* is not considered pathogenic or toxic, and is not a disease causing agent. Being a nonpathogenic virus, Phi29 bacteriophage has a great potential to serve as a gene delivery vector. The re-engineering of the bio-nanomotors for therapeutics loading and delivery, and the development of the controls will be highly useful towards the applications and operations of the motors.

As stated in the previous chapters, the motor is composed of a dodecameric connector at the vertex of the procapsid, geared by a hexameric pRNA ring (7) which encircles the N-terminus of the connector (55,272,273) , and a hexameric ring of gp16 which functions as an ATPase to drive the motor (6,9). To fully realize the potential of the bio-nanomotors, the motor components should be entirely understood. We have exploited nature's ingenious design of the Phi29 DNA packaging motor (59,139). For example, the connector has been successfully inserted into a lipid bilayer for single-molecule sensing of chemical and biopolymer, and potential DNA sequencing(28,29,139,228,229). Furthermore, the pRNA three-way junction motif has been used as a basis for design of ultrastable RNA nanoparticles as a therapeutic delivery device (59,70). We

may now move our steps further to use our extensive understanding of the phage and it's mechanism of packaging (100) to design an artificial motor with packaged therapeutics. The non-specificity of the ATPase of Phi29 allows the packaging of foreign substrates to high doses. The Phi29 bacteriophage has large packaging capacity with the phage coat serving as a protection from degradation. The phage particle can be incorporated with different functionalities and target the antigen presenting cells. The engineered motor may be used for loading and pumping therapeutic molecules into specifically targeted cells. Controlled packaging, external targeting moieties, and a multivalent nature are desired for targeted drug delivery, such a functional motor creates great opportunities to advance the field of nanotechnology and biomedicine.

REFERENCES

1. Grigoriev, D. N., Moll, W., Hall, J., and Guo, P. (2004) Bionanomotor. In Nalwa, H. S., editor. *Encyclopedia of Nanoscience and Nanotechnology*, American Scientific Publishers.,

2. Martin A, Baker TA, & Sauer RT (2005) Rebuilt AAA + Motors Reveal Operating Principles for ATP-Fuelled Machines. *Nature* 437: 1115-1120

3. Ammelburg M, Frickey T, & Lupas AN (2006) Classification of AAA+ Proteins. *J Struct Biol* 156: 2-11

4. Smith DE, Tans SJ, Smith SB, Grimes S, Anderson DL, & Bustamante C (2001) The Bacteriophage Phi29 Portal Motor Can Package DNA Against a Large Internal Force. *Nature* 413: 748-752

5. Guo P, Grimes S, & Anderson D (1986) A Defined System for *in Vitro* Packaging of DNA-Gp3 of the *Bacillus Subtilis* Bacteriophage Phi29. *Proc. Natl. Acad. Sci. USA* 83: 3505-3509

6. Guo P, Peterson C, & Anderson D (1987) Prohead and DNA-Gp3-Dependent ATPase Activity of the DNA Packaging Protein Gp16 of Bacteriophage Phi29. *J Mol Biol* 197: 229-236

7. Guo P, Erickson S, & Anderson D (1987) A Small Viral RNA Is Required for *in Vitro* Packaging of Bacteriophage Phi29 DNA. *Science* 236: 690-694

8. Lee TJ & Guo P (2006) Interaction of Gp16 With PRNA and DNA for Genome Packaging by the Motor of Bacterial Virus Phi29. *J. Mol Biol.* 356: 589-599

9. Ibarra B, Valpuesta JM, & Carrascosa JL (2001) Purification and Functional Characterization of P16, the ATPase of the Bacteriophage Phi29 Packaging Machinary. *Nucleic Acids Res.* 29: 4264-4273

10. Guo PX & Lee TJ (2007) Viral Nanomotors for Packaging of DsDNA and DsRNA. *Mol. Microbiol.* 64: 886-903

11. Zhang H, Schwartz C, De Donatis GM, & Guo P (2012) "Push Through One-Way Valve" Mechanism of Viral DNA Packaging. *Adv. Virus Res* 83: 415-465

12. Serwer P (2010) A Hypothesis for Bacteriophage DNA Packaging Motors. *Viruses* 2: 1821-1843

13. Yu J, Moffitt J, Hetherington CL, Bustamante C, & Oster G (2010) Mechanochemistry of a Viral DNA Packaging Motor. *J. Mol. Biol.* 400: 186-203

14. Moffitt JR, Chemla YR, Aathavan K, Grimes S, Jardine PJ, Anderson DL, & Bustamante C (2009) Intersubunit Coordination in a Homomeric Ring ATPase. *Nature* 457: 446-450

15. Aathavan K, Politzer AT, Kaplan A, Moffitt JR, Chemla YR, Grimes S, Jardine PJ, Anderson DL, & Bustamante C (2009) Substrate Interactions and Promiscuity in a Viral DNA Packaging Motor. *Nature* 461: 669-673

16. Hendrix RW (1978) Symmetry Mismatch and DNA Packaging in Large Bacteriophages. *Proc. Natl. Acad. Sci. USA* 75: 4779-4783

17. Sabanayagam CR, Oram M, Lakowicz JR, & Black LW (2007) Viral DNA Packaging Studied by Fluorescence Correlation Spectroscopy. *Biophys. J* 93: L17-L19

18. Khan SA, Hayes SJ, Wright ET, Watson RH, & Serwer P (1995) Specific Single-Stranded Breaks in Mature Bacteriophage T7 DNA. *Virology* 211: 329-331

19. Oram M, Sabanayagam C, & Black LW (2008) Modulation of the Packaging Reaction of Bacteriophage T4 Terminase by DNA Structure. *J Mol Biol* 381: 61-72

20. Fujisawa H & Morita M (1997) Phage DNA Packaging. *Genes Cells* 2: 537-545

21. Lebedev AA, Krause MH, Isidro AL, Vagin AA, Orlova EV, Turner J, Dodson EJ, Tavares P, & Antson AA (2007) Structural Framework for DNA Translocation *Via* the Viral Portal Protein. *EMBO J.* 26: 1984-1994

22. Guo P, Peterson C, & Anderson D (1987) Initiation Events in *in Vitro* Packaging of Bacteriophage Phi29 DNA-Gp3. *J Mol Biol* 197: 219-228

23. Serwer P (2003) Models of Bacteriophage DNA Packaging Motors. *J Struct. Biol* 141: 179-188

24. Chen DH, Baker ML, Hryc CF, DiMaio F, Jakana J, Wu W, Dougherty M, Haase-Pettingell C, Schmid MF, Jiang W, Baker D, King JA, & Chiu W (2011) Structural Basis for Scaffolding-Mediated Assembly and Maturation of a DsDNA Virus. *Proc. Natl. Acad. Sci. U. S. A* 108: 1355-1360

25. Donate LE, Herranz L, Secilla JP, Carazo JM, Fujisawa H, & Carrascosa JL (1988) Bacteriophage T3 Connector: Three-Dimensional Structure and Comparison With Other Viral Head-Tail Connecting Regions. *J Mol Biol* 201: 91-100

26. De-Donatis G, Zhao Z, Wang S, Huang PL, Schwartz C, Tsodikov VO, Zhang H, Haque F, & Guo P (2014) Finding of Widespread Viral and Bacterial Revolution DsDNA Translocation Motors Distinct From Rotation Motors by Channel Chirality and Size. *Cell Biosci* 4: 30

27. Guasch A, Pous J, Ibarra B, Gomis-Ruth FX, Valpuesta JM, Sousa N, Carrascosa JL, & Coll M (2002) Detailed Architecture of a DNA Translocating Machine: the High-Resolution Structure of the Bacteriophage Phi29 Connector Particle. *J. Mol. Biol.* 315: 663-676

28. Jing P, Haque F, Vonderheide A, Montemagno C, & Guo P (2010) Robust Properties of Membrane-Embedded Connector Channel of Bacterial Virus Phi29 DNA Packaging Motor. *Mol. Biosyst.* 6: 1844-1852

29. Jing P, Haque F, Shu D, Montemagno C, & Guo P (2010) One-Way Traffic of a Viral Motor Channel for Double-Stranded DNA Translocation. *Nano Lett.* 10: 3620-3627

30. Geng J, Fang H, Haque F, Zhang L, & Guo P (2011) Three Reversible and Controllable Discrete Steps of Channel Gating of a Viral DNA Packaging Motor. *Biomaterials* 32: 8234-8242

31. Fang H, Jing P, Haque F, & Guo P (2012) Role of Channel Lysines and "Push Through a One-Way Valve" Mechanism of Viral DNA Packaging Motor. *Biophysical Journal* 102: 127-135

32. Zhao Z, Khisamutdinov E, Schwartz C, & Guo P (2013) Mechanism of One-Way Traffic of Hexameric Phi29 DNA Packaging Motor With Four Electropositive Relaying Layers Facilitating Anti-Parallel Revolution. *ACS Nano* 7: 4082-4092

33. Schwartz C, De Donatis GM, Zhang H, Fang H, & Guo P (2013) Revolution Rather Than Rotation of AAA+ Hexameric Phi29 Nanomotor for Viral DsDNA Packaging Without Coiling. *Virology* 443: 28-39

34. Geng J, Wang S, Fang H, & Guo P (2013) Channel Size Conversion of Phi29 DNA-Packaging Nanomotor for Discrimination of Single- and Double-Stranded Nucleic Acids. *ACS Nano* 7: 3315-3323

35. Urbaneja MA, Rivqas S, Carrascosa JL, & Valpuesta JM (1994) An Intrinsic-Tryptophan-Fluorescence Study of Phage Phi29 Connector/Nucleic Acid Interactions. *Eur. J. Biochem.* 225: 747-753

36. Tolley AC & Stonehouse NJ (2008) Conformational Changes in the Connector Protein Complex of the Bacteriophage Phi29 DNA Packaging Motor. *Computational and Mathematical Methods in Medicine* 9: 327-337

37. Wang S, Ji Z, Yan E, Haque F, & Guo P (2016) Three-Step Channel Conformational Changes Common to DNA Packaging Motors of Bacterial Viruses T3, T4, SPP1, and Phi29. *Virology*

38. Tang JH, Olson N, Jardine PJ, Girimes S, Anderson DL, & Baker TS (2008) DNA Poised for Release in Bacteriophage Phi29. *Structure* 16: 935-943

39. Zhang CL, Lee C-S, & Guo P (1994) The Proximate 5' and 3' Ends of the 120-Base Viral RNA (PRNA) Are Crucial for the Packaging of Bacteriophage F29 DNA. *Virology* 201: 77-85

40. Zhang CL, Tellinghuisen T, & Guo P (1995) Confirmation of the Helical Structure of the 5'/3' Termini of the Essential DNA Packaging PRNA of Phage F29. *RNA* 1: 1041-1050

41. Zhang CL, Trottier M, & Guo PX (1995) Circularly Permuted Viral PRNA Active and Specific in the Packaging of Bacteriophage Phi29 DNA. *Virology* 207: 442-451

42. Zhang CL, Garver K, & Guo P (1995) Inhibition of Phage Phi29 Assembly by Antisense Oligonucleotides Targeting Viral PRNA Essential for DNA Packaging. *Virology* 211: 568-576

43. Zhang CL, Tellinghuisen T, & Guo P (1997) Use of Circular Permutation to Assess Six Bulges and Four Loops of DNA-Packaging PRNA of Bacteriophage Phi29. *RNA* 3: 315-322

44. Chen C & Guo P (1997) Magnesium-Induced Conformational Change of Packaging RNA for Procapsid Recognition and Binding During Phage Phi29 DNA Encapsidation. *J. Virol.* 71: 495-500

45. Chen C, Sheng S, Shao Z, & Guo P (2000) A Dimer As a Building Block in Assembling RNA: A Hexamer That Gears Bacterial Virus Phi29 DNA-Translocating Machinery. *J Biol Chem* 275(23): 17510-17516

46. Reid RJD, Bodley JW, & Anderson D (1994) Identification of Bacteriophage Phi29 Prohead RNA (PRNA) Domains Necessary for *in Vitro* DNA-Gp3 Packaging. *J. Biol. Chem.* 269: 9084-9089

47. Reid RJD, Zhang F, Benson S, & Anderson D (1994) Probing the Structure of Bacteriophage Phi29 Prohead RNA With Specific Mutations. *J Biol Chem* 269: 18656-18661

48. Reid RJD, Bodley JW, & Anderson D (1994) Characterization of the Prohead-PRNA Interaction of Bacteriophage Phi29. *J Biol Chem* 269: 5157-5162

49. Guo P, Zhang C, Chen C, Trottier M, & Garver K (1998) Inter-RNA Interaction of Phage Phi29 PRNA to Form a Hexameric Complex for Viral DNA Transportation. *Mol. Cell.* 2: 149-155

50. Zhang F, Lemieux S, Wu X, St.-Arnaud S, McMurray CT, Major F, & Anderson D (1998) Function of Hexameric RNA in Packaging of Bacteriophage Phi29 DNA in Vitro. *Mol. Cell.* 2: 141-147

51. Hendrix RW (1998) Bacteriophage DNA Packaging: RNA Gears in a DNA Transport Machine (Minireview). *Cell* 94: 147-150

52. Ibarra B, Caston J.R., Llorca O., Valle M, Valpuesta J.M., & Carrascosa J.L. (2000) Topology of the Components of the DNA Packaging Machinery in the Phage Phi29 Prohead. *J. Mol. Biol.* 298: 807-815

53. Shu D, Zhang H, Jin J, & Guo P (2007) Counting of Six PRNAs of Phi29 DNA-Packaging Motor With Customized Single Molecule Dual-View System. *EMBO J.* 26: 527-537

54. Moll D & Guo P (2007) Grouping of Ferritin and Gold Nanoparticles Conjugated to PRNA of the Phage Phi29 DNA-Packaging Motor. *J Nanosci and Nanotech (JNN)* 7: 3257-3267

55. Xiao F, Zhang H, & Guo P (2008) Novel Mechanism of Hexamer Ring Assembly in Protein/RNA Interactions Revealed by Single Molecule Imaging. *Nucleic Acids Res* 36: 6620-6632

56. Zhang H, Endrizzi JA, Shu Y, Haque F, Sauter C, Shlyakhtenko LS, Lyubchenko Y, Guo P, & Chi YI (2013) Crystal Structure of 3WJ Core Revealing Divalent Ion-Promoted Thermostability and Assembly of the Phi29 Hexameric Motor PRNA. *RNA* 19: 1226-1237

57. Chistol G, Liu S, Hetherington CL, Moffitt JR, Grimes S, Jardine PJ, & Bustamante C (2012) High Degree of Coordination and Division of Labor Among Subunits in a Homomeric Ring ATPase. *Cell* 151: 1017-1028

58. Morais MC, Koti JS, Bowman VD, Reyes-Aldrete E, Anderson D, & Rossman MG (2008) Defining Molecular and Domain Boundaries in the Bacteriophage Phi29 DNA Packaging Motor. *Structure* 16: 1267-1274

59. Shu D, Shu Y, Haque F, Abdelmawla S, & Guo P (2011) Thermodynamically Stable RNA Three-Way Junctions for Constructing Multifuntional Nanoparticles for Delivery of Therapeutics. *Nature Nanotechnology* 6: 658-667

60. Binzel DW, Khisamutdinov EF, & Guo P (2014) Entropy-Driven One-Step Formation of Phi29 PRNA 3WJ From Three RNA Fragments. *Biochemistry* 53: 2221-2231

61. Jasinski D, Khisamutdinov EF, Lyubchenko YL, & Guo P (2014) Physicochemically Tunable Poly-Functionalized RNA Square Architecture With Fluorogenic and Ribozymatic Properties. *ACS Nano* 8: 7620-7629

62. Khisamutdinov EF, Jasinski DL, & Guo P (2014) RNA As a Boiling-Resistant Anionic Polymer Material to Build Robust Structures With Defined Shape and Stoichiometry. *ACS Nano.* 8: 4771-4781

63. Khisamutdinov E, Li H, Jasinski D, Chen J, Fu J, & Guo P (2014) Enhancing Immunomodulation on Innate Immunity by Shape Transition Among RNA Triangle, Square, and Pentagon Nanovehicles. *Nucleic Acids Res.* 42: 9996-10004

64. Lee TJ, Haque F, Shu D, Yoo JY, Li H, Yokel RA, Horbinski C, Kim TH, Kim S-H, Nakano I, Kaur B, Croce CM, & Guo P (2015) RNA Nanoparticles As a Vector for Targeted SiRNA Delivery into Glioblastoma Mouse Model. *Oncotarget* 6: 14766-14776

65. Shu D, Li H, Shu Y, Xiong G, Carson WE, Haque F, Xu R, & Guo P (2015) Systemic Delivery of Anti-MiRNA for Suppression of Triple Negative Breast Cancer Utilizing RNA Nanotechnology. *ACS Nano* 9: 9731-9740

66. Shu Y, Haque F, Shu D, Li W, Zhu Z, Kotb M, Lyubchenko Y, & Guo P (2013) Fabrication of 14 Different RNA Nanoparticles for Specific Tumor Targeting Without Accumulation in Normal Organs. *RNA* 19: 766-777

67. Binzel D, Shu Y, Shu D, & Guo P (2015) Prostate Cancer Targeting Using PSMA Aptamer Incorporated in the 3WJ of the Phi29 Motor PRNA for Specific Delivery of MiRNA. *Nature Medicine* -Submitted

68. Cui D, Zhang C, Liu B, Shu Y, Du T, Shu D, Wang K, Dai F, Liu Y, Li C, Pan F, Yang Y, Ni J, Li H, Brand-Saberi B, & Guo P (2015) Regression of Gastric Cancer by Systemic Injection of RNA Nanoparticles Carrying Both Ligand and SiRNA. *Scientific reports* 5: 10726

69. Feng L, Li SK, Liu H, Liu CY, LaSance K, Haque F, Shu D, & Guo P (2014) Ocular Delivery of PRNA Nanoparticles: Distribution and Clearance After Subconjunctival Injection. *Pharmaceutical Research* 31: 1046-1058

70. Haque F, Shu D, Shu Y, Shlyakhtenko L, Rychahou P, Evers M, & Guo P (2012) Ultrastable Synergistic Tetravalent RNA Nanoparticles for Targeting to Cancers. *Nano Today* 7: 245-257

71. Abdelmawla S, Guo S, Zhang L, Pulukuri S, Patankar P, Conley P, Trebley J, Guo P, & Li QX (2011) Pharmacological Characterization of Chemically Synthesized Monomeric PRNA Nanoparticles for Systemic Delivery. *Molecular Therapy* 19: 1312-1322

72. Hoeprich S, ZHou Q, Guo S, Qi G, Wang Y, & Guo P (2003) Bacterial Virus Phi29 PRNA As a Hammerhead Ribozyme Escort to Destroy Hepatitis B Virus. *Gene Ther.* 10: 1258-1267

73. Khaled A, Guo S, Li F, & Guo P (2005) Controllable Self-Assembly of Nanoparticles for Specific Delivery of Multiple Therapeutic Molecules to Cancer Cells Using RNA Nanotechnology. *Nano Letters* 5: 1797-1808

74. Guo S, Tschammer N, Mohammed S, & Guo P (2005) Specific Delivery of Therapeutic RNAs to Cancer Cells Via the Dimerization Mechanism of Phi29 Motor PRNA. *Hum Gene Ther.* 16: 1097-1109

75. Guo S, Huang F, & Guo P (2006) Construction of Folate-Conjugated PRNA of Bacteriophage Phi29 DNA Packaging Motor for Delivery of Chimeric SiRNA to Nasopharyngeal Carcinoma Cells. *Gene Ther* 13: 814-820

76. Shu Y, Cinier M, Fox SR, Ben-Johnathan N, & Guo P (2011) Assembly of Therapeutic PRNA-SiRNA Nanoparticles Using Bipartite Approach. *Molecular Therapy* 19: 1304-1311

77. Shu Y, Cinier M, Shu D, & Guo P (2011) Assembly of Multifunctional Phi29 PRNA Nanoparticles for Specific Delivery of SiRNA and Other Therapeutics to Targeted Cells. *Methods* 54: 204-214

78. Guo P, Shu Y, Binzel D, & Cinier M (2012) Synthesis, Conjugation, and Labeling of Multifunctional PRNA Nanoparticles for Specific Delivery of SiRNA, Drugs and Other Therapeutics to Target Cells. *Methods in Molecular Biology* 928: 197-219

79. Guo P, Haque F, Hallahan B, Reif R, & Li H (2012) Uniqueness, Advantages, Challenges, Solutions, and Perspectives in Therapeutics Applying RNA Nanotechnology. *Nucleic Acid Ther.* 22: 226-245

80. Zhou J, Shu Y, Guo P, Smith D, & Rossi J (2011) Dual Functional RNA Nanoparticles Containing Phi29 Motor PRNA and Anti-Gp120 Aptamer for Cell-Type Specific Delivery and HIV-1 Inhibition. *Methods* 54: 284-294

81. Shukla GC, Haque F, Tor Y, Wilhelmsson LM, Toulme JJ, Isambert H, Guo P, Rossi JJ, Tenenbaum SA, & Shapiro BA (2011) A Boost for the Emerging Field of RNA Nanotechnology. *ACS Nano* 5: 3405-3418

82. Guo P (2010) The Emerging Field of RNA Nanotechnology. *Nature Nanotechnology* 5: 833-842

83. Schwartz C, De Donatis GM, Fang H, & Guo P (2013) The ATPase of the Phi29 DNA-Packaging Motor Is a Member of the Hexameric AAA+ Superfamily. *Virology* 443: 20-27

84. Chen C & Guo P (1997) Sequential Action of Six Virus-Encoded DNA-Packaging RNAs During Phage Phi29 Genomic DNA Translocation. *J. Virol.* 71: 3864-3871

85. Trottier M & Guo P (1997) Approaches to Determine Stoichiometry of Viral Assembly Components. *J. Virol.* 71: 487-494

86. Chen C, Trottier M, & Guo P (1997) New Approaches to Stoichiometry Determination and Mechanism Investigation on RNA Involved in Intermediate Reactions. *Nucleic Acids Symposium Series* 36: 190-193

87. Zhao Z, De-Donatis GM, Schwartz C, Fang H, Li J, & Guo P (2016) Arginine Finger Regulates Sequential Action of Asymmetrical Hexameric ATPase in DsDNA Translocation Motor. *Mol Cell Biol* in press:

88. Shu D & Guo P (2003) Only One PRNA Hexamer but Multiple Copies of the DNA-Packaging Protein Gp16 Are Needed for the Motor to Package Bacterial Virus Phi29 Genomic DNA. *Virology* 309(1): 108-113

89. Arai S, Saijo S, Suzuki K, Mizutani K, Kakinuma Y, Ishizuka-Katsura Y, Ohsawa N, Terada T, Shirouzu M, Yokoyama S, Iwata S, Yamato I, & Murata T (2013) Rotation Mechanism of Enterococcus Hirae V1-ATPase Based on Asymmetric Crystal Structures. *Nature* 493: 703-707

90. Lyubimov AY, Costa A, Bleichert F, Botchan MR, & Berger JM (2012) ATP-Dependent Conformational Dynamics Underlie the Functional Asymmetry of the Replicative Helicase From a Minimalist Eukaryote. *Proc. Natl. Acad. Sci. U. S. A* 109: 11999-12004

91. Snider J & Houry WA (2008) AAA+ Proteins: Diversity in Function, Similarity in Structure. *Biochemical Society Transactions* 36: 72-77

92. Aker J, Hesselink R, Engel R, Karlova R, Borst JW, Visser AJWG, & de Vries SC (2007) *In Vivo* Hexamerization and Characterization of the Arabidopsis AAA ATPase CDC48A Complex Using Forster Resonance Energy Transfer-Fluorescence Lifetime Imaging Microscopy and Fluorescence Correlation Spectroscopy. *Plant Physiology* 145: 339-350

93. White SR & Lauring B (2007) AAA+ ATPases: Achieving Diversity of Function With Conserved Machinery. *Traffic* 8: 1657-1667

94. Matias PM, Gorynia S, Donner P, & Carrondo MA (2006) Crystal Structure of the Human AAA+ Protein RuvBL1. *J. Biol. Chem.* 281: 38918-38929

95. Iyer LM, Leipe DD, Koonin EV, & Aravind L (2004) Evolutionary History and Higher Order Classification of AAA Plus ATPases. *J Struct Biol* 146: 11-31

96. Chen YJ, Yu X, & Egelman EH (2002) The Hexameric Ring Structure of the Escherichia Coli RuvB Branch Migration Protein. *J. Mol. Biol.* 319: 587-591

97. Singleton MR, Dillingham MS, & Wigley DB (2007) Structure and Mechanism of Helicases and Nucleic Acid Translocases. *Ann. Rev. Biochem.* 76: 23-50

98. Kainov DE, Tuma R, & Mancini EJ (2006) Hexameric Molecular Motors: P4 Packaging ATPase Unravels the Mechanism. *Cellular and Molecular Life Sciences* 63(10): 1095-1105

99. Hanson PI & Whiteheart SW (2005) AAA+ Proteins: Have Engine, Will Work. *Nat. Rev. Mol Cell Biol.* 6: 519-529

100. Schwartz C, Fang H, Huang L, & Guo P (2012) Sequential Action of ATPase, ATP, ADP, Pi and DsDNA in Procapsid-Free System to Enlighten Mechanism in Viral DsDNA Packaging. *Nucleic Acids Res.* 40: 2577-2586

101. Snider J, Thibault G, & Houry WA (2008) The AAA+ Superfamily of Functionally Diverse Proteins. *Genome Biol* 9: 216

102. Guo P, Schwartz C, Haak J, & Zhao Z (2013) Discovery of a New Motion Mechanism of Biomotors Similar to the Earth Revolving Around the Sun Without Rotation. *Virology* 446: 133-143

103. Guo P, Zhao Z, Haak J, Wang S, Wu D, Meng B, & Weitao T (2014) Common Mechanisms of DNA Translocation Motors in Bacteria and Viruses Using One-Way Revolution Mechanism Without Rotation. *Biotechnology Advances* 32: 853-872

104. Zhang YB, Yuan FH, Presnell SR, Tian KL, Gao Y, Tomkinson AE, Gu LY, & Li GM (2005) Reconstitution of 5 '-Directed Human Mismatch Repair in a Purified System. *Cell* 122: 693-705

105. Shu Y, Shu D, Haque F, & Guo P (2013) Fabrication of PRNA Nanoparticles to Deliver Therapeutic RNAs and Bioactive Compounds into Tumor Cells. *Nat Protoc.* 8: 1635-1659

106. Xiao F, Sun J, Coban O, Schoen P, Wang JC, Cheng RH, & Guo P (2009) Fabrication of Massive Sheets of Single Layer Patterned Arrays Using Lipid Directed Reengineered Phi29 Motor Dodecamer. *ACS Nano* 3: 100-107

107. Xiao F, Demeler B, & Guo P (2010) Assembly Mechanism of the Sixty-Subunit Nanoparticles *Via* Interaction of RNA With the Reengineered Protein Connector of Phi29 DNA-Packaging Motor. *ACS Nano.* 4: 3293-3301

108. Mehta A (2001) Myosin Learns to Walk. *J Cell Sci* 114: 1981-1998

109. Visscher K, Schnitzer MJ, & Block SM (1999) Single Kinesin Molecules Studied With a Molecular Force Clamp. *Nature* 400: 184-189

110. Vale RD, Funatsu T, Pierce DW, Romberg L, Harada Y, & Yanagida T (1996) Direct Observation of Single Kinesin Molecules Moving Along Microtubules. *Nature* 380: 451-453

111. Harada Y, Ohara O, Takatsuki A, Itoh H, Shimamoto N, & Kinosita K, Jr. (2001) Direct Observation of DNA Rotation During Transcription by Escherichia Coli RNA Polymerase. *Nature* 409: 113-115

112. Doering C, Ermentrout B, & Oster G (1998) Rotary DNA Motors. *Biophysical Journal* 69: 2256-2267

113. Ariga T, Masaike T, Noji H, & Yoshida M (2002) Stepping Rotation of F(1)-ATPase With One, Two, or Three Altered Catalytic Sites That Bind ATP Only Slowly. *J Biol. Chem* 277: 24870-24874

114. Casjens SR (2011) The DNA-Packaging Nanomotor of Tailed Bacteriophages. *Nat Rev. Microbiol.* 9: 647-657

115. Roos WH, Ivanovska IL, Evilevitch A, & Wuite GJL (2007) Viral Capsids: Mechanical Characteristics, Genome Packaging and Delivery Mechanisms. *Cellular and Molecular Life Sciences* 64: 1484-1497

116. Catalano CE (2000) The Terminase Enzyme From Bacteriophage Lambda: a DNA-Packaging Machine. *Cell Mol. Life Sci.* 57: 128-148

117. Hwang JS & Bogner E (2002) ATPase Activity of the Terminase Subunit PUL56 of Human Cytomegalovirus. *J Biol. Chem* 277: 6943-6948

118. Gual A, Camacho AG, & Alonso JC (2000) Functional Analysis of the Terminase Large Subunit, G2P, of Bacillus Subtilis Bacteriophage SPP1. *J. Biol. Chem.* 275: 35311-35319

119. Hang JQ, Tack BF, & Feiss M (2000) ATPase Center of Bacteriophage Lambda Terminase Involved in Post- Cleavage Stages of DNA Packaging: Identification of ATP-Interactive Amino Acids. *J. Mol. Biol.* 302: 777-795

120. Hwang Y, Catalano CE, & Feiss M (1996) Kinetic and Mutational Dissection of the Two ATPase Activities of Terminase, the DNA Packaging Enzyme of Bacteriophage Lambda. *Biochemistry* 35: 2796-2803

121. Rubinchik S, Parris W, & Gold M (1994) The in Vitro ATPases of Bacteriophage Lambda Terminase and Its Large Subunit, Gene Product A. The Relationship With Their DNA Helicase and Packaging Activities. *J Biol Chem* 269: 13586-13593

122. Morita M, Tasaka M, & Fujisawa H (1993) DNA Packaging ATPase of Bacteriophage T3. *Virology* 193: 748-752

123. Koonin EV, SENKEVICH TG, & Chernos VI (1993) Gene-A32 Product of Vaccinia Virus May Be an ATPase Involved in Viral-DNA Packaging As Indicated by Seuqnce Compareisons With Other Putative Viral ATPases. *Virus Genes* 7: 89-94

124. Valpuesta JM & Carrascosa J (1994) Structure of Viral Connectors and Their Funciton in Bacteriophage Assembly and DNA Packaging. *Quart. Rev. Biophys.* 27: 107-155

125. Olia AS, Prevelige PE, Johnson JE, & Cingolani G (2011) Three-Dimensional Structure of a Viral Genome-Delivery Portal Vertex. *Nat Struct Mol Biol* 18: 597-603

126. Baumann RG, Mullaney J, & Black LW (2006) Portal Fusion Protein Constraints on Function in DNA Packaging of Bacteriophage T4. *Mol Microbiol.* 61: 16-32

127. Hugel T, Michaelis J, Hetherington CL, Jardine PJ, Grimes S, Walter JM, Faik W, Anderson DL, & Bustamante C (2007) Experimental Test of Connector Rotation During DNA Packaging into Bacteriophage Phi29 Capsids. *Plos Biology* 5: 558-567

128. Chang C, Zhang H, Shu D, Guo P, & Savran C (2008) Bright-Field Analysis of Phi29 DNA Packaging Motor Using a Magnetomechanical System. *Appl. Phys. Lett.* 93: 153902-153903

129. Demarre G, Galli E, & Barre FX (2013) The FtsK Family of DNA Pumps. *Adv. Exp. Med. Biol* 767: 245-262

130. Barre FX (2007) FtsK and SpoIIIE: the Tale of the Conserved Tails. *Mol. Microbiol.* 66: 1051-1055

131. Crozat E & Grainge I (2010) FtsK DNA Translocase: the Fast Motor That Knows Where It's Going. *Chembiochem.* 11: 2232-2243

132. Bath J, Wu LJ, Errington J, & Wang JC (2000) Role of Bacillus Subtilis SpoIIIE in DNA Transport Across the Mother Cell-Prespore Division Septum. *Science* 290: 995-997

133. Lowe J, Ellonen A, Allen MD, Atkinson C, Sherratt DJ, & Grainge I (2008) Molecular Mechanism of Sequence-Directed DNA Loading and Translocation by FtsK. *Mol. Cell* 31: 498-509

134. Massey TH, Mercogliano CP, Yates J, Sherratt DJ, & Lowe J (2006) Double-Stranded DNA Translocation: Structure and Mechanism of Hexameric FtsK. *Mol. Cell* 23: 457-469

135. Pease PJ, Levy O, Cost GJ, Gore J, Ptacin JL, Sherratt D, Bustamante C, & Cozzarelli NR (2005) Sequence-Directed DNA Translocation by Purified FtsK. *Science* 307: 586-590

136. Saleh OA, Bigot S, Barre FX, & Allemand JF (2005) Analysis of DNA Supercoil Induction by FtsK Indicates Translocation Without Groove-Tracking. *Nat. Struct. Mol. Biol.* 12: 436-440

137. Iyer LM, Makarova KS, Koonin EV, & Aravind L (2004) Comparative Genomics of the FtsK-HerA Superfamily of Pumping ATPases: Implications for the Origins of Chromosome Segregation, Cell Division and Viral Capsid Packaging. *Nucleic Acids Res.* 32: 5260-5279

138. Bianco P & Kowalczykowski S (2000) Translocation Step Size and Mechanism of the RecBC DNA Helicase. *Nature* 405: 368-372

139. Wendell D, Jing P, Geng J, Subramaniam V, Lee TJ, Montemagno C, & Guo P (2009) Translocation of Double-Stranded DNA Through Membrane-Adapted Phi29 Motor Protein Nanopores. *Nat. Nanotechnol.* 4: 765-772

140. Li X, Yang X, Qi J, & Seeman N (1996) Antiparallel DNA Double Crossover Molecules As Components for Nanoconstruction. *J. Am. Chem. Soc.* 118: 6131-6140

141. Sun S, Kondabagil K, Draper B, Alam TI, Bowman VD, Zhang Z, Hegde S, Fokine A, Rossmann MG, & Rao VB (2008) The Structure of the Phage T4 DNA Packaging Motor Suggests a Mechanism Dependent on Electrostatic Forces. *Cell.* 135: 1251-1262

142. Enemark EJ & Joshua-Tor L (2008) On Helicases and Other Motor Proteins. *Curr. Opin. Struct. Biol.* 18: 243-257

143. Patel SS & Picha KM (2000) Structure and Function of Hexameric Helicases. *Annu. Rev. Biochem.* 69: 651-697

144. Itsathitphaisarn O, Wing RA, Eliason WK, Wang J, & Steitz TA (2012) The Hexameric Helicase DnaB Adopts a Nonplanar Conformation During Translocation. *Cell* 151: 267-277

145. Hacker KJ & Johnson KA (1997) A Hexameric Helicase Encircles One DNA Strand and Excludes the Other During DNA Unwinding. *Biochemistry* 36: 14080-14087

146. Dittrich M & Schulten K (2006) PcrA Helicase, a Prototype ATP-Driven Molecular Motor. *Structure* 14: 1345-1353

147. Phelps C, Lee W, Jose D, von Hippel PH, & Marcus AH (2013) Single-Molecule FRET and Linear Dichroism Studies of DNA Breathing and Helicase Binding at Replication Fork Junctions. *Proc. Natl. Acad. Sci. U. S. A* 110: 17320-17325

148. Fei J & Ha T (2013) Watching DNA Breath One Molecule at a Time. *Proc. Natl. Acad. Sci. U. S. A* 110: 17173-17174

149. Lee W, Jose D, Phelps C, Marcus AH, & von Hippel PH (2013) A Single-Molecule View of the Assembly Pathway, Subunit Stoichiometry, and Unwinding Activity of the Bacteriophage T4 Primosome (Helicase-Primase) Complex. *Biochemistry* 52: 3157-3170

150. Haque F, Wang S, Stites C, Chen L, Wang C, & Guo P (2015) Single Pore Translocation of Folded, Double-Stranded, and Tetra-Stranded DNA Through Channel of Bacteriophage Phi29 DNA Packaging Motor. *Biomaterials* 53: 744-752

151. Agirrezabala X, Martin-Benito J, Valle M, Gonzalez JM, Valencia A, Valpuesta JM, & Carrascosa JL (2005) Structure of the Connector of Bacteriophage T7 at 8A Resolution: Structural Homologies of a Basic Component of a DNA Translocating Machinery. *J. Mol Biol.* 347: 895-902

152. Xing X & Bell CE (2004) Crystal Structures of Escherichia Coli RecA in a Compressed Helical Filament. *J. Mol. Biol.* 342: 1471-1485

153. Pascal JM, Tsodikov OV, Hura GL, Song W, Cotner EA, Classen S, Tomkinson AE, Tainer JA, & Ellenberger T (2006) A Flexible Interface Between DNA Ligase and PCNA Supports Conformational Switching and Efficient Ligation of DNA. *Mol. Cell* 24: 279-291

154. Bailey S, Eliason WK, & Steitz TA (2007) Structure of Hexameric DnaB Helicase and Its Complex With a Domain of DnaG Primase. *Science* 318: 459-463

155. Enemark EJ & Joshua-Tor L (2006) Mechanism of DNA Translocation in a Replicative Hexameric Helicase. *Nature* 442: 270-275

156. Gomis-Ruth FX & Coll M (2001) Structure of TrwB, a Gatekeeper in Bacterial Conjugation. *Int. J. Biochem. Cell Biol.* 33: 839-843

157. Leipe DD, Wolf YI, Koonin EV, & Aravind L (2004) Classification and Evolution of P-Loop GTPases and Related ATPases. *J. Mol Biol. 2002. Mar. 15.* 317: 41-72

158. Chelikani V, Ranjan T, Zade A, Shukla A, & Kondabagil K (2014) Genome Segregation and Packaging Machinery in Acanthamoeba Polyphaga Mimivirus Is Reminiscent of Bacterial Apparatus. *J. Virol.*

159. Guo F, Liu Z, Vago F, Ren Y, Wu W, Wright ET, Serwer P, & Jiang W (2013) Visualization of Uncorrelated, Tandem Symmetry Mismatches in the Internal Genome Packaging Apparatus of Bacteriophage T7. *Proc. Natl. Acad. Sci. U. S. A* 110: 6811-6816

160. Pearson RK & Fox MS (1988) Effects of DNA Heterologies on Bacteriophage Lambda Packaging. *Genetics* 118: 5-12

161. Moll W-D & Guo P (2005) Translocation of Nicked but Not Gapped DNA by the Packaging Motor of Bacteriophage Phi29. *J Mol Biol* 351: 100-107

162. Simpson AA, Tao Y, Leiman PG, Badasso MO, He Y, Jardine PJ, Olson NH, Morais MC, Grimes S, Anderson DL, Baker TS, & Rossmann MG (2000) Structure of the Bacteriophage Phi29 DNA Packaging Motor. *Nature* 408: 745-750

163. Grimes S, Ma S, Gao J, Atz R, & Jardine PJ (2011) Role of Phi29 Connector Channel Loops in Late-Stage DNA Packaging. *J. Mol. Biol.* 410: 50-59

164. Lander GC, Tang L, Casjens SR, Gilcrease EB, Prevelige P, Poliakov A, Potter CS, Carragher B, & Johnson JE (2006) The Structure of an Infectious P22 Virion Shows the Signal for Headful DNA Packaging. *Science.* 312: 1791-1795

165. Molineux IJ & Panja D (2013) Popping the Cork: Mechanisms of Phage Genome Ejection. *Nat Rev. Microbiol.* 11: 194-204

166. Petrov AS & Harvey SC (2008) Packaging Double-Helical DNA into Viral Capsids: Structures, Forces, and Energetics. *Biophys. J.* 95: 497-502

167. Jiang W, Chang J, Jakana J, Weigele P, King J, & Chiu W (2006) Structure of Epsilon15 Bacteriophage Reveals Genome Organization and DNA Packaging/Injection Apparatus. *Nature.* 439: 612-616

168. Liu S, Chistol G, Hetherington CL, Tafoya S, Aathavan K, Schnitzbauer J, Grimes S, Jardine PJ, & Bustamante C (2014) A Viral Packaging Motor Varies Its DNA Rotation and Step Size to Preserve Subunit Coordination As the Capsid Fills. *Cell* 157: 702-713

169. Ray K, Ma J, Oram M, Lakowicz JR, & Black LW (2010) Single-Molecule and FRET Fluorescence Correlation Spectroscopy Analyses of Phage DNA Packaging: Colocalization of Packaged Phage T4 DNA Ends Within the Capsid. *J. Mol. Biol.* 395: 1102-1113

170. Kainov DE, Mancini EJ, Telenius J, Lisai J, Grimes JM, Bamford DH, Stuart DI, & Tuma R (2008) Structural Basis of Mechanochemical Coupling in a Hexameric Molecular Motor. *J Biol Chem* 283: 3607-3617

171. Mastrangelo IA, Hough PV, Wall JS, Dodson M, Dean FB, & Hurwitz J (1989) ATP-Dependent Assembly of Double Hexamers of SV40 T Antigen at the Viral Origin of DNA Replication. *Nature* 338: 658-662

172. Parsons CA, Stasiak A, Bennett RJ, & West SC (1995) Structure of a Multisubunit Complex That Promotes DNA Branch Migration. *Nature* 374: 375-378

173. Egelman HH, Yu X, Wild R, Hingorani MM, & Patel SS (1995) Bacteriophage T7 Helicase/Primase Proteins Form Rings Around Single- Stranded DNA That Suggest a General Structure for Hexameric Helicases. *Proc Natl Acad Sci U. S. A* 92: 3869-3873

174. Niedenzu T, Roleke D, Bains G, Scherzinger E, & Saenger W (2001) Crystal Structure of the Hexameric Replicative Helicase RepA of Plasmid RSF1010. *J. Mol. Biol.* 306: 479-487

175. Putnam CD, Clancy SB, Tsuruta H, Gonzalez S, Wetmur JG, & Tainer JA (2001) Structure and Mechanism of the RuvB Holliday Junction Branch Migration Motor. *J. Mol. Biol.* 311: 297-310

176. Willows RD, Hansson A, Birch D, Al-Karadaghi S, & Hansson M (2004) EM Single Particle Analysis of the ATP-Dependent BchI Complex of Magnesium Chelatase: an AAA(+) Hexamer. *J Struct Biol* 146: 227-233

177. Mueller-Cajar O, Stotz M, Wendler P, Hartl FU, Bracher A, & Hayer-Hartl M (2011) Structure and Function of the AAA+ Protein CbbX, a Red-Type Rubisco Activase. *Nature* 479: 194-199

178. Wang F, Mei Z, Qi Y, Yan C, Hu Q, Wang J, & Shi Y (2011) Structure and Mechanism of the Hexameric MecA-ClpC Molecular Machine. *Nature* 471: 331-335

179. Grainge I, Lesterlin C, & Sherratt DJ (2011) Activation of XerCD-Dif Recombination by the FtsK DNA Translocase. *Nucleic Acids Res.* 39: 5140-5148

180. Rao VB & Feiss M (2008) The Bacteriophage DNA Packaging Motor. *Annu. Rev. Genet.* 42: 647-681

181. Chemla YR, Aathavan K, Michaelis J, Grimes S, Jardine PJ, Anderson DL, & Bustamante C (2005) Mechanism of Force Generation of a Viral DNA Packaging Motor. *Cell.* 122: 683-692

182. Huang LP & Guo P (2003) Use of Acetone to Attain Highly Active and Soluble DNA Packaging Protein Gp16 of Phi29 for ATPase Assay. *Virology* 312: 449-457

183. Huang LP & Guo P (2003) Use of PEG to Acquire Highly Soluble DNA-Packaging Enzyme Gp16 of Bacterial Virus Phi29 for Stoichiometry Quantification. *J Virol Methods* 109: 235-244

184. Lee TJ, Zhang H, Liang D, & Guo P (2008) Strand and Nucleotide-Dependent ATPase Activity of Gp16 of Bacterial Virus Phi29 DNA Packaging Motor. *Virology* 380: 69-74

185. Grimes S & Anderson D (1990) RNA Dependence of the Bateriophage Phi29 DNA Packaging ATPase. *J. Mol. Biol.* 215: 559-566

186. Jimenez J, Santisteban A, Carazo JM, & Carrascosa JL (1986) Computer Graphic Display Method for Visualizing Three-Dimensional Biological Structures. *Science* 232: 1113-1115

187. Green DJ, Wang JC, Xiao F, Cai Y, Balhorn R, Guo P, & Cheng RH (2010) Self-Assembly of Heptameric Nanoparticles Derived From Tag-Functionalized Phi29 Connectors. *ACS Nano* 4: 7651-7659

188. Xiao F, Cai Y, Wang JC, Green D, Cheng RH, Demeler B, & Guo P (2009) Adjustable Ellipsoid Nanoparticles Assembled From Re-Engineered Connectors of the Bacteriophage Phi29 DNA Packaging Motor. *ACS Nano.* 3: 2163-2170

189. Guo Y, Blocker F, Xiao F, & Guo P (2005) Construction and 3-D Computer Modeling of Connector Arrays With Tetragonal to Decagonal Transition Induced by PRNA of Phi29 DNA-Packaging Motor. *J. Nanosci. Nanotechnol.* 5: 856-863

190. Carazo JM, Donate LE, Herranz L, Secilla JP, & Carrascosa JL (1986) Three-Dimensional Reconstruction of the Connector of Bacteriophage F29 at 1.8 Nm Resolution. *J Mol Biol* 192: 853-867

191. Haque F, Lunn J, Fang H, Smithrud D, & Guo P (2012) Real-Time Sensing and Discrimination of Single Chemicals Using the Channel of Phi29 DNA Packaging Nanomotor. *ACS Nano* 6: 3251-3261

192. Maluf NK, Gaussier H, Bogner E, Feiss M, & Catalano CE (2006) Assembly of Bacteriophage Lambda Terminase into a Viral DNA Maturation and Packaging Machine. *Biochemistry.* 45: 15259-15268

193. Maluf NK & Feiss M (2006) Virus DNA Translocation: Progress Towards a First Ascent of Mount Pretty Difficult. *Mol Microbiol.* 61: 1-4

194. Kondabagil K, Draper B, & Rao VB (2012) Adenine Recognition Is a Key Checkpoint in the Energy Release Mechanism of Phage T4 DNA Packaging Motor. *J Mol Biol* 415: 329-342

195. Shibayama Y, Dabbs ER, Yazawa K, & Mikami Y (2011) Functional Analysis of a Small Cryptic Plasmid PYS1 From Nocardia. *Plasmid* 66: 26-37

196. Lee CS & Guo P (1994) A Highly Sensitive System for the Assay of in Vitro Viral Assembly of Bacteriophage Phi29 of Bacillus Subtilis. *Virology* 202: 1039-1042

197. Lee TJ, Zhang H, Chang CL, Savran C, & Guo P (2009) Engineering of the Fluorescent-Energy-Conversion Arm of Phi29 DNA Packaging Motor for Single-Molecule Studies. *Small* 5: 2453-2459

198. Isidro A, Henriques AO, & Tavares P (2004) The Portal Protein Plays Essential Roles at Different Steps of the SPP1 DNA Packaging Process. *Virology.* 322: 253-263

199. Lee CS & Guo P (1995) *In Vitro* Assembly of Infectious Virions of Ds-DNA Phage F29 From Cloned Gene Products and Synthetic Nucleic Acids. *J. Virol.* 69: 5018-5023

200. Morais MC, Tao Y, Olsen NH, Grimes S, Jardine PJ, Anderson D, Baker TS, & Rossmann MG (2001) Cryoelectron-Microscopy Image Reconstruction of Symmetry Mismatches in Bacteriophage Phi29. *J Struct Biol* 135: 38-46

201. Ding F, Lu C, Zhao W, Rajashankar KR, Anderson DL, Jardine PJ, Grimes S, & Ke A (2011) Structure and Assembly of the Essential RNA Ring Component of a Viral DNA Packaging Motor. *Proc. Natl. Acad. Sci. U. S. A* 108: 7357-7362

202. Zhang X & Wigley DB (2008) The 'Glutamate Switch' Provides a Link Between ATPase Activity and Ligand Binding in AAA+ Proteins. *Nat. Struct. Mol. Biol.* 15: 1223-1227

203. Guo P, Noji H, Yengo CM, Zhao Z, & Grainge I (2016) Biological Nanomotors With Revolution, Linear, or Rotation Motion Mechanism. *Microbiology and Molecular Biology Reviews* 80: 161-186

204. Guo P, Grainge I, Zhao Z, & Vieweger M (2014) Two Classes of Nucleic Acid Translocation Motors: Rotation and Revolution Without Rotation. *Cell Biosci.* 4: 54

205. Soong RK, Bachand GD, Neves HP, Olkhovets AG, Craighead HG, & Montemagno CD (2000) Powering an Inorganic Nanodevice With a Biomolecular Motor. *Science* 290: 1555-1558

206. Hu B, Margolin W, Molineux IJ, & Liu J (2013) The Bacteriophage T7 Virion Undergoes Extensive Structural Remodeling During Infection. *Science* 339: 576-579

207. Walker JE, Saraste M, & Gay NJ (1982) E. Coli F1-ATPase Interacts With a Membrane Protein Component of a Proton Channel. *Nature* 298: 867-869

208. Walker JE, Saraste M, Runswick MJ, & Gay NJ (1982) Distantly Related Sequences in the Alpha- and Beta-Subunits of ATP Synthase, Myosin, Kinases and Other ATP-Requiring Enzymes and a Common Nucleotide Binding Fold. *EMBO J.* 1: 945-951

209. Jurado KA & Engelman A (2013) Multimodal Mechanism of Action of Allosteric HIV-1 Integrase Inhibitors. *Expert Rev. Mol. Med.* 15: e14

210. Karata K, Inagawa T, Wilkinson AJ, Tatsuta T, & Ogura T (1999) Dissecting the Role of a Conserved Motif (the Second Region of Homology) in the AAA Family of ATPases. Site-Directed Mutagenesis of the ATP-Dependent Protease FtsH. *J. Biol. Chem.* 274: 26225-26232

211. Hilbert BJ, Hayes JA, Stone NP, Duffy CM, Sankaran B, & Kelch BA (2015) Structure and Mechanism of the ATPase That Powers Viral Genome Packaging. *Proc. Natl. Acad. Sci. U. S. A* 112: E3792-E3799

212. Joly N, Zhang N, & Buck M (2012) ATPase Site Architecture Is Required for Self-Assembly and Remodeling Activity of a Hexameric AAA+ Transcriptional Activator. *Mol. Cell* 47: 484-490

213. Wendler P, Ciniawsky S, Kock M, & Kube S (2012) Structure and Function of the AAA+ Nucleotide Binding Pocket. *Biochim. Biophys. Acta* 1823: 2-14

214. Zeymer C, Fischer S, & Reinstein J (2014) Trans-Acting Arginine Residues in the AAA+ Chaperone ClpB Allosterically Regulate the Activity Through Inter- and Intradomain Communication. *J. Biol. Chem.* 289: 32965-32976

215. Yukawa A, Iino R, Watanabe R, Hayashi S, & Noji H (2015) Key Chemical Factors of Arginine Finger Catalysis of F1-ATPase Clarified by an Unnatural Amino Acid Mutation. *Biochemistry* 54: 472-480

216. Elles LM & Uhlenbeck OC (2008) Mutation of the Arginine Finger in the Active Site of Escherichia Coli DbpA Abolishes ATPase and Helicase Activity and Confers a Dominant Slow Growth Phenotype. *Nucleic Acids Res.* 36: 41-50

217. Roy A, Kucukural A, & Zhang Y (2010) I-TASSER: a Unified Platform for Automated Protein Structure and Function Prediction. *Nat. Protoc.* 5: 725-738

218. Humphrey W, Dalke A, & Schulten K (1996) VMD: Visual Molecular Dynamics. *J. Mol. Graph.* 14: 33-38

219. Volozhantsev NV, Oakley BB, Morales CA, Verevkin VV, Bannov VA, Krasilnikova VM, Popova AV, Zhilenkov EL, Garrish JK, Schegg KM, Woolsey R, Quilici DR, Line JE, Hiett KL, Siragusa GR, Svetoch EA, & Seal BS (2012) Molecular Characterization of Podoviral Bacteriophages Virulent for Clostridium Perfringens and Their Comparison With Members of the Picovirinae. *PLoS ONE* 7: e38283

220. Gomis-Ruth FX, Moncalian G, Perez-Luque R, Gonzalez A, Cabezon E, de la CF, & Coll M (2001) The Bacterial Conjugation Protein TrwB Resembles Ring Helicases and F1-ATPase. *Nature* 409: 637-641

221. Wallden K, Williams R, Yan J, Lian PW, Wang L, Thalassinos K, Orlova EV, & Waksman G (2012) Structure of the VirB4 ATPase, Alone and Bound to the Core Complex of a Type IV Secretion System. *Proc. Natl. Acad. Sci. U. S. A* 109: 11348-11353

222. Ogura T, Whiteheart SW, & Wilkinson AJ (2004) Conserved Arginine Residues Implicated in ATP Hydrolysis, Nucleotide-Sensing, and Inter-Subunit Interactions in AAA and AAA+ ATPases. *J. Struct. Biol.* 146: 106-112

223. Chen B, Sysoeva TA, Chowdhury S, Guo L, De CS, Hanson JA, Yang H, & Nixon BT (2010) Engagement of Arginine Finger to ATP Triggers Large Conformational Changes in NtrC1 AAA+ ATPase for Remodeling Bacterial RNA Polymerase. *Structure* 18: 1420-1430

224. Thomsen ND & Berger JM (2009) Running in Reverse: the Structural Basis for Translocation Polarity in Hexameric Helicases. *Cell* 139: 523-534

225. Mancini EJ, Kainov DE, Grimes JM, Tuma R, Bamford DH, & Stuart DI (2004) Atomic Snapshots of an RNA Packaging Motor Reveal Conformational Changes Linking ATP Hydrolysis to RNA Translocation. *Cell* 118: 743-755

226. Singleton MR, Sawaya MR, Ellenberger T, & Wigley DB (2000) Crystal Structure of T7 Gene 4 Ring Helicase Indicates a Mechanism for Sequential Hydrolysis of Nucleotides. *Cell* 101: 589-600

227. Kelley LA, Mezulis S, Yates CM, Wass MN, & Sternberg MJ (2015) The Phyre2 Web Portal for Protein Modeling, Prediction and Analysis. *Nat. Protoc.* 10: 845-858

228. Haque F, Li J, Wu H-C, Liang X-J, & Guo P (2013) Solid-State and Biological Nanopore for Real-Time Sensing of Single Chemical and Sequencing of DNA. *Nano Today* 8: 56-74

229. Wang S, Haque F, Rychahou PG, Evers BM, & Guo P (2013) Engineered Nanopore of Phi29 DNA-Packaging Motor for Real-Time Detection of Single Colon Cancer Specific Antibody in Serum. *ACS Nano* 7: 9814-9822

230. Fang H, Zhang P, Huang LP, Zhao Z, Pi F, Montemagno C, & Guo P (2014) Binomial Distribution for Quantification of Protein Subunits in Biological Nanoassemblies and Functional Nanomachines. *Nanomedicine.* 10: 1433-1440

231. Shu D, Pi F, Wang C, Zhang P, & Guo P (2015) New Approach to Develop Ultra-High Inhibitory Drug Using the Power-Function of the Stoichiometry of the Targeted Nanomachine or Biocomplex. *Nanomedicine* 10: 1881-1897

232. Kumar R & Grubmuller H (2014) Elastic Properties and Heterogeneous Stiffness of the Phi29 Motor Connector Channel. *Biophysical Journal* 106: 1338-1348

233. Ye Q, Rosenberg SC, Moeller A, Speir JA, Su TY, & Corbett KD (2015) TRIP13 Is a Protein-Remodeling AAA+ ATPase That Catalyzes MAD2 Conformation Switching. *Elife.* 4:

234. Stinson BM, Baytshtok V, Schmitz KR, Baker TA, & Sauer RT (2015) Subunit Asymmetry and Roles of Conformational Switching in the Hexameric AAA+ Ring of ClpX. *Nat. Struct. Mol. Biol.* 22: 411-416

235. Sun SX, Wang H, & Oster G (2004) Asymmetry in the F1-ATPase and Its Implications for the Rotational Cycle. *Biophys. J.* 86: 1373-1384

236. Wendler P, Shorter J, Snead D, Plisson C, Clare DK, Lindquist S, & Saibil HR (2009) Motor Mechanism for Protein Threading Through Hsp104. *Mol. Cell* 34: 81-92

237. Kravats AN, Tonddast-Navaei S, Bucher RJ, & Stan G (2013) Asymmetric Processing of a Substrate Protein in Sequential Allosteric Cycles of AAA+ Nanomachines. *J. Chem. Phys.* 139: 121921

238. Shu D, Moll WD, Deng Z, Mao C, & Guo P (2004) Bottom-Up Assembly of RNA Arrays and Superstructures As Potential Parts in Nanotechnology. *Nano Lett.* 4: 1717-1723

239. Liaw JW, Chen YS, & Kuo MK (2014) Rotating Au Nanorod and Nanowire Driven by Circularly Polarized Light. *Opt. Express* 22: 26005-26015

240. Loh IY, Cheng J, Tee SR, Efremov A, & Wang Z (2014) From Bistate Molecular Switches to Self-Directed Track-Walking Nanomotors. *ACS Nano* 8: 10293-10304

241. Li J, Gao W, Dong R, Pei A, Sattayasamitsathit S, & Wang J (2014) Nanomotor Lithography. *Nat. Commun.* 5: 5026

242. Balk AL, Mair LO, Mathai PP, Patrone PN, Wang W, Ahmed S, Mallouk TE, Liddle JA, & Stavis SM (2014) Kilohertz Rotation of Nanorods Propelled by Ultrasound, Traced by Microvortex Advection of Nanoparticles. *ACS Nano* 8: 8300-8309

243. Xuan M, Shao J, Lin X, Dai L, & He Q (2014) Self-Propelled Janus Mesoporous Silica Nanomotors With Sub-100 Nm Diameters for Drug Encapsulation and Delivery. *Chemphyschem* 15: 2255-2260

244. Kumar KR, Kamei T, Fukaminato T, & Tamaoki N (2014) Complete ON/OFF Photoswitching of the Motility of a Nanobiomolecular Machine. *ACS Nano* 8: 4157-4165

245. Ahmad Z & Cox JL (2014) ATP Synthase: the Right Size Base Model for Nanomotors in Nanomedicine. *ScientificWorldJournal.* 2014: 567398

246. Morozov KI & Leshansky AM (2014) The Chiral Magnetic Nanomotors. *Nanoscale.* 6: 1580-1588

247. Dong B, Zhou T, Zhang H, & Li CY (2013) Directed Self-Assembly of Nanoparticles for Nanomotors. *ACS Nano* 7: 5192-5198

248. Khataee HR & Ibrahim MY (2012) Modelling of Internal Architecture of Kinesin Nanomotor As a Machine Language. *IET. Nanobiotechnol.* 6: 87-92

249. Gao W, Manesh KM, Hua J, Sattayasamitsathit S, & Wang J (2011) Hybrid Nanomotor: a Catalytically/Magnetically Powered Adaptive Nanowire Swimmer. *Small* 7: 2047-2051

250. Thakur S, Chen JX, & Kapral R (2011) Interaction of a Chemically Propelled Nanomotor With a Chemical Wave. *Angew. Chem. Int. Ed Engl.* 50: 10165-10169

251. Bamrungsap S, Phillips JA, Xiong X, Kim Y, Wang H, Liu H, Hebard A, & Tan W (2011) Magnetically Driven Single DNA Nanomotor. *Small* 7: 601-605

252. Arai N, Yasuoka K, Koishi T, & Ebisuzaki T (2010) Asymmetric Brownian Motor Driven by Bubble Formation in a Hydrophobic Channel. *ACS Nano* 4: 5905-5913

253. Gibbs JG & Zhao Y (2010) Self-Organized Multiconstituent Catalytic Nanomotors. *Small* 6: 1656-1662

254. Klapper Y, Sinha N, Ng TW, & Lubrich D (2010) A Rotational DNA Nanomotor Driven by an Externally Controlled Electric Field. *Small* 6: 44-47

255. Kang H, Liu H, Phillips JA, Cao Z, Kim Y, Chen Y, Yang Z, Li J, & Tan W (2009) Single-DNA Molecule Nanomotor Regulated by Photons. *Nano Lett.* 9: 2690-2696

256. Besenbacher F & Norskov JK (2000) SURFACE SCIENCE: How to Power a Nanomotor. *Science* 290: 1520

257. Bishop JD & Klavins E (2007) An Improved Autonomous DNA Nanomotor. *Nano Lett.* 7: 2574-2577

258. Balzani V, Clemente-Leon M, Credi A, Ferrer B, Venturi M, Flood AH, & Stoddart JF (2006) Autonomous Artificial Nanomotor Powered by Sunlight. *Proc Natl Acad Sci U S A* 103: 1178-1183

259. Chen Y & Mao C (2004) Putting a Brake on an Autonomous DNA Nanomotor. *J. Am. Chem. Soc.* 126: 8626-8627

260. Kanatani K, Ochi Y, Okamoto A, & Saito I (2003) DNA Nanomotor Using Duplex-Quadruplex Conformational Transition. *Nucleic Acids Res. Suppl* 161-162

261. Lin C, Liu Y, & Yan H (2009) Designer DNA Nanoarchitectures. *Biochemistry* 48: 1663-1674

262. Aldaye FA, Palmer AL, & Sleiman HF (2008) Assembling Materials With DNA As the Guide. *Science* 321: 1795-1799

263. Seeman NC (2010) Nanomaterials Based on DNA. *Annu. Rev. Biochem.* 79: 65-87

264. Enemark EJ & Joshua-Tor L (2008) On Helicases and Other Motor Proteins. *Curr. Opin. Struct. Biol.* 18: 243-257

265. Kad NM, Wang H, Kennedy GG, Warshaw DM, & Van HB (2010) Collaborative Dynamic DNA Scanning by Nucleotide Excision Repair Proteins Investigated by Single- Molecule Imaging of Quantum-Dot-Labeled Proteins. *Mol. Cell* 37: 702-713

266. Pi F, Vieweger M, Zhao Z, Wang S, & Guo P (2015) Discovery of a New Method for Potent Drug Development Using Power Function of Stoichiometry of Homomeric Biocomplexes or Biological Nanomotors. *Expert Opin. Drug Deliv.* 1-14

267. Cai Y, Xiao F, & Guo P (2008) The Effect of N- or C-Terminal Alterations of the Connector of Bacteriophage Phi29 DNA Packaging Motor on Procapsid Assembly, PRNA Binding, and DNA Packaging. *Nanomedicine* 4: 8-18

268. Yang J, Yan R, Roy A, Xu D, Poisson J, & Zhang Y (2015) The I-TASSER Suite: Protein Structure and Function Prediction. *Nat. Methods* 12: 7-8

269. Zhang Y & Skolnick J (2005) TM-Align: a Protein Structure Alignment Algorithm Based on the TM-Score. *Nucleic Acids Res.* 33: 2302-2309

270. Marks DS, Colwell LJ, Sheridan R, Hopf TA, Pagnani A, Zecchina R, & Sander C (2011) Protein 3D Structure Computed From Evolutionary Sequence Variation. *PLoS ONE* 6: e28766

271. Spies, M. (2016) *DNA Helicases and DNA Motor Proteins,* Springer, New York

272. Xiao F, Moll D, Guo S, & Guo P (2005) Binding of PRNA to the N-Terminal 14 Amino Acids of Connector Protein of Bacterial Phage Phi29. *Nucleic Acids Res* 33: 2640-2649

273. Atz R, Ma S, Gao J, Anderson DL, & Grimes S (2007) Alanine Scanning and Fe-BABE Probing of the Bacteriophage Phi29 Prohead RNA-Connector Interaction. *J. Mol. Biol.* 369: 239-248

Vita

Zhengyi Zhao

Educational Institutions

Shenyang Pharmaceutical University	2006 – 2011	Bachelors of science	Pharmaceutical Sciences
University of Kentucky	2011 – 2016	Ph.D. Candidate	Pharmaceutical Sciences
The Ohio State University	2015 - 2016	Visiting Scholar	Pharmaceutical Sciences

Professional Publications

(1) Z. Zhao, E. F. Khisamutdinov, C. Schwartz and P. Guo. **"Mechanism of one-way traffic of hexameric phi29 DNA packaging motor with four electropositive relaying layers facilitating antiparallel revolution".** *ACS Nano.* 7:4082-4092 (May 2013).

(2) H. Zhang, C. Richards, Z. Zhao, and P. Guo. **"Single-Molecule Approach to Study RNA Nanoparticles".** *RNA Nanotechnology and Therapeutics.* pp. 263-282 (Jul. 2013).

(3) M. Qiu, E. F. Khisamutdinov, Z. Zhao, C. Pan, J. Choi, N. B. Leontis and P. Guo. **"RNA Nanotechnology for Computer Design and in vivo Computation".** *Philosophical Transactions of the Royal Society A.* 371: 20120310 (Sep. 2013).

(4) P. Guo, C. Schwartz, J. Haak, and Z. Zhao. **"Discovery of a New Motion Mechanism of Biomotors Similar to the Earth Revolving around the Sun without Rotation".** *Virology.* 446:133-143 (Nov. 2013).

(5) G. De-Donatis†, Z. Zhao† (co-first author), S. Wang, L. P. Huang, C. Schwartz, O. V. Tsodikov, H. Zhang, F. Haque and P. Guo. **"Finding of widespread viral and bacterial revolution dsDNA translocation motors distinct from rotation motors by channel chirality and size".** *Cell & Bioscience* 4:30 (Jun. 2014).

(6) P. Guo, Z. Zhao, J. Haak, S. Wang, D. Wu, B. Meng and T. Weitao. **"Common Mechanisms of DNA translocation motors in Cells, Bacteria and Viruses Using the Revolution Mechanism without Rotation".** *Biotechnology Advances*; 32:853 (2014).

(7) P. Guo, I. Grainge, Z. Zhao, M. Vieweger. **"Two classes of nucleic acid translocation motors: rotation and revolution without rotation".** *Cell & Bioscience.* 4:54 (Sep. 2014).

(8) H. Fang, P. Zhang, L. P. Huang, Z. Zhao, C. Montemagno, and P. Guo. **"Binomial distribution for quantification of protein subunits in biological nanoassemblies and functional**

nanomachines". *Nanomedicine.* 10:1433-40 (Oct. 2014).

(9) P. Guo, H. Noji, C. M. Yengo, Z. Zhao, I. Grainge. **"Biological nanomotors with revolution, linear, or rotation motion mechanism".** *Microbiology and Molecular Biology Reviews*. 80:161-186 (Mar. 2015).

(10) F. Pi, M. Vieweger, Z. Zhao, S. Wang, and P. Guo. **"Discovery of a new method for potent drug development using power function of stoichiometry of homomeric biocomplexes or biological nanomotors".** *Expert Opinion on Drug Delivery*. 26:1-14 (Aug. 2015).

(11) E. F. Khisamutdinov, M. N. Bui, D. Jasinski, Z. Zhao, Z. Cui, and P. Guo. **"Methods in Molecular Biology: Simple Method for Constructing RNA Triangle, Square, Pentagon by Tuning Interior RNA 3WJ Angle From 60˚ to 90˚ or 108˚".** 1316:181-93 (2015).

(12) T. Lee, S. Abels, E. F. Khisamutdinov, M. Qiu, D. L. Jasinski, Z. Zhao, T. Qu, J. Choi, and P. Guo. **"Conceptual, potential and advancements in computer design and in vivo computation applying RNA nanotechnology".** *Molecular Nanostructure and Nanotechnology.* (May 2016).

(13) Z. Zhao, G. De-Donatis, C. Schwartz, H. Fang, J. Li and P. Guo. **"Arginine fingers regulates sequential action of asymmetrical hexameric ATPase in dsDNA translocation motor".** *Molecular and Cellular Biology.* 36:2514-2523 (Sep. 2016).

(14) Z. Ji, S. Wang, Z. Zhao, Z. Zhou, F. Haque, P. Guo. **"Fingerprinting of Peptides with a Large Channel of Bacteriophage Phi29 DNA Packaging Motor".** *Small*. 12:4572-4578 (Jul. 2016).

(15) Z. Zhao, H. Zhang, D. Shu, C. Montemagno, J. Li and P. Guo. **"Construction of Asymmetrical Hexameric Biomimetic Motors with Continuous Single-Directional Motion by Sequential Coordination".** *Small*. *In press.* DOI: 10.1002/smll.201601600. (Oct. 2016).

(16) S. Wang, Z. Zhou, Z. Zhao, Z. Ji, H. Zhang, F. Haque, P. Guo. **"Nanopore of SPP1 DNA Packaging Motor for Dynamic Analysis of Protein Conformation and Folding in Real Time".** *Under revision* (2016).

(17) S. Wang, Z. Zhao, H. Farzin, P. Guo*. **"An Engineering Perspective of Biological Nanopores For Single Molecule Sensing and DNA Sequencing".** *Under submission* (2016).

(18) S. Wang, Z. Zhou, Z. Zhao, H. Zhang, F. Haque, P. Guo *. **"Channel of SPP1 DNA Packaging Motor for Real Time Kinetic Analysis of Peptide States".** *Under submission* (2016).

Scholastic and Professional Honors

Elite of Innovation (0.1%)	2006
Special prize (3%) in Shenyang Pharmaceutical University	2006

Second prize (8%) in Shenyang Pharmaceutical University	2007
United Pharmaceutical Co., Ltd Scholarship (1%)	2007
Second place in National English Contest for College Students	2007
First prize (6%) in Shenyang Pharmaceutical University	2007, 2008, 2010
Best Youth League Member of Shenyang Pharmaceutical University	2009
Single Item Scholarship in Shenyang Pharmaceutical University	2009
University of Kentucky COP Monthly Publication Highlight	2013
ASV 2014 Student Travel Award	2014